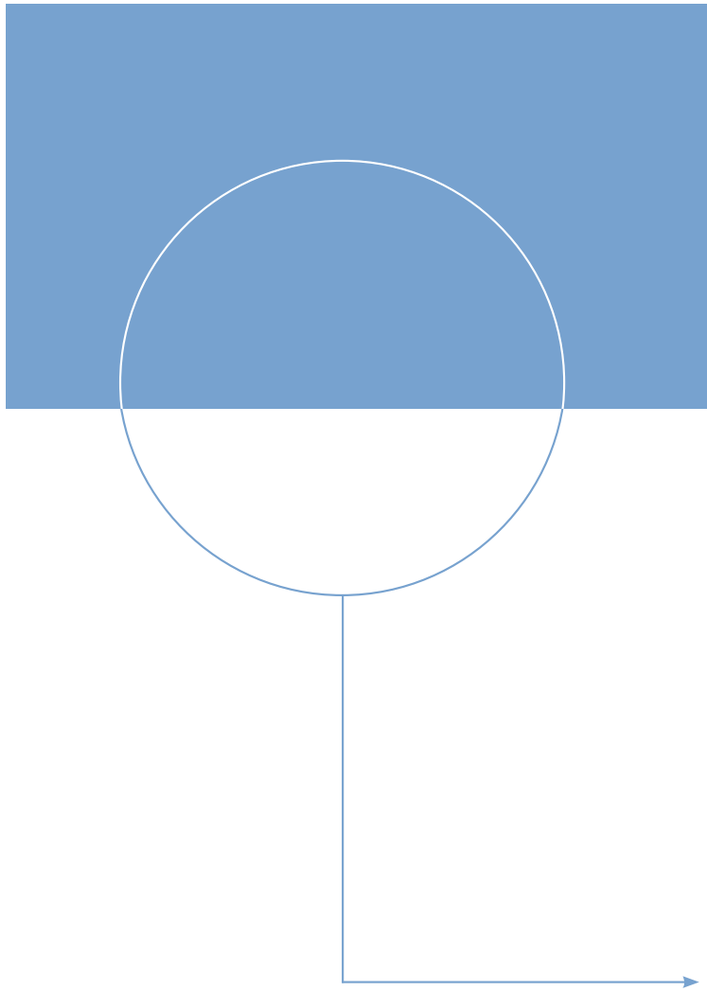

Master's thesis

2020

Aurora Haraldsen

NTNU
Norwegian University of
Science and Technology
Faculty of Information Technology and Electrical
Engineering
Department of Engineering Cybernetics

Aurora Haraldsen

Collision Avoidance using the Velocity Obstacle Algorithm for Underactuated Surface Vehicles

June 2020

NTNU
Norwegian University of
Science and Technology

NTNU
Norwegian University of
Science and Technology

NTNU
Norwegian University of
Science and Technology

Collision Avoidance using the Velocity Obstacle Algorithm for Underactuated Surface Vehicles

Aurora Haraldsen

MTTK
Submission date: June 2020
Supervisor: Kristin Y. Pettersen
Co-supervisor: Martin S. Wiig

Norwegian University of Science and Technology
Department of Engineering Cybernetics

Problem description

Autonomous vehicles are increasingly used in both scientific and commercial applications. During autonomous or semi-autonomous operations, the capability to avoid static and dynamic obstacles without human intervention is crucial for mission success and vehicle safety. In complex environments with dynamic obstacles the vehicle has to react quickly to obstacles, which can make the time consumption of motion planning algorithms unacceptable. Hence, there is a need for reactive collision avoidance algorithm for avoiding moving obstacles.

A common approach to reactive collision avoidance is the velocity obstacle approach, where obstacles are represented in the velocity space. The algorithm has been successfully applied to both non-holonomic systems and underactuated marine systems. The theoretical foundation of the algorithm, however, still needs to be expanded. In particular, it is interesting to investigate cases such as

- Analytical proof of vehicle safety when avoiding obstacles,
- Mathematical analysis of combining velocity obstacles with other goal-reaching behaviors, such as target reaching or path following.

The following subtasks are proposed for this assignment:

1. Perform a literature review on the topic of collision avoidance, with particular focus on velocity obstacles and on tools for analyzing a collision avoidance algorithm;
2. Implement the velocity obstacle method in a simulated environment;

3. Employ an analysis technique to prove safety for nonholonomic and underactuated vehicles avoiding a single, circular obstacle;
4. Combine the proof with target-reaching and path-following algorithms.

Abstract

This thesis presents a mathematical analysis of the velocity obstacle algorithm for collision avoidance of a moving obstacle in the plane. The velocity obstacle algorithm can be used for local navigation among dynamic obstacles by continually computing a set of unsafe velocities, and avoid the velocities inside this set. The method is commonly used for reactive collision avoidance as it requires only limited knowledge of the obstacle behaviour and is computationally inexpensive. A drawback of the previous analyses of the algorithm is the assumption that the vehicle and the obstacle are constrained to follow specific types of paths or that the velocities are assumed constant. Additionally, few consider the vehicle's dynamics when applying the algorithm, which in collision avoidance scenarios can be fatal if unaccounted for. In this thesis, we analyze the algorithm without these limitations. We provide conditions ensuring that a nonholonomic vehicle avoids a collision with an obstacle capable of both turning and accelerating towards the vehicle at any given moment in time. We extend the analysis to provide conditions under which safety is ensured for an underactuated vehicle, i.e. a vehicle unable to produce control forces in one or more of its degrees of freedom, in the presence of a moving obstacle. The theoretical proofs of collision avoidance are combined with proofs of target reaching and path following, and supported by numerical simulations.

Sammendrag

Denne masteravhandlingen presenterer en matematisk analyse av hastighet hindring algoritmen (eng. the velocity obstacle algorithm) for kollisjonsunngåelse i det horisontale planet. Algoritmen, som er hyppig brukt for reaktiv kollisjonsunngåelse, er basert på å regne ut samtlige hastighetsvektorer fartøyet kan inneha, som ved et ubestemt tidspunkt i fremtiden, fører til en kollisjon mellom fartøyet og en hindring. Ved å alltid unngå disse hastighetene unngår derav fartøyet en kollisjon med den spesifikke hindringen. En ulempe ved tidligere analyser av algoritmen er at fartøyet og hindringen er begrenset til å følge rette linjer, eller at hastighetene er antatt konstante. I tillegg tar få i betraktning dynamikken til fartøyet, som i kollisjonssituasjoner kan være avgjørende. I denne avhandlingen undersøker vi algoritmen uten slike begrensinger. Vi gir betingelser for at et ikke-holonomt fartøy unngår kollisjon med en hindring som beveger seg med tidsvarierende hastighet. Videre utvider vi analysen til å garantere kollisjonsunngåelse for et underaktuert fartøy, det vil si et fartøy som ikke kan styre en eller flere av sine frihetsgrader direkte. Vi kombinerer kollisjonsunngåelse med føring av fartøyet mot et ønsket mål eller en sti. Numeriske simuleringer er inkludert for å validere de teoretiske resultatene.

Contents

List of Figures

Preface

This master's thesis is submitted as a part of the requirements for the master degree at the Department of Engineering Cybernetics at the Norwegian University of Science and Technology. The work presented in this thesis has been carried out under the supervision of Prof. Kristin Y. Pettersen at the Department of Engineering Cybernetics and Dr. Martin S. Wiig at the Norwegian Defence Research Establishment (FFI).

During this project, I have been provided with multiple tools through Dr. Martin S. Wiig, who gave me access to his own doctoral thesis on collision avoidance, which provided me with a great deal of guidance throughout this work. I was also granted access to his Matlab files, containing simulation models of the systems described in Section 5.1, Section 6.1, Section 7.1 and Section 8.1, as well as several scripts for plotting the simulation results. During the masters project I have specifically implemented and applied the velocity obstacle algorithm presented in Chapter 5, the guidance laws described in Chapter 4, and all presented control laws in Chapter 6-8, to these simulation models.

Unless otherwise stated, all figures and illustrations have been created by the author.

I would like to thank my supervisor, Prof. Kristin Y. Pettersen, for her helpful thoughts and constant motivation throughout this work. I am especially grateful for the great deal of help I received in the midst of an uncertain period, when writing my first paper submission. I always feel very welcome in her presence, and could not ask for a more thoughtful or competent supervisor. I would also like to give a special

thanks to my co-supervisor, Dr. Martin S. Wiig, for the skillful guidance he has given me, and the great amount of time he has used to read and correct my work during this period. He is always available to answer questions, and has provided me with valuable tools, thoughts and tips. I honestly do not think I would have gotten here without him. Last, I want to thank my boyfriend, Simen Heimly, for the limitless support, and for keeping me grounded at times when work is all-consuming.

Aurora Haraldsen
Trondheim, June 2020

Chapter 1

Introduction

Autonomous vehicles have in recent years become a field of large interest. During autonomous operation, the vehicle must be able to navigate in complex, dynamic environments without human intervention, using inputs from sensors and/or cameras. To achieve the mission goal, the vehicle must depend on guidance and navigation systems. Avoiding obstacles along the path is a crucial part of the navigation, as a collision can in the worst case lead to an inoperable vehicle, and will in most cases involve mission failure. In this thesis, we will analyse a collision avoidance algorithm, the velocity obstacle (VO) algorithm [5], in combination with guidance laws for target reaching and path following. The guidance laws will ensure that the vehicle achieves the desired motion along a path or towards a target, while the collision avoidance algorithm makes the vehicle avoid obstacles that are present along the way.

The velocity obstacle algorithm is based on describing obstacles in the velocity space by computing, for each obstacle, and at each moment in time, the set of velocities resulting in a future collision. Collision-free navigation is achieved by maintaining velocities outside the union of these sets. The concept can be used for motion planning purposes by searching over a tree of successive, feasible maneuvers. However, we will analyze the algorithm for so-called *reactive* collision avoidance. Reactive algorithms compute only one next action at every instant, and can consequently cope with

highly dynamic and unpredictable environments. Such algorithms require only local information about the environment and are less computationally demanding than classical planning algorithms, which are both time-consuming and require an extensive world model. For vehicles with limited computational power, reactive algorithms present a suitable navigation method. Reactive algorithms can be employed in hybrid architectures, in order to reduce the search space of planning algorithms, or as a back-up algorithm for increased redundancy.

The analysis presented in this thesis will specifically consider *underactuated* vehicles. This class is very rich and includes vehicles such as automobiles, airplanes, and marine vehicles. In particular, we will investigate the algorithm applied to an underactuated marine vehicle modeled in 2D, also known as a surface vehicle. Surface vehicles equipped with stern propellers and steering rudders are able to generate a forward thrust (in the surge direction), and a momentum in yaw, but are unable to control the side-ways force (in the sway direction), and is thus underactuated in sway. Although the vehicle cannot explicitly control the force in the side-ways direction, such forces are induced by the vehicle's turning motion through dynamic coupling. Large swaying motions can in the worst case make the vehicle collide side-ways into an obstacle, it is therefore necessary to consider the underactuated dynamics during the control design and analysis of such systems.

Before analyzing the full model of an underactuated surface vehicle, we will study the kinematic model of the system for reactive collision avoidance of an obstacle. The analysis will be based on the unicycle model, subject to nonholonomic constraints. This model represents the kinematics of a large class of systems, the results are therefore applicable to many different vehicle types. The original formulation of the algorithm is furthermore based on constant velocities, and suggests that the concept does not deal well with nonholonomic constraints. The objective is to remove such limitations, and derive conditions for which safety is ensured in the general case.

Collision avoidance of obstacles will be combined with guidance of the vehicle. Analysis of guidance laws is not the primary goal of the thesis, but collision avoidance in combination with guidance systems is however interesting to investigate. The guidance algorithms we will consider can be classified as reactive algorithms; they

require no planning, and the next action is based on the current information. The guidance laws are furthermore easily implemented on a wide variety of vehicles and require few measurements. Since both algorithms are reactive, the control system can transition between collision avoidance and nominal guidance based on specific conditions, without any planning involved.

1.1 Motivation

Autonomous and unmanned vehicles present a large potential for both scientific and commercial applications. They have been employed in several areas, such as subsea inspection and intervention, surveillance, transportation, and space operation. The vehicles are required to navigate in unknown environments while performing autonomous or semi-autonomous operations, and the capability of avoiding static and dynamic obstacles is important for achieving the mission goal. Motion planning algorithms can be applied for avoiding obstacles if information about the environment is known. However, the information is often limited, non-existing or erroneous. The vehicle may therefore experience unexpected changes and must be able to react quickly to avoid collision, making the time-consumption of motion planning algorithms unacceptable. For this purpose, reactive algorithms present a more suitable approach. Reactive algorithms base decisions on the current information about the environment, meaning there is no planning involved. While reactive algorithms can be applied as the sole navigation method, they also work well in combination with, or as a backup to motion planning algorithms. Reactive algorithms are furthermore interesting when used to generate motion primitives for planning algorithms. Safe and efficient algorithms can significantly reduce the search space of an optimization problem, while also guaranteeing vehicle safety even in cases when the search does not converge to a solution [20].

A common approach to reactive collision avoidance in dynamic environments is the velocity obstacle approach [5], where obstacles are represented as cones in the velocity space. The cones, called velocity obstacles, represent the set of constant velocities causing a collision between the vehicle and an obstacle at some future time.

Maintaining velocities outside of the set guarantees a collision-free trajectory of the vehicle. The concept has been largely applied for reactive collision avoidance of moving obstacles, and for decentralized, reactive navigation in multi-agent systems.

Autonomous operations of marine vehicles require that guidance, navigation and control is performed with high safety, as the consequences of a collision can be severe. The International Regulations for Preventing Collisions at Sea (COLREGS) were originally made for ships operated by a crew, but have been successfully applied for autonomous sea navigation using velocity obstacles [9, 15]. The VO algorithm has furthermore been employed for unmanned and autonomous marine navigation in 2D for surface vehicles [9, 3, 15, 29], and in 3D for underwater vehicles [30]. Although COLREGS provides higher safety of the vehicle in scenarios with oncoming vehicles, an important consideration in the study of collision avoidance algorithms is the ability to *guarantee* vehicle safety. To be able to provide such a guarantee, the vehicle dynamics should be considered both in the design and analysis of the collision avoidance algorithm. It is therefore both relevant and important to consider the underactuated dynamics of marine vehicles when applying the VO algorithm in collision avoidance scenarios, which in previous work have been neglected. Underactuation in the sideways (sway) direction is common for surface vehicles, even though some vehicles can generate side-ways forces using e.g. tunnel thrusters. At maneuvering speeds, thrusters providing side-ways stabilizing forces loose their effectiveness [12], thus making the vehicle underactuated at those speed, causing the swaying motion to become significant at times. Uncontrolled forces in the lateral direction can be fatal in collision avoidance scenarios if they are not accounted for. In order to guarantee vehicle safety, such consideration must thus be included.

Another important consideration in the analysis of collision avoidance algorithms is the liveliness property, i.e. the algorithm ensures that the vehicle will progress towards its goals. It is so forth interesting to investigate the VO algorithm in combination with separate vehicle goals. Autonomous marine vehicles are commonly dependent on guidance systems to move from one place to another. It is in such cases relevant to analyse scenarios where the vehicle both navigates among moving obstacles, and moves towards a goal position or along a path.

1.2 Literature review

Collision avoidance (CA) is a critical part of autonomous operations due to the severe consequences of a failure. Surveys of existing CA algorithms are given in Hoy et al. [7] and Huang et al. [8], where the latter specifically considers methods for ship collision avoidance. CA algorithms are often divided in two groups, reactive algorithms and motion planning algorithms. As the name suggests, the latter group generally depends on planning, and often rely on optimization methods. This can be computationally expensive and time-consuming for autonomous vehicles with complex dynamics, navigating in dense environments. Optimization problems can furthermore become computationally intractable for large and complex search spaces. Hence, autonomous vehicles must generally rely on backup solutions that are computationally simpler and yet provably safe, i.e. reactive algorithms.

A common approach for reactive collision avoidance in the robotics community is the artificial potential field [14], which assumes the robot is moving in an abstract, artificial force field. The potential field has two components; an attractive force which makes the robot move towards it, and a repulsive force making the robot move in the opposite direction. The forces are generated by the goals (attractive) and the obstacles (repulsive), which are stronger near the goal or obstacle, and weaker at a distance. The method provides a continuous search for a solution as the robot moves under the influence of the potential field to reach the goal. Unfortunately, the method has several drawbacks in producing local minima causing the robot to get trapped, causing oscillations due to narrow passages or obstacles in general, and not generating passages between closely spaced obstacles.

A reactive algorithm that has been applied to both nonholonomic and underacted vehicles is the constant avoidance angle (CAA) algorithm [25, 26, 27]. The algorithm makes the vehicle avoid collision with an obstacle by steering the vehicle so that its velocity vector keeps a constant avoidance angle from the obstacle. To decide when collision avoidance is needed, the algorithm computes a vision cone of the obstacle, describing unsafe moving directions. If the obstacle is moving, the vision cone is expanded to yield a compensated vision cone, accounting for the obstacle velocity.

The algorithm has been mathematically analyzed and proven to guarantee safety of both kinematic and dynamical systems.

A similar concept to the CAA algorithm is the velocity obstacle algorithm [5]. The method is based on the computation of all velocities resulting in a collision between the vehicle and an obstacle, forming a cone-shaped set of unsafe velocities. Among several moving obstacles, the cones are combined to one unified set. Any velocity outside of this set ensures collision-free navigation of the vehicle, making the method flexible in the choice of solution. The vehicle can additionally maintain its nominal behaviour in the presence of obstacles as long as unsafe velocities are avoided. Thus, the method avoids restricting the vehicle motion more than necessary. The main drawback is however that the method is based on linear approximations of the obstacle and vehicle velocities, in addition to the assumption that the vehicle can change speed and orientation simultaneously.

Although the velocity obstacle algorithm works well for systems that are able to move in any direction, the concept struggles with systems subject to constraints restricting the overall motion. Several variations of the algorithm have been suggested to overcome this issue. Wilkie et al. [28] generalizes the velocity obstacle concept to include kinematic constraints of a car-like robot which can only move, at any instant, with a velocity parallel to the rear wheels. Owen and Montano [20] addresses the problem of avoiding moving and static obstacles while a robot drives towards a goal, by mapping the robot motion and dynamical environment into the velocity space. The robot is constrained to move along straight or circular paths, which is a common constraint imposed to nonholonomic robot motions. However, the obstacles are assumed to move with constant velocities and along straight paths. Thus, the method suffers from the same drawback as the original velocity obstacle algorithm in that regard.

The nonlinear velocity obstacle presented in Shiller et al. [21] can be used to handle obstacles moving along arbitrary trajectories, as is done in Large et al. [18]. Although the approach deals with one of the shortcomings of the algorithm, it introduces the assumption that the obstacle's trajectory can be exactly known or closely estimated.

The acceleration-velocity obstacles (AVO) is presented by van den Berg et al. [24],

which accounts for constraints in the vehicle's acceleration, inspired by the concept of velocity obstacles. The method combines velocity obstacles with acceleration constraints by letting the robot choose a velocity outside the AVO set, and apply proportional acceleration control to arrive at this velocity. The concept is extended to reciprocal collision avoidance [23], by evaluating the obstacles as other vehicles reacting to the changes in the environment, rather than passively moving entities. The concept of reciprocal collision avoidance was proposed by van den Berg et al. [23], and later generalized by Bareiss and van den Berg [2], called reciprocal velocity obstacles. The concept is designed for decentralized, real-time, multi-agent navigation. The behaviour of the other agents are taken into account by implicitly assuming that other agents makes the similar collision avoidance reasoning. The navigation method then avoids oscillating behaviour of the agents, while provably ensures agent safety.

Lalish et al. [17] presents a velocity obstacle approach to the n-vehicle collision avoidance problem, applied to unicycle-type vehicles with constant speeds and actuation constraints. Similar to the reciprocal velocity obstacles [23], proof of agent safety is derived by assuming that all agents follow the same collision avoidance algorithm. Other applications of velocity obstacles in multi-agent navigation include [16, 22].

The algorithm has been employed to prevent collision for several vehicle types, such as aerial vehicles in Alonso-Mora et al. [1] and Mercado Velasco et al. [19], underwater vehicles in Zhang et al. [29], and surface vehicles in Kuwata et al. [15] and Huang et al. [9] where the algorithm is used for implementing the International Regulations for Preventing Collisions at Sea (COLREGS). The velocity obstacle method is extended to 3D in Jenie et al. [10] and Jenie et al. [11], specifically designed for collision avoidance of unmanned aerial vehicles (UAVs). The 3D velocity space is divided into a set of discrete planes where the 2D velocity obstacle approach is applied to each plane. However, the 3D extension does not address vehicle constraints and dynamics which is a considerable drawback.

1.3 Assumptions

The general assumptions for restricting the scope of the thesis are as follows:

Assumption 1.1. No disturbances are present.

Assumption 1.2. Required measurements are available and perfectly measured.

Assumption 1.3. Motion is restricted to the horizontal plane.

1.4 Contributions

The main contributions of the work presented in this thesis are as follows:

- A mathematical analysis of the velocity obstacle method with time-varying velocities. The original VO method is based on linear approximations of the velocities of a vehicle and an obstacle. By describing the algorithm geometrically, we show by an analysis of the nonautonomous system that the same concept applies to time-varying velocities;
- A complete analysis of the performance of a nonholonomic vehicle following the velocity obstacle algorithm, for collision avoidance of a moving obstacle with time-varying velocity. The vehicle is required to maintain a constant forward speed, and has restricted turning rate. Despite this, the analysis shows that the vehicle can safely avoid a moving obstacle, even in the case where the obstacle is able to turn and accelerate towards the vehicle. This is in contrast to the original formulation of velocity obstacles, which both assumes that the obstacle maintains a constant velocity, and does not deal well with vehicles with restricted forward speed and nonholonomic constraints;
- A mathematical analysis of the algorithm applied to an underactuated surface vehicle, where we explicitly account for the dynamics of the vehicle when investigating safety in the presence of a moving obstacle. The vehicle is underactuated in the side-ways (sway) direction, and is hence unable to generate side-ways stabilizing forces. We show, for a proper choice of the vehicle's yaw rate (turning motion), that the magnitude of the sway speed can be upper bounded, and that

under these conditions, collision avoidance is achieved for the vehicle with underactuated dynamics;

- Proofs of collision avoidance of an obstacle are combined with proofs of target reaching and path following, by the pure pursuit and LOS guidance laws.
- Simulation studies of the algorithm applied to the specific systems validating the theoretical results.

1.5 Outline

The thesis is organized as follows:

Chapter 2 provides some mathematical preliminaries;

Chapter 3 presents the mathematical modeling of an underactuated marine vehicle, moving in 3 degrees of freedom. The model is derived using maneuvering theory;

Chapter 4 presents guidance laws for path following and target reaching. The relationship between the heading, course and crab angles is discussed;

Chapter 5 presents the velocity obstacle algorithm for collision avoidance in 2D. A preliminary analysis of the fundamental concept behind the algorithm is given, proving that a vehicle is ensured to maintain at least a minimum distance from an obstacle at all times, by continually avoiding the velocities inside the velocity obstacle set;

Chapter 6 applies the velocity obstacle algorithm to a unicycle-type vehicle subject to nonholonomic constraints. The vehicle is restricted to maintain a constant forward speed, and has limited turning rate. A minimum threshold distance is formulated deciding when the vehicle's avoidance maneuver must be initiated, and a lower bound on the vehicle's required turning rate is derived, ensuring that the vehicle can turn faster away from an obstacle than the obstacle is capable of turning and accelerating

towards it. These conditions are combined with proofs of target reaching and path following, ensuring that all goals of the vehicle are achieved. Simulations are included to verify the theoretical results;

Chapter 7 includes the underactuated sway dynamics of a surface vehicle in the unicycle-model. The vehicle is restricted to maintain a constant forward speed and is required to reach a target position in the world frame, maintain a limited sway speed, and avoid a moving obstacle in its path. The control system compensates for the vehicle's sway speed when controlling its heading as to steer the vehicle towards the right course, and the VO algorithm is set to generate course references rather than heading references. Conditions are derived under which the sway speed is bounded, combined with collision avoidance of a moving obstacle and target reaching by the pure pursuit guidance law. Simulations are provided to support the results of the analysis;

Chapter 8 applies the VO algorithm to the full model of an underactuated surface vehicle. The vehicle is, as before, required to maintain a constant forward speed. In addition, the vehicle is required to maintain a limited sway speed. Feedback linearizing controllers are employed to stabilize the surge and yaw dynamics exponentially. To deal with discontinuities in the yaw rate input, a yaw rate smoothing function is proposed. Conditions are given ensuring that the vehicle is guaranteed to avoid collision, in combination with both target reaching and path following, while maintaining a constant surge speed and limited sway speed. Simulations are presented to verify the theoretical results;

Chapter 9 gives the concluding remarks, and discusses some future research topics.

Chapter 2

Mathematical Preliminaries

This chapter presents some mathematical preliminaries to the following chapters. We will specify some frequently used notation, define the rotation matrices and convention for the principal rotations, and state some stability definitions and theorems.

2.1 Notation

We will here give an overview of the notation used in this thesis.

The space $\mathbb{R}^n$ is the Euclidean space of dimension n. The Euclidean norm of a vector $\boldsymbol{u} \in \mathbb{R}^n$ is denoted $\|\boldsymbol{u}\|$. A vector $\boldsymbol{u}$ in a reference frame a is denoted $\boldsymbol{u}^a$. The direction of a vector $\boldsymbol{u} = [u_x,\, u_y]^\top \in \mathbb{R}^2$ is denoted $\angle \boldsymbol{u}$, and is defined as

$$\angle \boldsymbol{u} \triangleq \text{atan2}(u_y,\, u_x). \tag{2.1}$$

The position of a reference frame b, with respect to a reference frame a, is denoted $\boldsymbol{p}_{ab}^a$. The velocity vector of frame b, with respect to frame a, is denoted $\boldsymbol{v}_{ab}^a \triangleq \dot{\boldsymbol{p}}_{ab}^a$. The rotation matrix used to rotate a vector from a reference frame b, to a reference frame a, is denoted $\boldsymbol{R}_b^a$, so that $\boldsymbol{v}^a = \boldsymbol{R}_b^a \boldsymbol{v}^b$.

Three different reference frames will commonly be seen in the thesis. The inertial

reference frame, approximated by the NED frame, denoted n, the Body attached reference frame of the vehicle, attached to the pivot point of the vehicle, denoted b, and the Body attached reference frame of an obstacle, attached to the center of the obstacle, denoted o.

Finally, the trigonometric functions $\sin(\cdot)$, $\cos(\cdot)$, and $\tan(\cdot)$ are, for brevity, denoted $\mathrm{s}(\cdot)$, $\mathrm{c}(\cdot)$ and $\mathrm{t}(\cdot)$, respectively.

2.2 Principal rotations

Using the zyx-convention, the Euler angles roll ϕ, pitch θ and yaw ψ, are used to decompose a rotation into three principal axis of rotation, given by

$$\boldsymbol{R}_{x,\phi} \triangleq \begin{bmatrix} 1 & 0 & 0 \\ 0 & \mathrm{c}(\phi) & -\mathrm{s}(\phi) \\ 0 & \mathrm{s}(\phi) & \mathrm{c}(\phi) \end{bmatrix}, \tag{2.2}$$

$$\boldsymbol{R}_{y,\theta} \triangleq \begin{bmatrix} \mathrm{c}(\theta) & 0 & \mathrm{s}(\theta) \\ 0 & 1 & 0 \\ -\mathrm{s}(\theta) & 0 & \mathrm{c}(\theta) \end{bmatrix}, \tag{2.3}$$

$$\boldsymbol{R}_{z,\psi} \triangleq \begin{bmatrix} \mathrm{c}(\psi) & -\mathrm{s}(\psi) & 0 \\ \mathrm{s}(\psi) & \mathrm{c}(\psi) & 0 \\ 0 & 0 & 1 \end{bmatrix}. \tag{2.4}$$

2.3 Stability definitions and theorems

We will here state some necessary definitions and theorems regarding the stability properties of nonautonomous systems. All of the presented material is found in Khalil [13].

Consider the nonautonomous system

$$\dot{x} = f(t, x), \tag{2.5}$$

where $f : [0, \infty) \times \mathcal{D} \to \mathbb{R}^n$ is piecewise continuous in t and locally Lipschitz[1] in x on $[0, \infty) \times \mathcal{D}$, and $\mathcal{D} \subset \mathbb{R}^n$ is a domain that contains the origin $x = 0$. Let the origin be an equilibrium of (2.5) for $t = 0$, i.e.:

$$f(t, 0) = 0, \ \forall t \geq 0. \tag{2.6}$$

Definition 2.1. Khalil [13, Definition 4.4]. *The equilibrium point $x = 0$ of (2.5) is*

- *stable if, for each $\epsilon > 0$, there is $\delta = \delta(t, \epsilon) > 0$ such that*

$$\|x(t_0)\| < \delta \implies \|x(t)\| < \epsilon, \ \forall t \geq t_0 \geq 0. \tag{2.7}$$

- *uniformly stable if, for each $\epsilon > 0$, there is $\delta = \delta(\epsilon)$ independent of t_0 such that (2.7) is satisfied.*

- *unstable if it is not stable.*

- *asymptotically stable (AS) if it is stable and there is a positive constant $c = c(t_0)$ such that $x(t) \to 0$ as $t \to \infty$, for all $\|x(t_0)\| < c$.*

- *uniformly asymptotically stable (UAS) if it is uniformly stable and there is a positive constant c, independent of t_0, such that for all $\|x(t_0)\| < c$, $x(t) \to 0$ as $t \to \infty$, uniformly in t_0; that is, for each $\eta > 0$, there is $T = T(\eta) > 0$ such that*

$$\|x(t)\| < \eta, \ \forall t \geq t_0 + T(\eta), \ \forall \|x(t_0)\| < c. \tag{2.8}$$

- *globally uniformly asymptotically stable (UGAS) if it is uniformly stable, $\delta(\epsilon)$ can be chosen to satisfy $\lim_{\epsilon \to \infty} \delta(\epsilon) = \infty$, and, for each pair of positive numbers η and*

[1] See Khalil [13, Lemma 3.2]

c, there is $T = T(\eta, c) > 0$ such that

$$\|x(t)\| < \eta, \ \forall t \geq t_0 + T(\eta, c), \forall \|x(t_0)\| < c. \tag{2.9}$$

2.3.1 Lyapunov stability

Lyapunov function candidates can be used to analyze the stability properties of a system. The following theorems are included for orientation.

Theorem 2.1. Khalil [13, Theorem 4.8]. *Let $x = 0$ be an equilibrium point for (2.5) and $\mathcal{D} \subset \mathbb{R}^n$ be a domain containing $x = 0$. Let $V : [0, \infty) \times \mathcal{D} \to \mathbb{R}$ be a continuously differentiable function such that*

$$W_1(x) \leq V(t, x) \leq W_2(x), \tag{2.10}$$

$$\frac{\partial V}{\partial t} + \frac{\partial V}{\partial x} f(t, x) \leq 0, \tag{2.11}$$

$\forall t \geq 0$ and $x \in \mathcal{D}$, where $W_1(x)$ and $W_2(x)$ are continuous positive definite functions on $\mathcal{D}$. Then, $x = 0$ is uniformly stable.

Theorem 2.2. Khalil [13, Theorem 4.9]. *Suppose the assumptions of Theorem 2.1 are satisfied with the inequality (2.11) strengthened to*

$$\frac{\partial V}{\partial t} + \frac{\partial V}{\partial x} f(t, x) \leq -W_3(x), \tag{2.12}$$

$\forall t \geq 0$ and $x \in \mathcal{D}$, where $W_3(x)$ is a continuous positive definite function on $\mathcal{D}$. Then, $x = 0$ is uniformly asymptotically stable (UAS). Moreover, if r and c are chosen such that $\mathcal{B}_r = \{\|x\| \leq r\} \subset \mathcal{D}$ and $c < \min_{\|x\|=r} W_1(x)$, then every trajectory starting in $\{x \in \mathcal{B}_r \,|\, W_2(x) \leq c\}$ satisfies

$$\|x(t)\| \leq \beta(\|x(t_0)\|, t - t_0), \ \forall t \geq t_0 \geq 0, \tag{2.13}$$

for some class of $\mathcal{KL}$[2] function β. Finally, if $\mathcal{D} = \mathbb{R}^n$ and $W_1(x)$ is radially unbounded, then $x = 0$ is globally uniformly asymptotically stable (UGAS).

[2] See Khalil [13, Definition 4.3]

Chapter 3

Modeling of Underactuated Surface Vehicles

In this chapter, we present the modeling of an underactuated surface vehicle. The surface vehicle is modeled using maneuvering theory, in 3 degrees of freedom (DOF). The modeling is based on Fossen [6], details regarding the presented theory can hence be found in [6].

3.1 Kinematics

To describe a marine craft moving in 6 DOF, six independent coordinates are needed to determine the position and orientation of the craft. The first three coordinates and their time-derivatives describe the position and translational motion of the vehicle along the x, y and z axes. The last three coordinates and time-derivatives describe the orientation and rotational motion about these axes. The first three motion components are called *surge*, *sway* and *heave*, and the last three are called *roll*, *pitch* and *yaw*.

3.1.1 Reference frames

The vehicle kinematics must be described with respect to a reference frame. The inertial frame, often referred to as the world frame, is an important frame to identify. This frame is where Newton's equations of motion apply, and is a frame whose points do not accelerate. Moreover, the inertial frame acts as a reference for all other reference frames, and must be defined before any other frames can be assigned. In local navigation, the inertial frame can be approximated by the North-East-Down (NED) frame, and these terms will be used somewhat interchangeably. In the NED frame, denoted n, the x^n axis points towards the true North, the y^n axis points towards East, and the z^n axis points downwards, normal to the Earth's surface.

The Body frame, denoted b, is a non-inertial coordinate frame, attached to the body of the vehicle. The x^b axis points along the surge motion, the y^b axis along the sway motion, and the z^b axis along the heave motion. The body-attached reference frame is commonly used to describe the linear and angular velocity of the craft, while the position and orientation of the craft is usually described in the NED frame.

3.1.2 6 DOF Kinematics

The generalized positions and velocities of a marine vehicle are given by

$$\boldsymbol{\eta} = [x^n\,, y^n\,, z^n\,, \phi\,, \theta\,, \psi\,]^\top\,, \tag{3.1}$$

$$\dot{\boldsymbol{\eta}} = \left[\dot{x}^n\,, \dot{y}^n\,, \dot{z}^n\,, \dot{\phi}\,, \dot{\theta}\,, \dot{\psi}\right]^\top\,, \tag{3.2}$$

where $\boldsymbol{\Theta} = [\phi\,, \theta\,, \psi\,]^\top$ are the Euler angles, representing roll, pitch and yaw. The velocities of the vehicle can be described in the Body frame as

$$\boldsymbol{\nu} = [u\,, v\,, w\,, p\,, q\,, r\,]^\top\,, \tag{3.3}$$

where $\boldsymbol{\nu}_1 = [u\,, v\,, w]^\top$ represents the surge, sway and heave speeds, and $\boldsymbol{\nu}_2 = [p\,, q\,, r\,]^\top$ represents the roll, pitch and yaw rates.

The following notation will be adopted for vectors in the coordinate systems b and

n:

$$\boldsymbol{p}_{nb}^{n} = \begin{bmatrix} x_b^n \\ y_b^n \\ z_b^n \end{bmatrix} \in \mathbb{R}^3 \text{ Position in } n, \qquad \boldsymbol{v}_{nb}^{n} = \begin{bmatrix} \dot{x}_b^n \\ \dot{y}_b^n \\ \dot{z}_b^n \end{bmatrix} \in \mathbb{R}^3 \text{ Linear velocity in } n,$$

$$\boldsymbol{v}_{nb}^{b} = \begin{bmatrix} u_b \\ v_b \\ w_b \end{bmatrix} \in \mathbb{R}^3 \text{ Linear velocity in } b, \quad \boldsymbol{\omega}_{nb}^{b} = \begin{bmatrix} p_b \\ q_b \\ r_b \end{bmatrix} \in \mathbb{R}^3 \text{ Angular velocity in } b,$$

$$\boldsymbol{\Theta}_{nb} = \begin{bmatrix} \phi_b \\ \theta_b \\ \psi_b \end{bmatrix} \in \mathbb{R}^3 \text{ Euler angles from } n \text{ to } b, \; \dot{\boldsymbol{\Theta}}_{nb} = \begin{bmatrix} \dot{\phi}_b \\ \dot{\theta}_b \\ \dot{\psi}_b \end{bmatrix} \in \mathbb{R}^3 \text{ Euler angle rates},$$

$$\boldsymbol{\eta} = \begin{bmatrix} \boldsymbol{p}_{nb}^{n} \\ \boldsymbol{\Theta}_{nb} \end{bmatrix} \in \mathbb{R}^6 \text{ Generalized coordinates}, \; \boldsymbol{\nu} = \begin{bmatrix} \boldsymbol{v}_{nb}^{b} \\ \boldsymbol{\omega}_{nb}^{b} \end{bmatrix} \in \mathbb{R}^6 \text{ Body velocities.}$$

The linear velocity in n, $\boldsymbol{v}_{nb}^{n}$, can be obtained from the body-fixed linear velocity, $\boldsymbol{v}_{nb}^{b}$, by the Euler angle rotation matrix, defined as

$$\boldsymbol{R}_b^n \coloneqq \boldsymbol{R}_{z,\psi_b} \boldsymbol{R}_{y,\theta_b} \boldsymbol{R}_{x,\phi_b}, \tag{3.4}$$

where the matrices $\boldsymbol{R}_{z,\psi}$, $\boldsymbol{R}_{y,\theta}$ and $\boldsymbol{R}_{x,\phi}$ are defined in Chapter 2. Moreover,

$$\boldsymbol{v}_{nb}^{n} = \boldsymbol{R}_b^n \boldsymbol{v}_{nb}^{b}. \tag{3.5}$$

The body-fixed angular velocity vector, $\boldsymbol{\omega}_{nb}^{b}$, is related to the Euler rate vector,

$\dot{\Theta}_{nb}$, through a transformation matrix $\boldsymbol{T}(\Theta_{nb})$ according to

$$\dot{\Theta}_{nb} = \boldsymbol{T}(\Theta_{nb})\boldsymbol{\omega}_{nb}^{b}. \tag{3.6}$$

The transformation matrix $\boldsymbol{T}(\Theta_{nb})$ is not unique, and can be found in several ways, for instance:

$$\boldsymbol{\omega}_{nb}^{n} = \begin{bmatrix} \dot{\phi}_b \\ 0 \\ 0 \end{bmatrix} + \boldsymbol{R}_{x,\phi_b}^{\top} \begin{bmatrix} 0 \\ \dot{\theta}_b \\ 0 \end{bmatrix} + \boldsymbol{R}_{x,\phi_b}^{\top} \boldsymbol{R}_{y,\theta_b}^{\top} \begin{bmatrix} 0 \\ 0 \\ \dot{\psi}_b \end{bmatrix}. \tag{3.7}$$

By comparing (3.6) and (3.7) we find this particular transformation matrix as

$$\boldsymbol{T}^{-1}(\Theta_{nb}) = \begin{bmatrix} 1 & 0 & -\mathrm{s}\theta_b \\ 0 & \mathrm{c}\phi_b & \mathrm{c}\theta_b\mathrm{s}\phi_b \\ 0 & -\mathrm{s}\phi_b & \mathrm{c}\theta_b\mathrm{s}\phi_b \end{bmatrix} \implies \boldsymbol{T}(\Theta_{nb}) = \begin{bmatrix} 1 & \mathrm{s}\phi_b\mathrm{t}\theta_b & \mathrm{c}\phi_b\mathrm{t}\theta_b \\ 0 & \mathrm{c}\phi_b & -\mathrm{s}\phi_b \\ 0 & \mathrm{s}\phi_b/\mathrm{c}\theta_b & \mathrm{c}\phi_b/\mathrm{s}\theta_b \end{bmatrix} \tag{3.8}$$

It can be noticed that the transformation matrix is non-singular for pitch angles equal to $\theta_b = \pm\frac{\pi}{2}$. Moreover, $\boldsymbol{T}^{-1}(\Theta_{nb}) \neq \boldsymbol{T}^{\top}(\Theta_{nb})$, meaning $\boldsymbol{T}(\Theta_{nb}) \notin SO(3)$. To circumvent this issue, an alternative representation of the vehicle's orientation can be used, the quaternion representation. However, this is not a problem for surface vessels restricted to move in the horizontal plane.

The 6 DOF kinematic equations can be summarized as

$$\begin{aligned} \dot{\eta} &= \boldsymbol{J}_{\boldsymbol{\Theta}}(\boldsymbol{\eta})\boldsymbol{\nu} \\ &\Updownarrow \\ \begin{bmatrix} \boldsymbol{v}_{nb}^{n} \\ \dot{\boldsymbol{\Theta}}_{nb} \end{bmatrix} &= \begin{bmatrix} \boldsymbol{R}(\boldsymbol{\Theta}_{nb}) & \boldsymbol{0}_{3\times3} \\ \boldsymbol{0}_{3\times3} & \boldsymbol{T}(\boldsymbol{\Theta}_{nb}) \end{bmatrix} \begin{bmatrix} \boldsymbol{v}_{nb}^{b} \\ \boldsymbol{\omega}_{nb}^{b} \end{bmatrix}. \end{aligned} \tag{3.9}$$

3.1.3 3 DOF Kinematics

A common simplification of (3.9) is the 3 DOF representation, obtained by the assumption that the roll and pitch angles are small during normal operation. Most

surface vehicles are passively stabilized in roll at maneuvering speeds, and the unmodeled dynamics in heave and pitch can be considered as wave-induced disturbances. Assuming $\phi_b \approx 0$, $\theta_b \approx 0$, the Euler angle rotation matrix from Equation (3.4) is reduced to $\boldsymbol{R}_b^n \approx \boldsymbol{R}_{z,\psi_b}$, and the transformation matrix from Equation (3.8) becomes $\boldsymbol{T}(\boldsymbol{\Theta}_{nb}) \approx \boldsymbol{I}_3$.

The 3 DOF kinematic equations can be written in the simple form:

$$\begin{bmatrix} \boldsymbol{v}_{nb}^n \\ \dot{\psi}_b \end{bmatrix} = \begin{bmatrix} \cos(\psi_b) & -\sin(\psi_b) & 0 \\ \sin(\psi_b) & \cos(\psi_b) & 0 \\ 0 & 0 & 1 \end{bmatrix} \begin{bmatrix} \boldsymbol{v}_{nb}^b \\ r_b \end{bmatrix}, \tag{3.10}$$

where $\boldsymbol{v}_{nb}^n = [\dot{x}_b^n \, , \dot{y}_b^n]^\top$, and $\boldsymbol{v}_{nb}^b = [u_b \, , v_b]^\top$. Note that when considering the 3 DOF model, the notation presented in the previous section may still be employed, however, the vectors will only contain the modeled dynamics, and thus have a different dimension.

3.2 Dynamics

The dynamics of the vehicle can be described using maneuvering theory [6]. In maneuvering theory, the frequency-dependent added mass and potential damping are approximated by constant values, under the assumption that the vehicle is moving with constant, maneuvering speed. The hydrodynamic coefficients can be assumed frequency-independent at those speeds, enabling fluid-memory effects to be neglected. The resulting model is a nonlinear mass-damper-spring system, with constant coefficients.

The maneuvering equations of motion can be written in the general form:

$$\boldsymbol{M}\dot{\boldsymbol{\nu}} + \boldsymbol{C}(\boldsymbol{\nu})\boldsymbol{\nu} + \boldsymbol{D}(\boldsymbol{\nu})\boldsymbol{\nu} + \boldsymbol{g}(\boldsymbol{\eta}) = \boldsymbol{B}\boldsymbol{u}, \tag{3.11}$$

where $\boldsymbol{M} = \boldsymbol{M}^\top$ is the inertia matrix comprehensive the added mass, $\boldsymbol{C}(\boldsymbol{\nu})$ is the Coriolis-centripetal matrix including added mass, $\boldsymbol{D}(\boldsymbol{\nu})$ contains the hydrodynamic

damping terms, and $\boldsymbol{g}(\boldsymbol{\eta})$ contains the gravitational/buoyancy forces and moments. The hydrodynamic damping terms become nonlinear when quadratic damping is included. For convenience, we only model the linear damping, rendering the damping matrix constant, $\boldsymbol{D}(\boldsymbol{\nu}) \coloneqq \boldsymbol{D}$.

The control input from the vehicle's actuators are contained in the vector $\boldsymbol{u}$. $\boldsymbol{B}$ is the input matrix, mapping the input signals to control forces and moments. The model (3.11) will be explained in greater detail in the following section.

3.2.1 3 DOF Dynamics

In 3 DOF, the state vectors become $\boldsymbol{\nu} = [u_b\,, v_b\,, r_b\,]^\top$ and $\boldsymbol{\eta} = [x_b^n\,, y_b^n\,, \psi_b\,]^\top$. The dimension of the matrices $\boldsymbol{M}$, $\boldsymbol{C}$, and $\boldsymbol{D}$ is hence $\mathbb{R}^{3\times 3}$. Since the vehicle is moving in the horizontal plane, gravitational and buoyancy effects can be neglected, i.e. $\boldsymbol{g}(\boldsymbol{\eta}) = 0$. We assume that the vehicle has a homogeneous mass distribution, is port-starboard symmetric, and that the origin of the body, o_b, lies along the center-line of the craft. For this particular geometry, the structure of the inertia matrix (included added mass), $\boldsymbol{M}$, and the hydrodynamic damping matrix, $\boldsymbol{D}$, becomes

$$\boldsymbol{M} = \begin{bmatrix} m_{11} & 0 & 0 \\ 0 & m_{22} & m_{23} \\ 0 & m_{32} & m_{33} \end{bmatrix}, \quad \boldsymbol{D} = \begin{bmatrix} d_{11} & 0 & 0 \\ 0 & d_{22} & d_{23} \\ 0 & d_{32} & d_{33} \end{bmatrix}, \tag{3.12}$$

where $m_{32} \coloneqq m_{23}$. The Coriolis-centripetal matrix (included added mass), $\boldsymbol{C}$, can be computed directly from $\boldsymbol{M}$, as presented in Fossen [6]:

$$\boldsymbol{C} = \begin{bmatrix} \boldsymbol{0}_{3\times 3} & -S(\boldsymbol{M}_{11}\boldsymbol{\nu}_1 + \boldsymbol{M}_{12}\boldsymbol{\nu}_2) \\ -S(\boldsymbol{M}_{11}\boldsymbol{\nu}_1 + \boldsymbol{M}_{12}\boldsymbol{\nu}_2) & -S(\boldsymbol{M}_{21}\boldsymbol{\nu}_1 + \boldsymbol{M}_{22}\boldsymbol{\nu}_2) \end{bmatrix}, \tag{3.13}$$

where

$$\boldsymbol{M}_{\text{6DOF}} \coloneqq \begin{bmatrix} \boldsymbol{M}_{11} & \boldsymbol{M}_{12} \\ \boldsymbol{M}_{21} & \boldsymbol{M}_{22} \end{bmatrix},$$

$\boldsymbol{\nu}_1 = [u,\, v,\, w]^\top$, and $\boldsymbol{\nu}_2 = [p,\, q,\, r]^\top$. For the 3 DOF state space, we find $\boldsymbol{C}$ as

$$\boldsymbol{C} = \begin{bmatrix} 0 & 0 & -(m_{22}v_b + m_{23}r_b) \\ 0 & 0 & m_{11}u_b \\ m_{22}v_b + m_{23}r_b & -m_{11}u_b & 0 \end{bmatrix}. \tag{3.14}$$

It can be noticed that $\boldsymbol{C}$ is skew-symmetric: $\boldsymbol{C} = -\boldsymbol{C}^\top$.

The vehicle is equipped with a thruster generating force in the surge direction, and a rudder to generate yaw momentum. The input vector takes the form $\boldsymbol{u} = [\delta_u\,, \delta_r\,]^\top$ where δ_u is the surge input, and δ_r is the rudder input. We assume that the surge thrust only affects the surge dynamics. The rudder angle can however both affect the yaw and sway dynamics. The structure of the input matrix, $\boldsymbol{B}$, becomes

$$\boldsymbol{B} = \begin{bmatrix} b_{11} & 0 \\ 0 & b_{22} \\ 0 & b_{32} \end{bmatrix}. \tag{3.15}$$

To remove the effect of the rudder on the sway dynamics, we can perform a coordinate transform. The procedure is described in Fossen [6], and is quite common in order to take advantage of the crafts geometry. The origin of the body, o_b, is translated by the distance

$$\xi \triangleq -\frac{b_{22}m_{33} - b_{32}m_{23}}{m_{22}m_{33} - m_{23}^2} \tag{3.16}$$

along the center-line of the craft to the point o_c.

Remark 3.1. The coordinate transform corresponds to placing the origin of the body-attached reference frame of the vehicle to its pivot point, i.e. the point in which the vehicle rotates about.

The position of o_b with respect to o_c is given by $\boldsymbol{r}_b^c \triangleq [-\xi\,, 0\,, 0\,]$. The transformation

matrix is then straight-forward to compute:

$$\boldsymbol{H} = \begin{bmatrix} 1 & 0 & 0 \\ 0 & 1 & -\xi \\ 0 & 0 & 1 \end{bmatrix}. \tag{3.17}$$

The equations of motion about o_c is given by

$$\boldsymbol{H}^\top \boldsymbol{M}\boldsymbol{H}\dot{\boldsymbol{\nu}} + \boldsymbol{H}^\top \boldsymbol{C}(\boldsymbol{\nu})\boldsymbol{H}\boldsymbol{\nu} + \boldsymbol{H}^\top \boldsymbol{D}\boldsymbol{H}\boldsymbol{\nu} = \boldsymbol{H}^\top \boldsymbol{B}\boldsymbol{u}. \tag{3.18}$$

Remark 3.2. The coordinate transform does not change the structure, nor the properties of the matrices $\boldsymbol{M}$, $\boldsymbol{C}$, $\boldsymbol{D}$ and $\boldsymbol{B}$.

The effects of the rudder input on the sway dynamics are now removed:

$$(\boldsymbol{H}^\top \boldsymbol{M}\boldsymbol{H})^{-1}\boldsymbol{H}^\top \boldsymbol{B}\boldsymbol{u} = [g_u,\, 0,\, g_r]^\top, \tag{3.19}$$

where g_u and g_r are the control forces in surge and yaw respectively, defined as

$$g_u \triangleq \delta_u \frac{b_{11}}{m_{11}}, \tag{3.20}$$

$$g_r \triangleq \delta_r \frac{b_{32}m_{22} - b_{22}m_{23}}{m_{22}m_{33} - m_{23}^2}. \tag{3.21}$$

Since the coordinate transform preserves the original structure of the inertia, Coriolis, and damping matrix, we will adopt the notation of (3.12) and (3.14) for the transformed matrices to this end. The notation (3.19) will be employed for the control forces.

Solving the 3 DOF equations of motion with respect to $\dot{\boldsymbol{v}}_{nb}^b = [\dot{u}_b\,, \dot{v}_b,\ \dot{r}_b\,]^\top$ yields

$$\begin{aligned} \dot{u}_b &= f_u(v_b, r_b) + g_u, \\ \dot{v}_b &= f_v(u_b, v_b, r_b), \\ \dot{r}_b &= f_r(u_b, v_b, r_b) + g_r, \end{aligned} \tag{3.22}$$

where

$$f_u \triangleq r_b \frac{r_b m_{23} + v_b m_{22}}{m_{11}} - v_b \frac{d_{11}}{m_{11}}, \tag{3.23}$$

$$\begin{aligned} f_v \triangleq\ & v_b \frac{d_{22} m_{23} - d_{32} m_{22} - u_b m_{22} (m_{22} + m_{11})}{m_{22} m_{33} - m_{23}^2} \\ & + r_b \frac{d_{32} m_{23} - d_{33} m_{22} + u_b m_{23} (m_{11} - m_{22})}{m_{22} m_{33} - m_{23}^2}, \end{aligned} \tag{3.24}$$

$$\begin{aligned} f_r \triangleq\ & v_b \frac{d_{32} m_{23} - d_{22} m_{33} + u_b m_{23} (m_{11} + m_{22})}{m_{22} m_{33} - m_{23}^2} \\ & + r_b \frac{d_{33} m_{23} - d_{23} m_{33} + u_b \left(m_{23}^2 - m_{11} m_{33}\right)}{m_{22} m_{33} - m_{23}^2}. \end{aligned} \tag{3.25}$$

3.3 Assumptions overview

We present an overview of the model assumption in this section.

Assumption 3.1. The vehicle model is expressed in the Body frame, in reference to the NED frame, attached to the center line of the craft at the pivot point.

Assumption 3.2. The vehicle has a homogeneous mass distribution and is port-starboard symmetric.

Assumption 3.3. Pitch and heave motions are treated as wave induced disturbances, and are hence neglected.

Assumption 3.4. The vehicle is passively stabilized in roll; roll motions can be neglected.

Assumption 3.5. The vehicle is moving in the horizontal plane; gravitational and buoyancy forces can be neglected.

Assumption 3.6. Nonlinear damping can be neglected, only linear damping is modeled.

Assumption 3.7. The control input in surge only affects the surge dynamics.

Chapter 4

Guidance Laws

In this chapter, we will present the guidance laws used for generating references for the vehicle to reach a target position, and follow a straight line path, in the NED frame. Guidance systems are in general used to achieve the desired motion of the vehicle towards a static or moving point, or along a path. We will describe two separate methods for these purposes, which later in the thesis will be applied to the vehicle, in combination with collision avoidance of an obstacle. The theory presented is based on Fossen [6].

4.1 Definitions of heading, course and crab angles

The relationship between the heading, course and crab angles is important to address before presenting the guidance laws.

Definition 4.1 (*Heading angle ψ*). *The angle ψ from the x^n axis to the x^b axis, where n denotes the NED frame and b denotes the Body frame, by a positive rotation about the z^n axis by the right-hand screw convention.*

The heading angle can be measured using a magnetic compass, and is defined even for zero speeds.

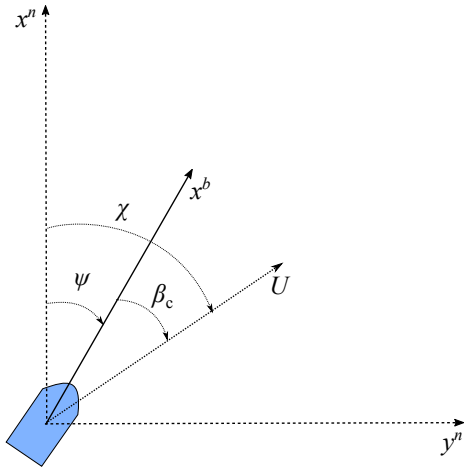

Figure 4.1: The heading, course and crab angles.

Definition 4.2 (*Course* χ). *The angle χ from the x^n axis to the velocity vector of the vehicle, where n denotes the NED frame, by a positive rotation about the z^n axis by the right-hand screw convention.*

The course angle describes the direction in which the vehicle is moving in the NED frame. The course is thus only defined for positive speeds.

The motion of the vehicle moving in the horizontal plane can be described kinematically by (3.10), as

$$\dot{x}^n = u\cos(\psi) - v\sin(\psi), \tag{4.1}$$
$$\dot{y}^n = u\sin(\psi) + v\cos(\psi). \tag{4.2}$$

These equations can be expressed in the form

$$\dot{x}^n = U\cos(\psi + \beta_c) := U\cos(\chi), \tag{4.3}$$
$$\dot{y}^n = U\sin(\psi + \beta_c) := U\sin(\chi), \tag{4.4}$$

where $U = \sqrt{u^2 + v^2}$ is the speed of the vehicle. The course χ can be written as

$$\chi = \psi + \beta_c, \tag{4.5}$$

where β_c is the crab angle, given by

$$\beta_c = \tan^{-1}\left(\frac{v}{u}\right) = \sin^{-1}\left(\frac{v}{U}\right). \tag{4.6}$$

Definition 4.3 (*Crab angle* β_c). *The angle β_c from the x^b axis to the velocity vector of the vehicle, where b denotes the Body frame, by a positive rotation about the z^b axis by the right-hand screw convention.*

The relationship between the heading, course and crab angles is shown in Figure 4.1. When the vehicle is guided towards a goal, it will be given *course* commands. If the vehicle controls its heading angle, it must account for the crab angle, β_c, induced by the side-ways (sway) speed, in order to maintain the desired course.

4.2 Line of sight guidance

Line of sight (LOS) guidance is a three-point guidance scheme, which involves the use of a reference point in order to construct a straight line-path going to the position of the target. The LOS guidance vector points from the interceptor (i.e. the vehicle), towards a point on this line, denoted $\boldsymbol{p}^n_{\text{los}} = [x^n_{\text{los}}, y^n_{\text{los}}]^\top$. Two main methods exist for computing the desired course of the vehicle using LOS guidance. We will consider the lookahead-based steering, which employs a lookahead distance to direct the vehicle towards the path. This method has several advantages over the similar, enclosure-based steering.

In lookahead-based steering, the point $\boldsymbol{p}^n_{\text{los}}$ is situated a constant lookahead distance $\Delta > 0$ from the direct projection of the vehicle position $\boldsymbol{p}^n_{nb}$ on to the path, illustrated in Figure 4.2. The desired course is computed through two components, as

$$\chi^n_{\text{los}}(y_{\text{e}}) \triangleq \chi_{\text{p}} + \chi_{\text{r}}(y_{\text{e}}), \tag{4.7}$$

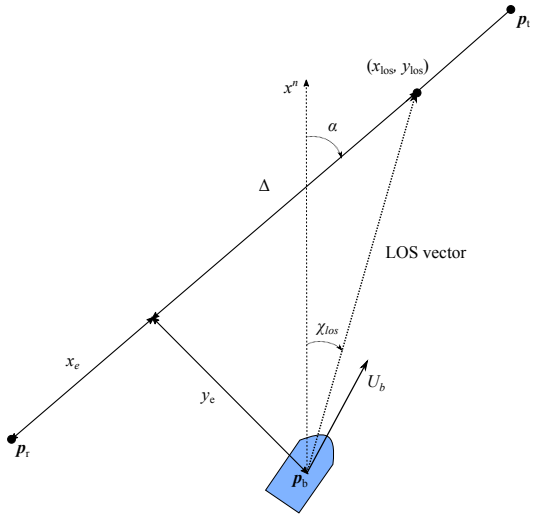

Figure 4.2: Geometry of the line of sight (LOS) guidance.

where

$$\chi_{\mathrm{p}} = \alpha \tag{4.8}$$

is the path-tangential angle (see Figure 4.2), and

$$\chi_{\mathrm{r}}(y_{\mathrm{e}}) = \arctan\left(\frac{-y_{\mathrm{e}}}{\Delta}\right) \tag{4.9}$$

is the velocity-path relative angle, ensuring that the vehicle is steered towards the point $\boldsymbol{p}^n_{\mathrm{los}}$. The path-tangential angle, α, and cross-track error, y_{e}, are computed by

$$\alpha = \mathrm{atan2}\left(y^n_{\mathrm{t}} - y^n_{\mathrm{r}}, x^n_{\mathrm{t}} - x^n_{\mathrm{r}}\right), \tag{4.10}$$

$$y_{\mathrm{e}} = -\left(x^n_b - x^n_{\mathrm{t}}\right)\sin(\alpha) + \left(y^n_b - y^n_{\mathrm{t}}\right)\cos(\alpha), \tag{4.11}$$

where $\boldsymbol{p}^n_{\mathrm{t}} = [x^n_{\mathrm{t}}, y^n_{\mathrm{t}}]^\top$ is the target position, and $\boldsymbol{p}^n_{\mathrm{r}} = [x^n_{\mathrm{r}}, y^n_{\mathrm{r}}]^\top$ is the reference point.

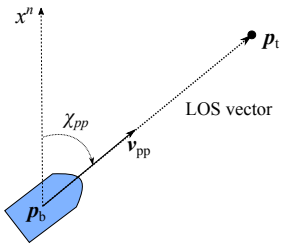

Figure 4.3: Geometry of the pure pursuit guidance.

The steering law (4.9) can be interpreted as a saturated control input:

$$\chi_r(y_e) = \arctan\left(-K_p y_e\right) : \mathbb{R} \to [-\pi/2,\, \pi/2]\,, \tag{4.12}$$

where $K_p = \frac{1}{\Delta} > 0$. The lookahead distance determines the convergence of the vehicle to the path, where a short distance yields an aggressive steering. A larger distance yields a more delicate steering, but longer convergence time. If the course reference is tracked, the guidance law (4.7) ensures that the cross-track error converges to the origin, i.e. $\lim_{t\to\infty} y_e(t) = 0$.

4.3 Pure pursuit guidance

Pure pursuit guidance belongs to the two-point guidance schemes, only involving the interceptor and the target. The guidance velocity is aligned with the LOS vector between the interceptor and the target, thus generating a motion directly towards the target's current position. The method is similar to a predator chasing its pray, and often leads to a tail-chase of moving targets.

The geometry of the guidance law is shown in Figure 4.3. The pure pursuit guidance velocity is given by

$$\boldsymbol{v}_{pp}^n \triangleq -\kappa \frac{\tilde{\boldsymbol{p}}}{\|\tilde{\boldsymbol{p}}\|}, \tag{4.13}$$

where $\tilde{\boldsymbol{p}} \triangleq \boldsymbol{p}_{nb}^n - \boldsymbol{p}_t^n$, and $\kappa > 0$ is effectively the speed of the vehicle. The desired

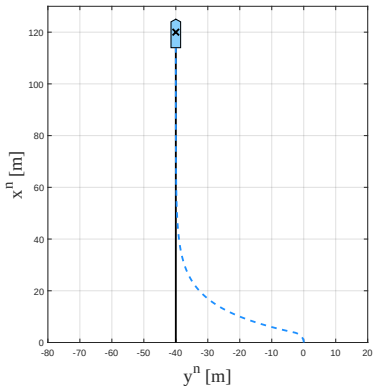

(a) Simulation of the LOS guidance law, with lookahead distance $\Delta = 10$ m.

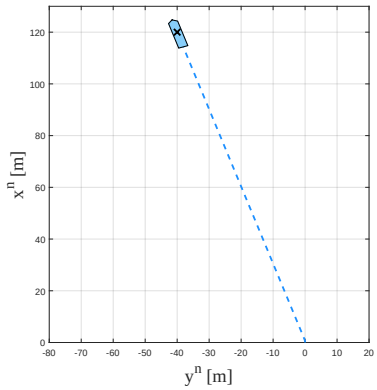

(b) Simulation of the pure pursuit guidance law, with $\kappa = 2$ m/s.

Figure 4.4: The vehicle following of the LOS and pure pursuit guidance laws. The target position is equal to $\boldsymbol{p}_{\mathrm{t}}^n = [120, -40]^\top$ marked by an 'X'. The vehicle, with initial position $[0, 0]^\top$, maintains a constant surge speed $u = 2$ m/s, and zero sway speed.

course is found from (4.13) as $\chi_{\mathrm{pp}}^n \triangleq \mathrm{atan2}(y_{\mathrm{t}}^n - y_b^n, x_{\mathrm{t}}^n - x_b^n)$.

To illustrate the presented methods, trajectories of the kinematic vehicle (3.10) following the LOS and pure pursuit guidance laws can be seen in Figure 4.4, for reaching a static target. The reference point for the LOS guidance was chosen as $[0, -40]$. The LOS guidance law yields a gradual convergence of the vehicle to the path, on which it eventually reaches the target. When employing the pure pursuit guidance law, the vehicle takes the shortest path towards the target.

Chapter 5

The Velocity Obstacle Algorithm

This chapter presents the velocity obstacle algorithm in 2D. The main concept behind the algorithm is to compute the set of velocities, which at any future point in time, result in a collision between the vehicle and an obstacle. By maintaining velocities outside of this set, the vehicle is ensured to avoid a collision with the obstacle. We will employ this algorithm for reactive collision avoidance of a circular obstacle, moving with time-varying velocity.

Collision avoidance of an obstacle will be combined with other goal-reaching behaviour of the vehicle. In particular, the vehicle's nominal behaviour consists of traveling towards a target or along a path, by the use of guidance laws. For this reason, the vehicle's control system has two modes; *guidance mode* and *collision avoidance mode*. The control system transitions between these two modes based on specific safety conditions.

In collision avoidance mode, the vehicle reactively avoids an obstacle by following the VO algorithm. As stated before, the collision avoidance scheme is based on the computation of all velocities resulting in a collision between the vehicle and a nearby

obstacle. If the vehicle maintains an unsafe velocity simultaneously as the obstacle is within a close range of the vehicle, then the vehicle should perform an avoidance maneuver and change its current velocity to a safe one. Evidently, the vehicle should avoid unsafe velocities until it can safely exit collision avoidance mode, and nominal guidance can resume.

A preliminary analysis of the collision avoidance algorithm will be given. We will prove that the fundamental concept behind the algorithm guarantees collision avoidance, regardless of the kinematic and dynamical properties of the system. That is, by consistently maintaining velocities outside the set of unsafe velocities, the distance between the vehicle and an obstacle will always remain larger than a chosen minimum distance.

5.1 Obstacle model

In this section we will define the model used to describe a moving obstacle. We will state some necessary assumptions regarding the obstacle model and describe the required obstacle measurements for the implementation of the algorithm.

The velocity obstacle algorithm can deal with obstacles of any shape. However, we consider an obstacle with circular shape for convenience. The obstacle is modeled as a moving, circular domain $\mathcal{D}_o$, with radius R_o. Since it can be difficult to estimate the dynamics of the obstacle, it is modeled as a nonholonomic vehicle to capture the essential motion of any moving hindrance:

$$\dot{x}_o^n = u_o \cos(\psi_o^n), \tag{5.1a}$$

$$\dot{y}_o^n = u_o \sin(\psi_o^n), \tag{5.1b}$$

$$\dot{\psi}_o^n = r_o, \tag{5.1c}$$

$$\dot{u}_o = a_o, \tag{5.1d}$$

where x_o^n and y_o^n are the Cartesian coordinates of the obstacle center, u_o is the forward speed, a_o is the forward acceleration, and ψ_o^n and r_o are the obstacle heading and heading rate, respectively. The position of the obstacle center is denoted $\boldsymbol{p}_{no}^n \triangleq$

$[x_o^n, y_o^n]^\top$, with associated velocity vector $\boldsymbol{v}_{no}^n \triangleq [\dot{x}_o^n, \dot{y}_o^n]^\top$.

We require the obstacle's turning rate and forward acceleration to be bounded:

Assumption 5.1. The obstacle's heading rate, r_o, and forward acceleration, a_o, are bounded by

$$\begin{aligned} r_o &\in [-r_{o,\max},\, r_{o,\max}] \\ a_o &\in [-a_{o,\max},\, a_{o,\max}]\,, \end{aligned} \tag{5.2}$$

where $r_{o,\max} \geq 0$ and $a_{o,\max} \geq 0$ are constant parameters.

And finally, the obstacle's speed cannot be arbitrarily large, i.e. it needs to meet the following condition:

Assumption 5.2. The obstacle's forward speed $u_o \geq 0$ is bounded by

$$u_o \leq u_{o,\max}, \tag{5.3}$$

where $u_{o,\max} \geq 0$ is a constant parameter.

5.1.1 Extended obstacle domain

To implement the algorithm, we map the the vehicle into the configuration space of the obstacle, by reducing the vehicle to a point, and extending the obstacle domain by a radius that compensates for at least the area of the vehicle. The extended obstacle domain is denoted $\mathcal{D}_{o|\epsilon}$, with radius defined as $R_{o|\epsilon} \triangleq R_o + d_\epsilon$, where $d_\epsilon > 0$ is a constant design parameter. To this end, the extended obstacle domain will be represented by a dotted line encircling the obstacle, as e.g. in Figure 5.1.

5.1.2 Required obstacle measurements

Consider Figure 5.1. As previously stated, the algorithm can deal with obstacles of any shape. A requirement is however that the obstacle shape can be measured, in addition to the obstacle size. In our case, this corresponds to the circular domain $\mathcal{D}_o$, and the

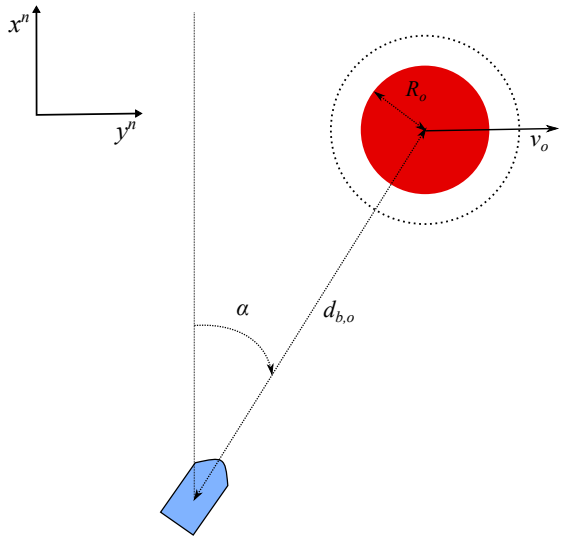

Figure 5.1: Required obstacle measurements, in reference to the NED frame.

radius R_o. Moreover, the vehicle must be able to detect the obstacle, and sense the distance $d_{b,o} \triangleq \|\boldsymbol{p}^n_{nb} - \boldsymbol{p}^n_{no}\|$ and the orientation $\alpha \triangleq \text{atan2}(y^n_b - y^n_o, x^n_b - x^n_o)$. Note that $\boldsymbol{p}^n_{nb} \triangleq [x^n_b,\, y^n_b]^\top$ denotes the vehicle's Cartesian coordinates, in correspondence with the notation presented in Chapter 3. The required measurements are available through a variety of sensors, such as lasers, radars and sonars, or alternatively through cameras.

In order to compensate for the obstacle's motion, the velocity of the obstacle, $\boldsymbol{v}^n_{no}$, must be measured. If the previously mentioned sensors provide Doppler measurements, then the obstacle velocity is available as well. The obstacle velocity can alternatively be computed using tracking algorithms.

5.2 Algorithm definition

In this section, we will present the velocity obstacle algorithm for reactive collision avoidance of a circular obstacle. We will present the concept as it is done in Fiorini

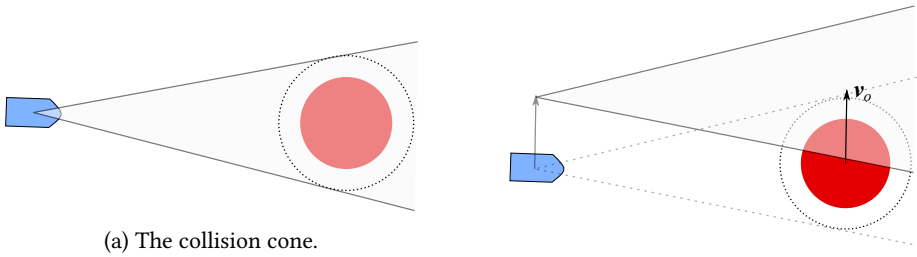

(a) The collision cone.

(b) The velocity obstacle.

Figure 5.2: Illustration of the collision cone and the velocity obstacle.

and Shiller [5], and subsequently describe the algorithm geometrically, in order to locate unsafe directions for the vehicle to avoid. We will state the specific conditions for deciding if the vehicle's control system should switch from nominal guidance to collision avoidance and vice versa, and finally present the heuristics deciding the structure of the avoidance maneuver for the vehicle to avoid a collision with a moving obstacle.

5.2.1 Terminology

In this section, we introduce the concept of the velocity obstacle for a single obstacle. The concept is based on the computation of all instantaneous velocities resulting in a collision between the vehicle and an obstacle:

Definition 5.1 (*Collision*). *A collision occurs between the vehicle and the obstacle if* $\|\boldsymbol{p}^n_{nb} - \boldsymbol{p}^n_{no}\| < d_{sep}$*, where* d_{sep} *is the minimum allowed separation distance between the vehicle and obstacle centers.*

Let the vehicle's velocity vector be denoted as $\boldsymbol{v}^n_{nb} \triangleq \dot{\boldsymbol{p}}^n_{nb}$, and define the ray $l(\boldsymbol{p}, \boldsymbol{v})$ going from the position $\boldsymbol{p}$, along the direction of $\boldsymbol{v}$, as

$$l(\boldsymbol{p}, \boldsymbol{v}) \triangleq \{\, \boldsymbol{p} + \boldsymbol{v}t \mid t \geq 0 \,\}. \tag{5.4}$$

We are now ready to present what is commonly known as the collision cone [5]:

Definition 5.2 (*Collision cone*). *The set of relative velocities* $\boldsymbol{v}_{nbo}^n \triangleq \boldsymbol{v}_{nb}^n - \boldsymbol{v}_{no}^n$ *resulting in a collision between the obstacle and the vehicle, assuming the velocity vectors* $\boldsymbol{v}_{nb}^n$ *and* $\boldsymbol{v}_{no}^n$ *are constant over time, is defined as*

$$\mathcal{CC} \triangleq \{ \boldsymbol{v}_{nbo}^n \mid l(\boldsymbol{p}_{nb}^n, \boldsymbol{v}_{nbo}^n) \cap \mathcal{D}_{o|\epsilon} \neq \varnothing \}. \tag{5.5}$$

Definition 5.2 corresponds to any relative velocity of the vehicle with respect to the obstacle, whose ray intersects the extended obstacle domain, seen in Figure 5.2a.

The condition can equivalently be described in terms of absolute velocities by adding the obstacle velocity, $\boldsymbol{v}_{no}^n$, to each velocity in the collision cone, as illustrated in Figure 5.2b. This is known as the velocity obstacle [5]:

Definition 5.3 (*Velocity obstacle*). *The set of absolute velocities* $\boldsymbol{v}_{nb}^n$ *resulting in a collision between the obstacle and the vehicle, assuming the velocity vectors* $\boldsymbol{v}_{nb}^n$ *and* $\boldsymbol{v}_{no}^n$ *are constant over time, is defined as*

$$\mathcal{VO} \triangleq \mathcal{CC} \oplus \boldsymbol{v}_{no}^n, \tag{5.6}$$

where the operator $\oplus$ *denotes the Minkowski sum.*

5.2.2 Geometrical representation

The purpose of this section is to describe the previously introduced concepts geometrically. This allows us to formulate the conditions for a collision in terms of the vehicle's direction.

The geometry of the collision cone is illustrated in Figure 5.3. The edges of the collision cone can be described by the angles

$$\psi_{\mathrm{t}}^{\pm} \triangleq \alpha \pm \beta \tag{5.7}$$

with respect to the positive x^n axis, where

$$\beta \triangleq \sin^{-1}\left(\frac{R_{o|\epsilon}}{d_{b,o}}\right) \in \left(0, \frac{\pi}{2}\right]. \tag{5.8}$$

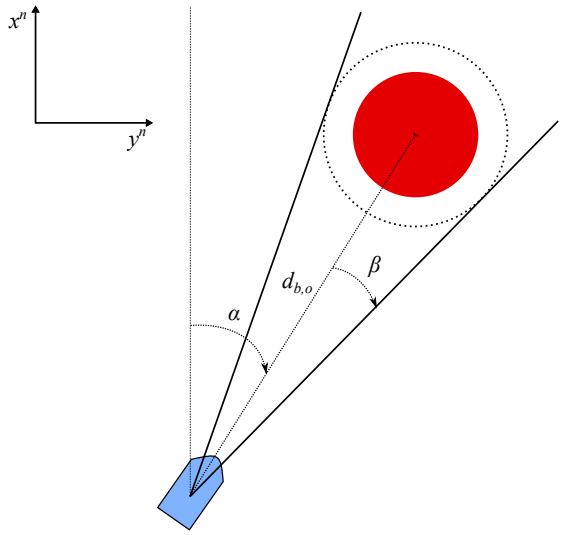

Figure 5.3: Geometry of the collision cone, $\mathcal{CC}$.

We employ the superscript $\pm$ to distinguish between the two edges of the cone. Notice that the angular area within the cone increases as the vehicle moves closer to the obstacle, or as the obstacle radius increases, yielding a larger area to be avoided. Define the relative heading of the vehicle with respect to the obstacle as

$$\psi_{bo}^n \triangleq \angle \boldsymbol{v}_{nbo}^n. \tag{5.9}$$

Then, by Definition 5.2, the condition for a collision to occur at some future time may be written as

$$\psi_{bo}^n \in \left(\psi_{\mathrm{t}}^-, \psi_{\mathrm{t}}^+\right). \tag{5.10}$$

Substituting (5.7) in (5.10) and solving the inequality leads to the following condition:

Definition 5.4 (*Conflict*). *The vehicle is in a conflict with the obstacle if they are not currently in a collision, but with zero control input, the vehicle will collide with the*

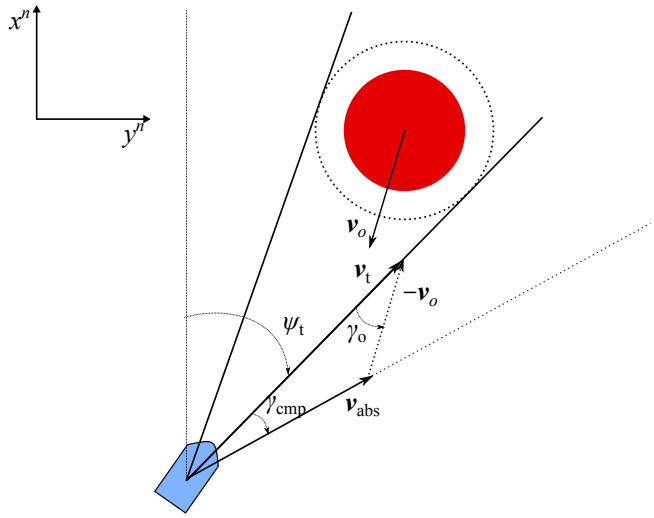

Figure 5.4: Geometric representation of the angles γ^+_{cmp} and γ^+_o.

obstacle at some point in the future, assuming the obstacle maintains its current velocity:

$$|\psi^n_{bo} - \alpha| < \beta. \tag{5.11}$$

It can be convenient to describe the edges of the collision cone in terms absolute velocities. The *absolute collision cone* can be obtained by compensating for the obstacle velocity. Let the vectors $\boldsymbol{v}^\pm_\mathrm{t}$ denote the edges of the collision cone, with orientation $\angle \boldsymbol{v}^\pm_\mathrm{t} \triangleq \psi^\pm_\mathrm{t}$. Furthermore, let the vectors $\boldsymbol{v}^\pm_{\text{abs}} \triangleq \boldsymbol{v}^\pm_\mathrm{t} + \boldsymbol{v}^n_{no}$ lie along the edges of the absolute collision cone, with length $\|\boldsymbol{v}^\pm_{\text{abs}}\| \triangleq U_b$, where $U_b \triangleq \sqrt{u_b^2 + v_b^2}$ is the speed of the vehicle. The direction of these vectors are found geometrically by considering Figure 5.4, as

$$\psi^\pm_{\text{abs}} \triangleq \gamma^\pm_{\text{cmp}} + \psi^\pm_\mathrm{t}. \tag{5.12}$$

The compensation angle $\gamma^\pm_{\text{cmp}}$ is computed by using the sine rule on the triangle

consisting of $\boldsymbol{v}_{\text{abs}}^{\pm}$, $\boldsymbol{v}_{\text{t}}^{\pm}$ and $\boldsymbol{v}_{no}^{n}$, as

$$\gamma_{\text{cmp}}^{\pm} = \sin^{-1}\left(\frac{u_o \sin(\gamma_o^{\pm})}{U_b}\right), \tag{5.13}$$

where $u_o \triangleq \|\boldsymbol{v}_{no}^{n}\|$ by (5.1). Furthermore, the angle $\gamma_o^{\pm}$ is found geometrically as

$$\gamma_o^{\pm} = \pi + \psi_{\text{t}}^{\pm} - \psi_o^n. \tag{5.14}$$

A measure of the angular distances to a conflict can be formulated as, [17]:

$$\gamma_{\text{ad}}^{\pm} \triangleq \pm\psi_b^n \mp \psi_{\text{abs}}^{\pm}, \tag{5.15}$$

where the angles $\gamma_{\text{ad}}^{\pm}$ are wrapped into the domain $(-2\pi, 2\pi]$ such that the distance is negative when the vehicle is in a conflict, and positive otherwise. An illustration of the angles can be seen in Figure 5.5, corresponding to the angular distances the vehicle must turn in both directions in order to enter (or exit) a conflict. The shortest angular distance to a conflict, denoted γ_{ad}, can be computed from the definition (5.11), as

$$\gamma_{\text{ad}} \triangleq \begin{cases} \gamma_{\text{ad}}^{+}, & \text{if } \psi_{bo}^n - \alpha \geq 0, \\ \gamma_{\text{ad}}^{-}, & \text{if } \psi_{bo}^n - \alpha < 0, \end{cases} \tag{5.16}$$

where the angular difference is mapped to the domain $\left(\psi_{bo}^n - \alpha\right) \in (-\pi, \pi]$.

5.2.3 Switching conditions

The velocity obstacle is the basis for deciding if the vehicle is headed for a collision with the obstacle. In the previous section we formulated the conditions of the velocity obstacle in terms of direction. The presented theory can be used to construct an avoidance maneuver for the vehicle so that it avoids a collision. However, we have not yet addressed when the vehicle should perform such a maneuver.

To not constrain the vehicle needlessly, the obstacle should pose a significant threat before it is necessary for the vehicle to change its course. The original VO

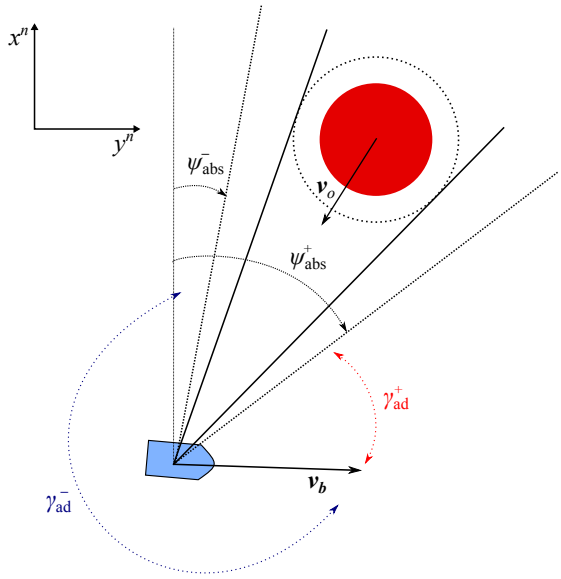

Figure 5.5: Angular distances to a conflict, $\gamma^{\pm}_{\text{ad}}$. The shortest distance, $\gamma_{\text{ad}} = \gamma^{+}_{\text{ad}}$, is marked in red.

method [5] employs a time-horizon to distinguish between obstacles with imminent collision and long time to collision. If the obstacle will cause a collision within a suitable time-horizon then it is handled immediately, otherwise it is ignored. Although the time-horizon is intuitive, we will instead decide if the vehicle's control system should switch to collision avoidance mode based on the distance between the obstacle and vehicle, motivated by Wiig et al. [27].

Recall that the vehicle nominally is in guidance mode, traveling towards a target or a path. The control system is switched to collision avoidance mode at the time $t_1 \geq t_0$ if the obstacle is within a chosen threshold distance of the vehicle, simultaneously as the guidance velocity, denoted $\boldsymbol{v}^n_{ndg}$, is unsafe:

$$d_{b,o}(t_1) \leq d_{\text{threshold}}, \quad \boldsymbol{v}^n_{ndg}(t_1) \in \mathcal{VO}(t_1). \tag{5.17}$$

The control system exits CA mode at $t_2 > t_1$ when the guidance velocity is safe:

$$\boldsymbol{v}_{ndg}^{n}(t_2) \notin \mathcal{VO}(t_2). \tag{5.18}$$

It can be noticed that the vehicle may enter collision avoidance mode several times before it escapes the obstacle completely.

5.2.4 Turning rules

Recall that the edges of the absolute collision cone can be described by the angles $\psi_{\text{abs}}^{\pm}$ defined in (5.12). In collision avoidance mode, the vehicle's velocity vector should lie along, or outside these boundaries, to ensure that a collision is avoided. When the vehicle enters CA mode, the vehicle's turning direction towards safety will be chosen based on the distance to the obstacle at this moment in time, and the angular distances to each of these edges.

In particular, if the distance satisfies $d_{b,o} = d_{\text{threshold}}$ when collision avoidance mode is entered, the turning direction is chosen to make the vehicle seek to pass behind the obstacle. This is obtained by maximizing the angular differences between the obstacle's heading, ψ_o^n, and the edges of the absolute collision cone, as presented in Wiig et al. [27]:

$$d_{b,o} = d_{\text{threshold}}, \quad j = \underset{j \in \{\pm\}}{\arg\max} \left| \psi_o^n - \psi_{\text{abs}}^{(j)} \right|, \tag{5.19}$$

where the angular difference is mapped to the interval $(-\pi, \pi]$. This can be interpreted as turning in the direction that is farthest away from the direction the obstacle is traveling in.

Remark 5.1. The threshold distance should be chosen large enough to ensure that the vehicle can safely turn in the desired direction, without being in danger of a collision during the maneuver.

If the obstacle turns, the vehicle may enter collision avoidance mode as the distance satisfies $d_{b,o} < d_{\text{threshold}}$. To ensure safety, the turning direction will make the vehicle

turn away from the nearest edge of the absolute collision cone, so that it avoid entering the conflict. The correct turning direction is obtained by minimizing the angular distances to a conflict defined in (5.15), as

$$d_{b,o} < d_{\text{threshold}}, \quad j = \arg\min_{j\in\{\pm\}} \left|\psi_b^n - \psi_{\text{abs}}^{(j)}\right|. \tag{5.20}$$

Notice that one of the distances will be zero in this case. The vehicle may then pass on either side of the obstacle, whichever is safest.

5.3 Preliminary analysis

We will here provide a preliminary analysis of the collision avoidance algorithm, proving that the vehicle, following heading references along or outside the edges of the absolute collision cone, will maintain at least a distance $R_{o|\epsilon}$ from the obstacle. To prove this, we consider the condition of a conflict, defined in (5.11).

Lemma 5.1. *Consider a static obstacle, and let the vehicle and the obstacle initially be separated by a distance $d_{b,o}(t_0) > R_{o|\epsilon}$. If the vehicle maintains a heading angle, ψ_b^n, satisfying*

$$|\psi_b^n(t) - \alpha(t)| = \beta(t), \quad \forall t \geq t_0, \tag{5.21}$$

where β is defined in (5.8), then the vehicle will converge to a circle with radius $R_{o|\epsilon}$ and center in the obstacle center, $\boldsymbol{p}_{no}^n$. Moreover, if the vehicle maintains a heading angle satisfying

$$|\psi_b^n(t) - \alpha(t)| \geq \beta(t), \quad \forall t \geq t_0, \tag{5.22}$$

then

$$d_{b,o}(t) \geq R_{o|\epsilon}, \quad \forall t \geq t_0. \tag{5.23}$$

Proof. Consider the line segment going from the origin of the vehicle, $\boldsymbol{p}_{nb}^n$, to the origin of the obstacle, $\boldsymbol{p}_{no}^n$, with length $d_{b,o}$ and orientation α. The time-derivative of

$d_{b,o}$ is found geometrically as

$$\dot{d}_{b,o} = -U_b \cos(\psi_b^n - \alpha). \tag{5.24}$$

Let the vehicle satisfy (5.21) where β is defined in (5.8). We can then write (5.24) as

$$\dot{d}_{b,o} = -U_b \sqrt{1 - \left(\frac{R_{o|\epsilon}}{d_{b,o}}\right)^2}. \tag{5.25}$$

Solving (5.25) for $d_{b,o}$, it can be seen that $d_{b,o}$ has a minimum value equal to $R_{o|\epsilon}$, when $\dot{d}_{b,o} = 0$. Hence, we have established that $d_{b,o}$ is lower bounded by $R_{o|\epsilon}$. Since the vehicle initially satisfies $d_{b,o}(t_0) > R_{o|\epsilon}$, then by (5.25) $\dot{d}_{b,o}(t_0) < 0$. Moreover, $\dot{d}_{b,o} < 0 \; \forall d_{b,o} > R_{o|\epsilon}$, and $\dot{d}_{b,o} = 0$ if and only if $d_{b,o} = R_{o|\epsilon}$. Thus, $\dot{d}_{b,o} \leq 0 \; \forall t \geq t_0$. Since $\dot{d}_{b,o} \leq 0$ and $d_{b,o}$ is lower bounded, then $d_{b,o} \to R_{o|\epsilon}$ as $t \to \infty$. Hence, the position of the vehicle, $\boldsymbol{p}_{nb}^n$, converges to a circle with radius $R_{o|\epsilon}$ and center in $\boldsymbol{p}_{no}^n$.

Now, let the vehicle satisfy (5.22). The time-derivative of $d_{b,o}$ from (5.24) then satisfies

$$\dot{d}_{b,o} \geq -U_b \sqrt{1 - \left(\frac{R_{o|\epsilon}}{d_{b,o}}\right)^2}. \tag{5.26}$$

Hence,

$$d_{b,o} \geq R_{o|\epsilon}, \quad \forall t \geq t_0, \tag{5.27}$$

which concludes the proof. □

Lemma 5.2. *Consider an obstacle moving with a time-varying velocity $\boldsymbol{v}_{no}^n(t)$, and let the vehicle and the obstacle initially be separated by a distance $d_{b,o}(t_0) > R_{o|\epsilon}$. If the vehicle maintains a heading angle satisfying*

$$|\psi_{bo}^n(t) - \alpha(t)| \geq \beta(t), \quad \forall t \geq t_0, \tag{5.28}$$

then

$$d_{b,o}(t) \geq R_{o|\epsilon}, \quad \forall t \geq t_0. \tag{5.29}$$

Proof. Consider a coordinate frame n_o attached to the obstacle and aligned with the

inertial frame n, moving with the obstacle velocity $\boldsymbol{v}_{no}^n$. In this frame, the obstacle is static and the vehicle has the velocity $\boldsymbol{v}_{nbo}^n \triangleq \boldsymbol{v}_{nb}^n - \boldsymbol{v}_{no}^n$. Hence, Lemma 5.1 can be applied for the vehicle with the relative velocity $\boldsymbol{v}_{nbo}^n$ and heading $\psi_{bo}^n \triangleq \angle \boldsymbol{v}_{nbo}^n$. $\square$

Chapter 6

The Velocity Obstacle Algorithm for Unicycles

In this chapter, we will apply the velocity obstacle algorithm to a kinematic unicycle subject to nonholonomic constraints, for reactive collision avoidance of a moving obstacle. The unicycle model describes the kinematics of a large class of vehicles, including the underactuated surface vehicle modeled in Chapter 3.

The vehicle is restricted to maintain a constant forward speed, and has limited turning rate. To ensure that the vehicle is able to turn away from a nearby obstacle, we derive a lower bound on the required turning rate of the vehicle. With this bound satisfied, the vehicle is always able to turn away from a conflict without entering it, even in cases where the obstacle accelerates or turns towards the vehicle. Furthermore, we derive a minimum distance ensuring that the vehicle is able to turn out of a conflict if one is entered, before a collision can occur. The lower bound is used to choose the threshold distance introduced in the previous chapter.

Collision avoidance will achieved while also guaranteeing that the vehicle will reach its separate goals. It can be recalled that the vehicle's control system switches between guidance and collision avoidance. The nominal goal of the vehicle is thus

to reach a target or converge to a path, dependent on the current guidance mode the vehicle is in, by the use of guidance laws. Guarantees of collision avoidance combined with target reaching and path following will be provided through a mathematical analysis. The theoretical proofs are supported by numerical simulations in the last section.

6.1 System description

In this section, we present the vehicle model with associated control objective, and state the model used to describe a moving obstacle in the vehicle's presence.

6.1.1 Vehicle model

The vehicle is modeled as a kinematic unicycle-type vehicle, representing the kinematic model (3.10) with zero sway speed:

$$\begin{aligned} \dot{x}_b^n &= u_b \cos(\psi_b^n), \\ \dot{y}_b^n &= u_b \sin(\psi_b^n), \\ \dot{\psi}_b^n &= r_b, \end{aligned} \tag{6.1}$$

where $\boldsymbol{p}_{nb}^n \triangleq [x_b^n \, , y_b^n]^\top$ are the Cartesian coordinates of the vehicle center, u_b is the forward speed, and ψ_b^n and r_b are the heading and heading rate, respectively. The vehicle's velocity vector is denoted $\boldsymbol{v}_{nb}^n \triangleq [\dot{x}_b^n \, , \dot{y}_b^n]^\top$.

For convenience, we assume that the vehicle maintains a constant forward speed given by an arbitrary outer-loop controller, but directly controls the turning rate, r_b, in order to follow the heading reference generated by the control system:

Assumption 6.1. The vehicle's forward speed $u_b > 0$ is constant.

Assumption 6.2. The vehicle's heading rate, r_b, is directly controlled and bounded

by

$$r_b \in [-r_{b,\max},\, r_{b,\max}]\,, \tag{6.2}$$

where $r_{b,\max} > 0$ is a constant parameter.

6.1.2 Control objective

The vehicle's control objective varies, depending on the nominal guidance mode of the vehicle. We distinguish between two guidance modes; target reaching and path following.

In target reaching mode, the control objective of the vehicle is to come within an acceptable distance of a target position $\boldsymbol{p}_{\mathrm{t}}^n \triangleq [x_{\mathrm{t}}^n\,, y_{\mathrm{t}}^n]^\top$, at an unspecified point in time $t_{\mathrm{f}} \in [t_0, \infty)$. The control objective may be written

$$\|\boldsymbol{p}_{\mathrm{t}}^n - \boldsymbol{p}_{nb}^n(t_{\mathrm{f}})\| \leq d_{\mathrm{a}}, \tag{6.3}$$

where $d_{\mathrm{a}} > 0$ is the acceptance distance.

In path following mode, the control objective of the vehicle is to converge to, and follow a straight line path parallel to the positive x^n axis, defined as

$$\mathcal{P} \triangleq \{(x, y) \in \mathbb{R}^2 \mid y = y_{\mathrm{t}}^n\}, \tag{6.4}$$

where y_{t}^n is the desired vehicle position along the y^n axis. Furthermore, both goals should be achieved while keeping at least a minimum safety distance d_ϵ to the obstacle:

$$d_{b,o}(t) - R_o \geq d_\epsilon > 0,\ \forall t \geq t_0, \tag{6.5}$$

where $d_{b,o} \triangleq \|\boldsymbol{p}_{nb}^n - \boldsymbol{p}_{no}^n\|$ is the distance between the vehicle and obstacle centers. Note that d_ϵ both compensates for the vehicle's own area, and an unspecified separation distance between the vehicle and the obstacle.

6.1.3 Obstacle model

The obstacle model is described in Chapter 5, but is summarized here for convenience. The obstacle is modeled as the nonholonomic vehicle:

$$\dot{x}_o^n = u_o \cos(\psi_o^n), \tag{6.6a}$$
$$\dot{y}_o^n = u_o \sin(\psi_o^n), \tag{6.6b}$$
$$\dot{\psi}_o^n = r_o, \tag{6.6c}$$
$$\dot{u}_o = a_o. \tag{6.6d}$$

The position of the obstacle center is denoted $\boldsymbol{p}_{no}^n \triangleq [x_o^n\,, y_o^n]^\top$, with associated velocity vector $\boldsymbol{v}_{no}^n \triangleq [\dot{x}_o^n\,, \dot{y}_o^n]^\top$. The obstacle is modeled as a moving, circular domain $\mathcal{D}_o$, with radius R_o, subject to the kinematic constraints:

Assumption 6.3. The obstacle's heading rate, r_o, and forward acceleration, a_o, are bounded by

$$\begin{aligned} r_o &\in [-r_{o,\max},\, r_{o,\max}]\,, \\ a_o &\in [-a_{o,\max},\, a_{o,\max}]\,, \end{aligned} \tag{6.7}$$

where $r_{o,\max} \geq 0$ and $a_{o,\max} \geq 0$ are constant parameters.

Assumption 6.4. The obstacle's forward speed $u_o \geq 0$ is bounded by

$$u_o \leq u_{o,\max}, \tag{6.8}$$

where $u_{o,\max} < u_b$ is a constant parameter.

Remark 6.1. By Assumption 6.4 we assume that the vehicle is able to maintain a higher forward speed than the the obstacle. This is a general assumption that needs to met in order to prove safety of the vehicle when the obstacle is not cooperating. If

the obstacle is restricted in other ways, then safety could be investigated without this assumption. Such scenarios will not be analyzed in this thesis.

6.2 Guidance and control

The vehicle's control system switches between two modes: nominal guidance mode, and collision avoidance mode. In this section, we will present the former of these two modes.

In guidance mode, the vehicle's heading references will be generated by one of the guidance laws presented in Chapter 4. We will employ the pure pursuit guidance law for target reaching, and the line of sight guidance law for path following. Both of the guidance schemes are summarized below. In order to follow the references generated by the guidance system, the vehicle will employ a kinematic heading controller, stated in the last section.

6.2.1 Pure pursuit guidance

When the control system is in target reaching mode, the vehicle's nominal heading references will be generated by the pure pursuit guidance law described in Section 4.3. The guidance law generates a velocity vector along the line of sight vector between the vehicle and the target, given by

$$\boldsymbol{v}_{\text{pp}}^n \triangleq -u_b \frac{\tilde{\boldsymbol{p}}^n}{\|\tilde{\boldsymbol{p}}^n\|}, \tag{6.9}$$

where $\tilde{\boldsymbol{p}}^n \triangleq \boldsymbol{p}_{nb}^n - \boldsymbol{p}_{\text{t}}^n$, and $u_b > 0$ is the forward speed of the vehicle. The desired heading is given by

$$\psi_{\text{pp}}^n \triangleq \angle \boldsymbol{v}_{\text{pp}}^n. \tag{6.10}$$

The pure pursuit guidance law ensures that the vehicle reaches a static target. However, it can result in a tail chase of moving targets.

6.2.2 Line of sight guidance

In path following mode, the vehicle's heading references will be generated by the line of sight (LOS) guidance law described in Section 4.2. LOS guidance is a three point guidance scheme, based on guiding the vehicle towards a straight line path constructed from two points, denoted as $\boldsymbol{p}_{k-1}^n = \left[x_{k-1}^n \, , y_{k-1}^n\right]^\top$ and $\boldsymbol{p}_k^n = [x_k^n \, , y_k^n]^\top$. The points are chosen to comply with the desired path defined in (6.4).

The line of sight vector points towards a point on the path, located a constant lookahead distance $\Delta > 0$ from the direct projection of the vehicle position onto the path. The desired heading is computed as

$$\psi_{\text{los}}^n(y_{\text{e}}) \triangleq \chi_p + \arctan\left(\frac{-y_{\text{e}}}{\Delta}\right), \tag{6.11}$$

where the path-tangential angle χ_p, and the cross-track error y_{e}, are defined as

$$\chi_p = \text{atan2}\left(y_k^n - y_{k-1}^n, x_k^n - x_{k-1}^n\right), \tag{6.12}$$

$$y_{\text{e}} = -\left(x_b^n - x_k^n\right)\sin(\chi_p) + \left(y_b^n - y_k^n\right)\cos(\chi_p). \tag{6.13}$$

The guidance velocity during LOS guidance is computed from (6.11), as

$$\boldsymbol{v}_{\text{los}}^n \triangleq u_b \left[\cos(\psi_{\text{los}}^n), \, \sin(\psi_{\text{los}}^n)\right]^\top. \tag{6.14}$$

6.2.3 Heading controller

In order to follow the heading references generated by the guidance system, the vehicle employs a kinematic heading controller:

$$r_b = \begin{cases} 0, & \text{if } \tilde{\psi} = 0, \\ -r_{b,\max}, & \text{if } \tilde{\psi} = (0, \pi], \\ r_{b,\max}, & \text{if } \tilde{\psi} = (-\pi, 0). \end{cases} \tag{6.15}$$

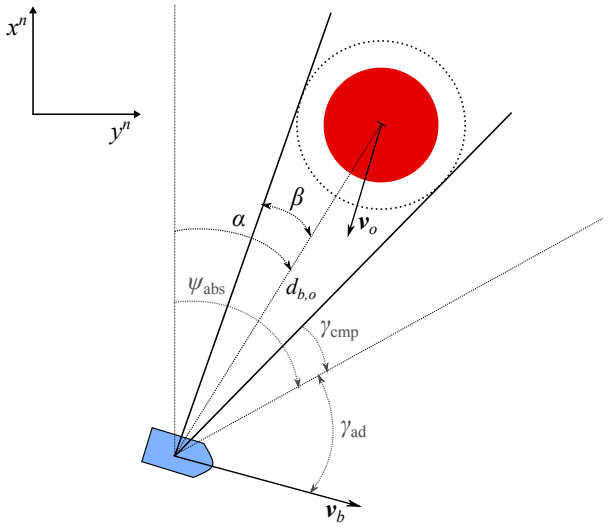

Figure 6.1: Geometric representation of the VO algorithm.

The error variable $\tilde{\psi} \triangleq \psi_b^n - \psi_{dg}^n$ is chosen to belong in the interval $(-\pi, \pi]$ to ensure that the vehicle always takes the shortest turn to the desired heading.

6.3 Collision avoidance

The collision avoidance algorithm presented in Chapter 5 will be used to generate heading references for the vehicle when the control system is in collision avoidance mode. We will summarize the algorithm in this section, and furthermore define the control input for the nonholonomic vehicle to avoid collision with an obstacle.

The vehicle is headed for a collision with a nearby obstacle if it satisfies the condition:

$$\boldsymbol{v}_{nbo}^n \in \mathcal{CC} \iff \boldsymbol{v}_{nb}^n \in \mathcal{VO}, \tag{6.16}$$

where $\mathcal{CC}$ is the collision cone, $\mathcal{VO}$ is the velocity obstacle, and $\boldsymbol{v}_{nbo}^n \triangleq \boldsymbol{v}_{nb}^n - \boldsymbol{v}_{no}^n$ is the relative velocity of the vehicle with respect to the obstacle. The edges of the collision cone, represented by the solid, tangent lines in Figure 6.1, can be described

geometrically as

$$\psi_{\text{t}}^{\pm} \triangleq \alpha \pm \beta, \tag{6.17}$$

where

$$\beta \triangleq \sin^{-1}\left(\frac{R_{o|\epsilon}}{d_{b,o}}\right) \in \left(0, \frac{\pi}{2}\right]. \tag{6.18}$$

The vehicle is said to be in a conflict with the obstacle if $\psi_{bo}^{n} \triangleq \angle \boldsymbol{v}_{nbo}^{n}$ lies within the angular boundaries of the collision cone:

$$|\psi_{bo}^{n} - \alpha| < \beta. \tag{6.19}$$

The edges of the absolute collision cone is defined geometrically as

$$\psi_{\text{abs}}^{\pm} \triangleq \gamma_{\text{abs}}^{\pm} + \psi_{\text{t}}^{\pm}, \tag{6.20}$$

where the compensation angle $\gamma_{\text{cmp}}^{\pm}$ is computed by the following relation:

$$\gamma_{\text{cmp}}^{\pm} = \sin^{-1}\left(\frac{u_o \sin(\gamma_o^{\pm})}{u_b}\right). \tag{6.21}$$

Remark 6.2. Assumption 6.4 ensures that (6.21) is well-defined.

The angle $\gamma_o^{\pm}$ is found geometrically as

$$\gamma_o^{\pm} = \pi + \psi_{\text{t}}^{\pm} - \psi_o^{n}. \tag{6.22}$$

A measure of the angular distances to a conflict can be formulated as follows:

$$\gamma_{\text{ad}}^{\pm} \triangleq \pm\psi_b^{n} \mp \psi_{\text{abs}}^{\pm}, \tag{6.23}$$

corresponding to the angular distances the vehicle must turn in both directions in order to enter (or exit) a conflict. The shortest distance to a conflict, denoted γ_{ad}, is

defined as

$$\gamma_{\text{ad}} \triangleq \begin{cases} \gamma_{\text{ad}}^{+}, & \text{if } \psi_{bo}^{n} - \alpha \geq 0, \\ \gamma_{\text{ad}}^{-}, & \text{if } \psi_{bo}^{n} - \alpha < 0, \end{cases} \tag{6.24}$$

where the angular difference is mapped to the interval $\left(\psi_{bo}^{n} - \alpha\right) \in (-\pi, \pi]$.

The control system is switched to collision avoidance mode if the vehicle is too close to the obstacle, simultaneously as the guidance velocity, denoted $\boldsymbol{v}_{ndg}^{n}$, is unsafe:

$$d_{b,o}(t_1) \leq d_{\text{threshold}}, \;\; \boldsymbol{v}_{ndg}^{n}(t_1) \in \mathcal{VO}(t_1). \tag{6.25}$$

Nominal guidance will resume when the guidance velocity is safe:

$$\boldsymbol{v}_{ndg}^{n}(t_2) \notin \mathcal{VO}(t_2). \tag{6.26}$$

If the distance equals $d_{b,o} = d_{\text{threshold}}$ at the time in which the vehicle enters CA mode, the vehicle will seek to pass behind the obstacle:

$$d_{b,o} = d_{\text{threshold}}, \;\; j = \underset{j \in \{\pm\}}{\arg\max} \left| \psi_{o}^{n} - \psi_{\text{abs}}^{(j)} \right|, \tag{6.27}$$

where j is the turning parameter. If the distance is less than $d_{\text{threshold}}$, the vehicle will instead turn away from the nearest conflict:

$$d_{b,o} < d_{\text{threshold}}, \;\; j = \underset{j \in \{\pm\}}{\arg\min} \left| \psi_{b}^{n} - \psi_{\text{abs}}^{(j)} \right|. \tag{6.28}$$

The collision avoidance law is stated as

$$r_b = \begin{cases} r_{b,\max}, & \text{if } j = + \mid \gamma_{\text{ad}}^{+} \leq \sigma, \\ -r_{b,\max}, & \text{if } j = - \mid \gamma_{\text{ad}}^{-} \leq \sigma, \end{cases} \tag{6.29}$$

where j is chosen by the turning rules presented above. The vehicle will then turn with maximum turning power, until it acquires a heading that is an angular safety

distance $\sigma > 0$ away from a conflict, where σ is a constant design parameter.

6.4 Analysis

This section presents a mathematical analysis of the collision avoidance algorithm presented in Section 6.3 applied to the kinematic vehicle (6.1), for avoiding a moving obstacle described by (6.6), while the vehicle drives towards a goal, or follows a path.

6.4.1 Staying out of conflict

The first theorem will provide the conditions ensuring that the vehicle avoids entering a conflict with the obstacle, if it starts outside of conflict. If the vehicle stays out of conflict, we can recall from Lemma 5.2 that the vehicle then avoids a collision with the obstacle as well. This requires, as we will show, that the vehicle is able to turn faster than the obstacle can turn or accelerate towards it.

Theorem 6.1. *Consider an obstacle described by (6.6) and a vehicle described by (6.1). Let Assumption 6.1-6.4 hold, and suppose the vehicle starts outside a conflict, i.e.:*

$$|\psi_{bo}^{n}(t_0) - \alpha(t_0)| \geq \beta(t_0). \tag{6.30}$$

If the vehicle maintains a continuous control input satisfying

$$\begin{aligned} \gamma_{\text{ad}}^{+} = 0 &\implies r_b = r_{b,\max}, \\ \gamma_{\text{ad}}^{-} = 0 &\implies r_b = -r_{b,\max}, \end{aligned} \tag{6.31}$$

where

$$r_{b,\max} \geq r_{o,\max}\frac{u_{o,\max}}{u_b} + \frac{a_{o,\max}}{\sqrt{u_b^2 - u_{o,\max}^2}}. \tag{6.32}$$

Then, the vehicle will remain outside the conflict, and furthermore maintain a distance

to the obstacle satisfying

$$d_{b,o}(t) - R_o \geq d_\epsilon, \quad \forall t \geq t_0. \tag{6.33}$$

Proof. The proof of the theorem follows along the lines of the proof presented in Lalish et al. [17], which argues that if the vehicle starts conflict-free, and continuously turns away from the nearest conflict or exerts no control input $r_b = 0$, then the vehicle avoids a collision with another vehicle following the same collision avoidance algorithm. We extend the analysis to the case where the vehicle avoids a non-cooperating obstacle, and show that safety can be guaranteed as long as the vehicle's turning rate is lower bounded by a sufficient minimum value.

We compute the angular distances to a conflict, $\gamma^{\pm}_{\text{ad}}$, by substituting (6.17) and (6.20) into (6.23), as

$$\gamma^{\pm}_{\text{ad}} = \pm\psi^n_b \mp (\alpha \pm \beta + \gamma^{\pm}_{\text{cmp}}), \tag{6.34}$$

which has the time-derivative:

$$\dot{\gamma}^{\pm}_{\text{ad}} = \pm r_b \mp \left(\dot{\alpha} \pm \dot{\beta}\right) \mp \dot{\gamma}^{\pm}_{\text{cmp}}. \tag{6.35}$$

The time-derivative of α is found geometrically as

$$\dot{\alpha} = -\frac{U_{bo}}{d_{b,o}} \sin(\psi^n_{bo} - \alpha), \tag{6.36}$$

where $U_{bo} \triangleq \|\boldsymbol{v}^n_{nb} - \boldsymbol{v}^n_{no}\|$, while the time-derivative of β can be computed from (6.18) as

$$\dot{\beta} = \frac{d}{dt}\left(\sin^{-1}\left(\frac{R_{o|\epsilon}}{d_{b,o}}\right)\right) \tag{6.37}$$

$$= -\dot{d}_{b,o}\frac{R_{o|\epsilon}}{d_{b,o}\sqrt{d^2_{b,o} - R^2_{o|\epsilon}}} \tag{6.38}$$

$$= \frac{U_{bo}}{d_{b,o}} \cos(\psi^n_{bo} - \alpha)\tan(\beta), \tag{6.39}$$

where $\dot{d}_{b,o}$ is found geometrically. The time-derivative of $\gamma^{\pm}_{\text{cmp}}$ can be computed from (6.21) as

$$\dot{\gamma}^{\pm}_{\text{cmp}} = \frac{\partial\left(\gamma^{\pm}_{\text{cmp}}\right)}{\partial \gamma^{\pm}_{o}}\dot{\gamma}^{\pm}_{o} + \frac{\partial\left(\gamma^{\pm}_{\text{cmp}}\right)}{\partial u_o}\dot{u}_o, \tag{6.40}$$

where $\gamma^{\pm}_{o}$ is defined in (6.22). We compute the terms as

$$\frac{\partial\left(\gamma^{\pm}_{\text{cmp}}\right)}{\partial \gamma^{\pm}_{o}}\dot{\gamma}^{\pm}_{o} = \tag{6.41}$$

$$= \frac{\partial}{\partial \gamma^{\pm}_{o}}\left(\sin^{-1}\left(\frac{u_o \sin(\gamma^{\pm}_{o})}{u_b}\right)\right)\dot{\gamma}^{\pm}_{o} \tag{6.42}$$

$$= (-r_o + \dot{\alpha} \pm \dot{\beta})\frac{(u_o/u_b)\cos(\gamma^{\pm}_{o})}{\sqrt{1-(u_o/u_b)^2\sin^2(\gamma^{\pm}_{o})}}, \tag{6.43}$$

and

$$\frac{\partial\left(\gamma^{\pm}_{\text{cmp}}\right)}{\partial u_o}\dot{u}_o = \tag{6.44}$$

$$= \frac{\partial}{\partial u_o}\left(\sin^{-1}\left(\frac{u_o \sin(\gamma^{\pm}_{o})}{u_b}\right)\right)\dot{u}_o \tag{6.45}$$

$$= a_o \frac{\sin(\gamma^{\pm}_{o})}{u_b\sqrt{1-(u_o/u_b)^2\sin^2(\gamma^{\pm}_{o})}}. \tag{6.46}$$

For convenience, we define

$$P(\gamma_o) \triangleq \frac{(u_o/u_b)\cos(\gamma_o)}{\sqrt{1-(u_o/u_b)^2\sin^2(\gamma_o)}}, \tag{6.47a}$$

$$Q(\gamma_o) \triangleq \frac{\sin(\gamma_o)}{u_b\sqrt{1-(u_o/u_b)^2\sin^2(\gamma_o)}}. \tag{6.47b}$$

Finally, we find the derivative of $\gamma_{\text{ad}}^{\pm}$ as

$$\begin{aligned}\dot{\gamma}_{\text{ad}}^{\pm} = \pm r \pm r_o P(\gamma_o^{\pm}) \mp a_o Q(\gamma_o^{\pm}) + \frac{U_{bo}}{d_{b,o}}(1 + P(\gamma_o^{\pm})) \dots \\ (\pm \sin(\psi_{bo}^n - \alpha) - \cos(\psi_{bo}^n - \alpha)\tan(\beta)) \,.\end{aligned} \tag{6.48}$$

The shortest distance to a conflict, γ_{ad}, satisfies (6.24). Hence,

$$\pm \sin(\psi_{bo}^n - \alpha) = |\sin(\psi_{bo}^n - \alpha)|. \tag{6.49}$$

The vehicle starts outside a conflict, i.e. satisfies (6.30). Hence, $|\tan(\psi_{bo}^n - \alpha)| \geq \tan(\beta)$, implying that

$$|\sin(\psi_{bo}^n - \alpha)| - \cos(\psi_{bo}^n - \alpha)\tan(\beta) \geq 0. \tag{6.50}$$

Furthermore, (6.47a) and (6.47b) are bounded by Assumption 6.4:

$$P(\gamma_o) \in \left[-\frac{u_o}{u_b}, \frac{u_o}{u_b}\right], \tag{6.51a}$$

$$Q(\gamma_o) \in \left[-\frac{1}{\sqrt{u_b^2 - u_o^2}}, \frac{1}{\sqrt{u_b^2 - u_o^2}}\right]. \tag{6.51b}$$

Since $u_b > u_o$, then $P(\gamma_o^{\pm}) \in (-1, 1)$. By the previous observations, (6.48) can be reduced to

$$\dot{\gamma}_{\text{ad}}^{\pm} \geq \pm r_b \pm r_o P(\gamma_o^{\pm}) \mp a_o Q(\gamma_o^{\pm}). \tag{6.52}$$

From (6.52) we can formulate a lower bound on the vehicle's required turning rate, based on Assumption 6.3 bounding the obstacle's turning rate and acceleration, Assumption 6.4 bounding the obstacle's speed, and the bounds (6.51). Thus, if vehicle satisfies

$$r_{b,\max} \geq r_{o,\max}\frac{u_{o,\max}}{u_b} + \frac{a_{o,\max}}{\sqrt{u_b^2 - u_{o,\max}^2}}, \tag{6.53}$$

then a continuous control input satisfying (6.31) also ensures that

$$\dot{\gamma}_{\text{ad}}(t) \geq 0, \quad \forall t \geq t_0, \tag{6.54}$$

meaning that the shortest angular distance to a conflict is either constant or increasing with time. Hence,

$$|\psi_{bo}^n(t) - \alpha(t)| \geq \beta(t), \quad \forall t \geq t_0, \tag{6.55}$$

which ensures that

$$d_{b,o}(t) - R_o \geq d_\epsilon, \quad \forall t \geq t_0, \tag{6.56}$$

by Lemma 5.2. □

Theorem 6.1 agrees with intuition. As long as the vehicle turns in the opposite direction of the nearest conflict, it will stay out of the conflict regardless of the obstacle's motion, on the condition that the vehicle's turning rate is large enough to compensate for any change in the obstacle's direction and/or speed. Intuitively, as the obstacle's maximum turning rate, forward acceleration or speed increases, the vehicle's required turning rate increases as well. We state the following assumption in order to ensure that the conditions of Theorem 6.1 are satisfied for the remainder of the analysis:

Assumption 6.5. The vehicle's maximum turning rate, $r_{b,\max}$, satisfies

$$r_{b,\max} \geq r_{o,\max}\frac{u_{o,\max}}{u_b} + \frac{a_{o,\max}}{\sqrt{u_b^2 - u_{o,\max}^2}}. \tag{6.57}$$

6.4.2 Turning out of conflict

Notice that the control input (6.29) satisfies the conditions of Theorem 6.1. The result is useful, because it proves that the vehicle, satisfying Assumption 6.5, will avoid a collision with the obstacle if the vehicle is able to turn out of a conflict before a collision occurs. In order to ensure this, we must choose the threshold distance of the switching condition (6.25) above a lower bound, derived in the following lemma.

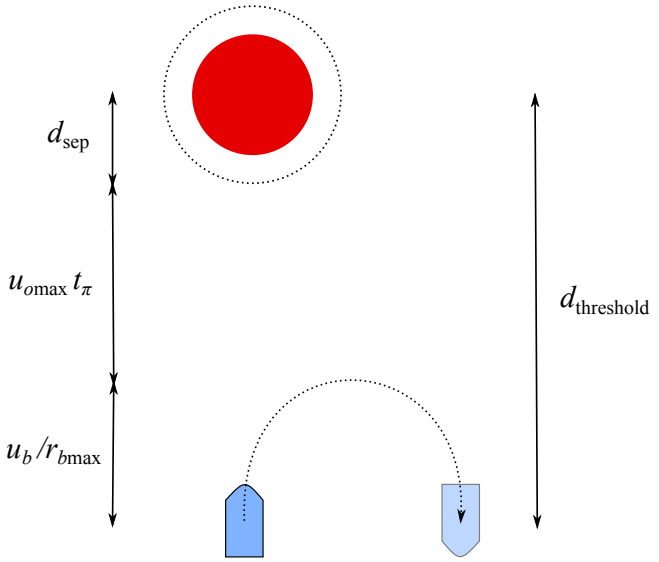

Figure 6.2: Representation of the minimum threshold distance.

Lemma 6.1. *Consider an obstacle described by* (6.6)*, and a vehicle described by* (6.1)*. Let the vehicle enter collision avoidance mode according to the switching rule* (6.25)*, and suppose the distance satisfies* $d_{b,o} = d_{\text{threshold}}$ *at this point in time. Let the control input be given by the collision avoidance algorithm* (6.29)*, and the turning direction be chosen by the turning rules* (6.27)-(6.28)*. Finally, let Assumption 6.1-6.5 hold. If the threshold distance satisfies*

$$d_{\text{threshold}} \geq u_{o,\max} t_\pi + d_{\text{sep}} + d_{\text{turn}}, \tag{6.58}$$

where

$$t_\pi := \frac{\pi}{r_{b,\max}}, \; d_{\text{turn}} := \frac{u_b}{r_{b,\max}}. \tag{6.59}$$

Then, the vehicle will successfully turn out of the conflict and reach a safe heading, before the obstacle is within the distance d_{sep} *of the vehicle.*

Proof. To prove this lemma, we will formulate an upper bound of the distance traveled by the vehicle and the obstacle during the vehicle's avoidance maneuver.

Figure 6.2 illustrates the worst case collision avoidance scenario in consideration. Let the obstacle move with maximum forward speed $u_o = u_{o,\max}$ towards the vehicle, and let the radius of the obstacle be infinitely large, such that $\beta \to \pi/2$. The angular distance to a safe heading can then at most be π. The vehicle will turn with maximum turning rate towards safety, by (6.29). Hence, the vehicle's trajectory lies on a circle with radius

$$d_{\text{turn}} = \frac{u_b}{r_{b,\max}}, \tag{6.60}$$

and time it takes for the vehicle obtain a safe heading is upper bounded by

$$t_\pi = \frac{\pi}{r_{b,\max}}. \tag{6.61}$$

It follows that if $d_{\text{threshold}}$ satisfies (6.58), then the vehicle will have successfully turned out of the conflict before the distance between the vehicle and the obstacle is reduced to less than d_{sep}. □

6.4.3 Safe target reaching

In this section, we will provide the conditions ensuring that the kinematic vehicle (6.1), following the collision avoidance algorithm presented in Section 6.3, will navigate safely in the presence of a moving obstacle, while being guided towards a static target by the guidance law (6.9). Before presenting the main theorem, we state the following, well-known result:

Lemma 6.2. *Consider a static target $\boldsymbol{p}_{\text{t}}^n$. The origin of the pure pursuit guidance law*

$$\boldsymbol{v}_{\text{pp}}^n = -\kappa \frac{\tilde{\boldsymbol{p}}^n}{\|\tilde{\boldsymbol{p}}^n\|}, \tag{6.62}$$

where $\tilde{\boldsymbol{p}}^n = \boldsymbol{p}_{nb}^n - \boldsymbol{p}_{\text{t}}^n$ and $\kappa > 0$, is then UGAS.

Proof. Consider the Lyapunov function candidate

$$V = \frac{1}{2} (\tilde{\boldsymbol{p}}^n)^\top \tilde{\boldsymbol{p}}^n. \tag{6.63}$$

The time-derivative of V along the trajectories of $\tilde{\boldsymbol{p}}^n$ is

$$\dot{V} = \left(\tilde{\boldsymbol{p}}^n\right)^\top \tilde{\boldsymbol{v}}^n. \tag{6.64}$$

The target is static, hence $\tilde{\boldsymbol{v}}^n = \boldsymbol{v}_{\text{pp}}^n - \boldsymbol{v}_{\text{t}}^n = \boldsymbol{v}_{\text{pp}}^n$, which yields

$$\dot{V} = -\kappa \frac{\left(\tilde{\boldsymbol{p}}^n\right)^\top \tilde{\boldsymbol{p}}^n}{\|\tilde{\boldsymbol{p}}^n\|} < 0 \ \forall \tilde{\boldsymbol{p}}^n \neq 0. \tag{6.65}$$

The Lyapunov function candidate (6.63) is positive definite and radially unbounded, and its derivative with respect to time, $\dot{V}$, is negative definite. Hence, the origin $\tilde{\boldsymbol{p}} = 0$ is UGAS. □

Theorem 6.2. *Consider an obstacle described by (6.6), and a vehicle described by (6.1). Let the acceptance distance satisfy*

$$d_a \geq \frac{u_b}{r_{b,\max}}. \tag{6.66}$$

If Assumption 6.1-6.5 hold, the vehicle follows the pure pursuit guidance law (4.13) with the heading controller (6.15), the switching rules (6.25)-(6.26), and the turning rules (6.27)-(6.29). Then, the vehicle will come within an acceptable distance, d_a, of the target position $\boldsymbol{p}_{\text{t}}^n$, while maintaining a distance to the obstacle satisfying

$$d_{b,o}(t) - R_o \geq d_\epsilon, \ \forall t \in [t_0, \, t_{\text{f}}], \tag{6.67}$$

where $t_{\text{f}} < \infty$ is the time of arrival at $\boldsymbol{p}_{\text{t}}^n$, provided the vehicle and the obstacle are initially separated by the distance:

$$d_{b,o}(t_0) \geq d_{\text{threshold}}, \tag{6.68}$$

satisfying

$$d_{\text{threshold}} \geq R_o + d_\epsilon + \frac{u_b + \pi u_{o,\max}}{r_{b,\max}}. \tag{6.69}$$

Proof. Let the vehicle enter collision avoidance mode at the time $t_1 \geq t_0$ as the distance

satisfies $d_{b,o}(t_1) = d_{\text{threshold}}$. Lemma 6.1 and condition (6.69) then ensures that the vehicle will reach a safe heading, satisfying

$$|\psi_{bo}^n - \alpha| \geq \beta, \tag{6.70}$$

before the obstacle is within the safety distance of the vehicle. Since the vehicle maintains a continuous control input satisfying (6.29) until the control system exits collision avoidance mode at the time $t_2 > t_1$, it is ensured that $d_{b,o}(t) - R_o \geq d_\epsilon, \ \forall t \in [t_0, t_2]$, by Theorem 6.1.

The obstacle may turn, causing the vehicle to enter collision avoidance mode as the distance satisfies $d_{b,o} < d_{\text{threshold}}$. It follows from the turning rule (6.28) and the control input (6.29) that the vehicle will then immediately turn away from the conflict at maximum turning rate, thus ensuring that the vehicle cannot enter the conflict, i.e. satisfies (6.70) at all times. Hence, by Theorem 6.1 the vehicle satisfies

$$d_{b,o}(t) - R_o \geq d_\epsilon, \ \forall t \in [t_0, t_\text{f}], \tag{6.71}$$

where t_f is the time of arrival at $\boldsymbol{p}_\text{t}^n$.

Finally, since $u_b > u_{o,\max}$ the vehicle will escape the obstacle at some point in time and proceed to the target $\boldsymbol{p}_\text{t}^n$. An upper bound of the required turning rate when the vehicle follows the pure pursuit guidance law can be found geometrically as

$$|r_b| \leq \frac{u_b}{d_a}. \tag{6.72}$$

Hence, the acceptance distance must satisfy

$$\frac{u_b}{d_a} \leq r_{b,\max}, \tag{6.73}$$

by Assumption 6.2. Since the origin of the pure pursuit guidance law is globally uniformly asymptotically stable for a static target by Lemma 6.2, and the acceptance distance satisfies (6.66), it is ensured that the vehicle position $\boldsymbol{p}_{nb}^n$ converges to within d_a of the target position $\boldsymbol{p}_\text{t}^n$, in finite time. □

6.4.4 Safe path following

In this section, we will provide the conditions to ensure that the vehicle safely converges to, and follows a predefined path in the presence of a moving obstacle, when the vehicle follows the line of sight guidance law (6.11), and the collision avoidance algorithm described in Section 6.3. Before presenting the final theorem of the chapter, we state the following, well-known result:

Lemma 6.3. *Let the path-tangential angle χ_p be defined as (6.12), the cross-track error y_e be defined as (6.13), and the lookahead distance satisfy $\Delta > 0$. Then, the LOS guidance law*

$$\psi_{\mathrm{los}}^n(y_\mathrm{e}) = \chi_p + \arctan\left(\frac{-y_\mathrm{e}}{\Delta}\right) \tag{6.74}$$

ensures that the cross-track error y_e of the system (6.1) converges globally uniformly asymptotically to the origin.

Proof. Consider the Lyapunov function candidate

$$\frac{1}{2}y_\mathrm{e}^2. \tag{6.75}$$

The time-derivative of V along the trajectories of y_e is

$$\dot{V} = y_\mathrm{e}\dot{y}_\mathrm{e}. \tag{6.76}$$

The time-derivative of the cross-track error y_e is computed from (6.13) and (6.1) as

$$\dot{y}_\mathrm{e} = -\dot{x}_b^n \sin(\chi_p) + \dot{y}_b^n \cos(\chi_p) \tag{6.77}$$

$$= -u_b \cos(\psi_{\mathrm{los}}^n) \sin(\chi_p) + u_b \sin(\psi_{\mathrm{los}}^n) \cos(\chi_p). \tag{6.78}$$

Inserting the LOS guidance law (6.74) we obtain:

$$\dot{y}_{\mathrm{e}} = u_b \sin\left(\arctan\left(\frac{-y_{\mathrm{e}}}{\Delta}\right)\right) \tag{6.79}$$

$$= -u_b \frac{y_{\mathrm{e}}}{\Delta\sqrt{\left(\frac{y_{\mathrm{e}}}{\Delta}\right)^2 + 1}}. \tag{6.80}$$

Hence,

$$\dot{V} = -u_b \frac{y_{\mathrm{e}}^2}{\Delta\sqrt{\left(\frac{y_{\mathrm{e}}}{\Delta}\right)^2 + 1}} < 0, \ \forall y_{\mathrm{e}} \neq 0. \tag{6.81}$$

The Lyapunov function candidate (6.75) is radially unbounded and positive definite, and its derivative with respect to time, $\dot{V}$, is negative definite. Hence, the cross-track error y_{e} converges globally uniformly asymptotically to the origin, i.e. $\lim_{t\to\infty} y_{\mathrm{e}} = 0$. □

Theorem 6.3. *Consider an obstacle described by (6.6), and a vehicle described by (6.1). Let the lookahead distance satisfy*

$$\Delta \geq \frac{u_b}{r_{b,\max}}. \tag{6.82}$$

If Assumption 6.1-6.5 hold, the vehicle follows the line of sight guidance law (6.11) with the heading controller (6.15), the switching rules (6.25)-(6.26), and the turning rules (6.27)-(6.29). Then, the vehicle will converge to, and follow the path $\mathcal{P}$, while maintaining a distance to the obstacle satisfying

$$d_{b,o}(t) - R_o \geq d_\epsilon, \ \forall t \geq t_0, \tag{6.83}$$

provided the vehicle and the obstacle initially are separated by a distance:

$$d_{b,o}(t_0) \geq d_{\text{threshold}}, \tag{6.84}$$

satisfying

$$d_{\text{threshold}} \geq R_o + d_\epsilon + \frac{u_b + \pi u_{o,\max}}{r_{b,\max}}. \tag{6.85}$$

Proof. The proof of Theorem 6.2 ensures that (6.83) is satisfied when the stated conditions hold. Since $u_b > u_{o,\max}$, the vehicle will at some point in time escape the obstacle, and proceed towards the path. The required turning rate when the vehicle follows the LOS guidance law is computed from (6.11) as

$$\dot{\psi}^n_{\text{los}} = -\frac{\Delta \dot{y}_e}{\Delta^2 + y_e^2}, \tag{6.86}$$

where y_e is the cross-track error defined in (6.13), and $\Delta > 0$ is the lookahead distance. An upper bound of the required turning rate is found from (6.86), as

$$|r_b| \leq \frac{u_b}{\Delta}. \tag{6.87}$$

Hence, the lookahead distance must satisfy

$$\frac{u_b}{\Delta} \leq r_{b,\max}, \tag{6.88}$$

by Assumption 6.2. Since the line of sight guidance law ensures global uniform asymptotic convergence of the vehicle onto a given path by Lemma 6.3, and the lookahead distance satisfies (6.82), the vehicle is ensured to converge to the path $\mathcal{P}$ in finite time, and for the remainder of the time, follow along it. □

6.5 Simulations

This section presents two numerical simulations of the kinematic vehicle (6.1), following the collision avoidance algorithm presented in Section 6.3, for avoiding a moving obstacle described by (6.6). In the first scenario, the vehicle's control objective is to reach a target position. In the second scenario, the objective is to converge to, and follow a straight line path in this frame. Both objectives are given with respect to the NED frame.

In both simulations the vehicle's forward speed is constant and equal to $u_b = 2$ m/s, and the maximum turning rate is equal to $r_{b,\max} = 0.5$ rad/s. The initial position of the vehicle was chosen as $[0,\ 0]$ m. The obstacle's radius was chosen as $R_o = 10$ m,

the safety distance as $d_\epsilon = 5$ m, and the angular safety distance as $\sigma = 0.09$ rad, or approximately 5 degrees. The speed, acceleration and turning rate of the obstacle will be specified for each simulation example.

6.5.1 Target reaching

This section presents a numerical simulation of the vehicle traveling towards a target position, chosen as $\boldsymbol{p}_{\mathrm{t}}^n = [140,\ 0]$ m, by following the pure pursuit guidance law (6.9), while avoiding a collision with a moving obstacle by following the VO algorithm. The obstacle both turns and accelerates as the vehicle approaches it, with constant acceleration $a_o = a_{o,\max} = 0.05$ m/s^2, and constant turning rate $r_o = r_{o,\max} = 0.1$ rad/s. The initial speed of the obstacle was chosen as $u_o(t_0) = 0$ m/s, and the maximum speed as $u_{o,\max} = 1.8$ m/s, satisfying Assumption 6.4. With these parameters, the threshold distance was computed as $d_{\text{threshold}} = 30.3$ m, in accordance with Theorem 6.2. Assumption 6.5 holds as well, verified by direct calculation. The acceptance distance was chosen as $d_a = 4$ m, satisfying the condition of Theorem 6.2.

Trajectories of the vehicle and the obstacle are shown in Figure 6.3. The relative guidance velocity, denoted $\boldsymbol{v}_{\mathrm{ndgo}}^n \triangleq \boldsymbol{v}_{\mathrm{ndg}}^n - \boldsymbol{v}_{no}^n$, is shown as the blue arrow, in order to demonstrate when the vehicle enters and exits collision avoidance mode. The obstacle can be seen to move in a clockwise circle as it increases its forward speed. The vehicle enters collision avoidance mode as the distance satisfies $d_{b,o} < d_{\text{threshold}}$, and turns right according to the turning rule (6.28), seen in Figure 6.3a and 6.3b. Even though the obstacle turns directly towards the vehicle for some time, while increasing its forward speed, the vehicle avoids a collision by continuously turning away from the conflict. The vehicle safely exits collision avoidance mode at $t = 54$ s, seen in Figure 6.3c. Finally, at $t = 80$ s, the vehicle reaches the target without collision.

The distance between the obstacle and the vehicle, $d_{b,o}(t)$, is plotted against the threshold distance $d_{\text{threshold}}$, and the minimum safety distance $R_{o|\epsilon} \triangleq R_o + d_\epsilon$, in Figure 6.4a. The obstacle's forward speed, $u_o(t)$, is plotted as well. It can be seen that the vehicle is able to maintain at least the minimum safety distance from the obstacle at all times during the collision avoidance scenario. Hence, the simulation result agrees

with the theoretical result of Theorem 6.2.

6.5.2 Path following

In this section, we present a numerical simulation of the vehicle following the LOS guidance law (6.11), while also avoiding a collision with a moving obstacle by following the VO algorithm. The path $\mathcal{P}$ was chosen parallel to the x^n axis, with target position along the y^n axis equal to $y_{\text{t}}^n = 10$ m. The lookahead distance was chosen as $\Delta = 10$, satisfying the condition of Theorem 6.3.

In this scenario, the obstacle approaches the vehicle head on and increases its forward speed, with constant acceleration $a_o = a_{o,\max} = 0.05$ m/s^2. The initial speed of the obstacle was chosen as $u_o(t_0) = 0$ m/s, and the maximum speed as $u_{o,\max} = 1.9$ m/s, satisfying Assumption 6.4. The obstacle does not turn, i.e. $r_o = r_{o,\max} = 0$ rad/s. The required threshold distance is then computed as $d_{\text{threshold}} = 30.9$ m, in accordance with Theorem 6.3. Assumption 6.5 holds with the current parameters.

Trajectories of the vehicle and the obstacle are shown in Figure 6.5. The vehicle converges to the path, but is forced to leave it once the obstacle comes within the threshold distance of the vehicle. The vehicle enters collision avoidance mode as the distance satisfies $d_{b,o} = d_{\text{threshold}}$, and turns right according to the turning rule (6.27), as seen in Figure 6.5a and 6.5b. During this time, the obstacle accelerates in the direction of the vehicle. Despite this, the vehicle safely maneuvers around the obstacle by maintaining a continuous control input satisfying (6.29), and finally exits collision avoidance mode at $t = 35$ s, seen in Figure 6.5c. The vehicle then escapes the obstacle completely, and converges to the path once again, as seen in Figure 6.5d.

The distance between the obstacle and the vehicle, $d_{b,o}(t)$, is plotted against the threshold distance $d_{\text{threshold}}$, and the minimum safety distance $R_{o|\epsilon}$, in Figure 6.4b. The obstacle's forward speed, $u_o(t)$, is plotted as well. It can be seen that the distance remains above the minimum safety distance at all times during the collision avoidance scenario. Hence, the simulation result supports the theoretical result of Theorem 6.3.

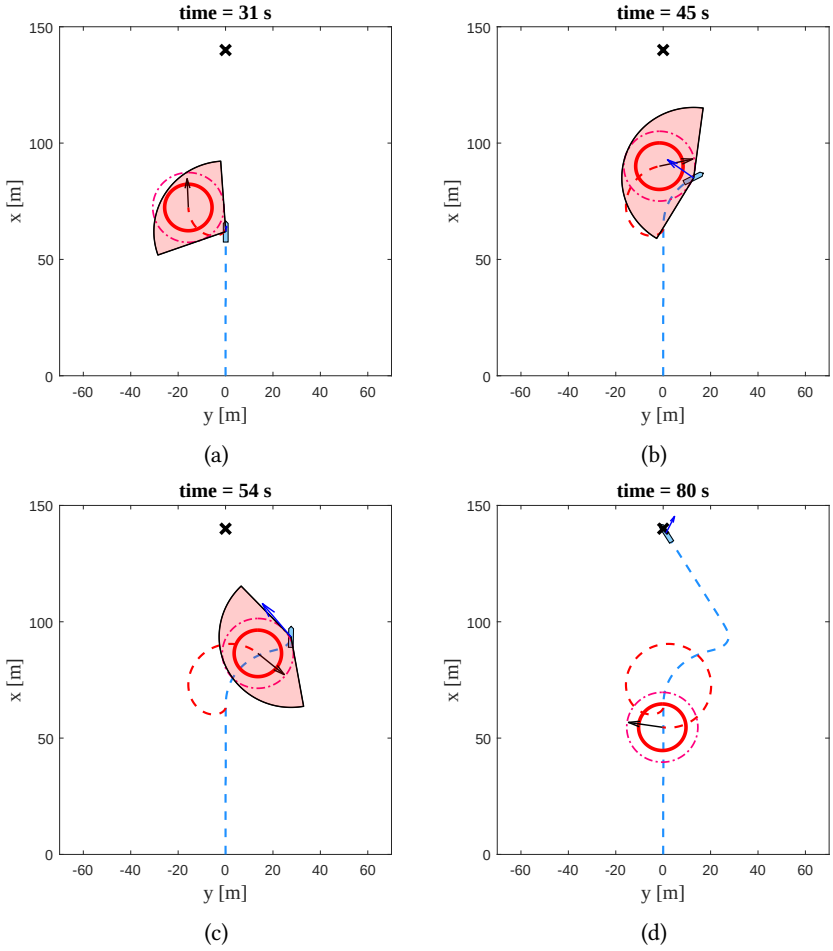

Figure 6.3: First simulation scenario of a nonholonomic vehicle reactively avoiding collision, guided by the pure pursuit guidance law. The obstacle is the red circle, the vehicle is the blue polygon, and the safety distance is the magenta line encircling the obstacle. The trajectories of the vehicle and the obstacle are the blue and red, dashed lines, respectively. The collision cone, $\mathcal{CC}$, is the red cone, and the relative guidance velocity, $\boldsymbol{v}^n_{ndgo}$, is the blue arrow. The target position is marked as an 'X'.

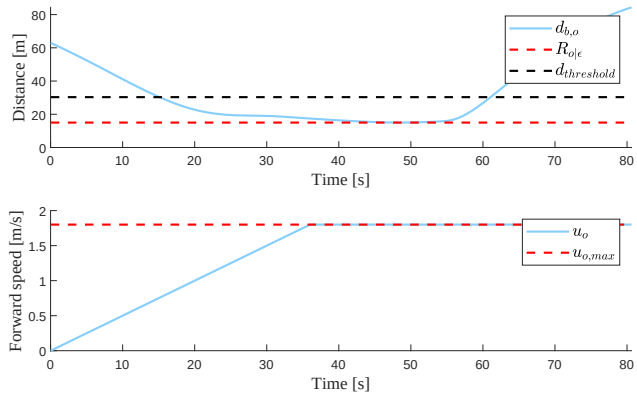

(a) Distance, $d_{b,o}$, and forward speed of the obstacle, u_o, during the first simulation.

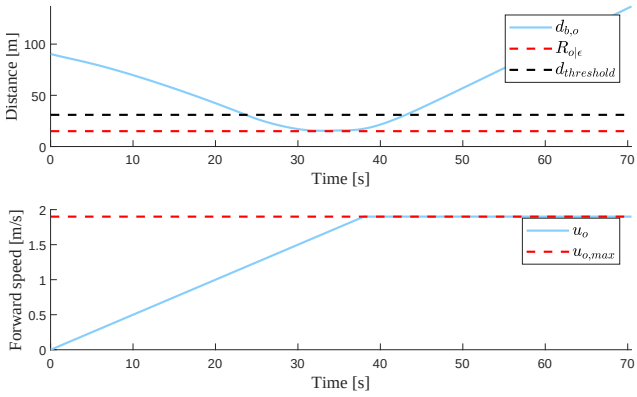

(b) Distance, $d_{b,o}$, and forward speed of the obstacle, u_o, during the second simulation.

Figure 6.4: Distance between the vehicle and the obstacle, and forward speed of the obstacle, during both simulations.

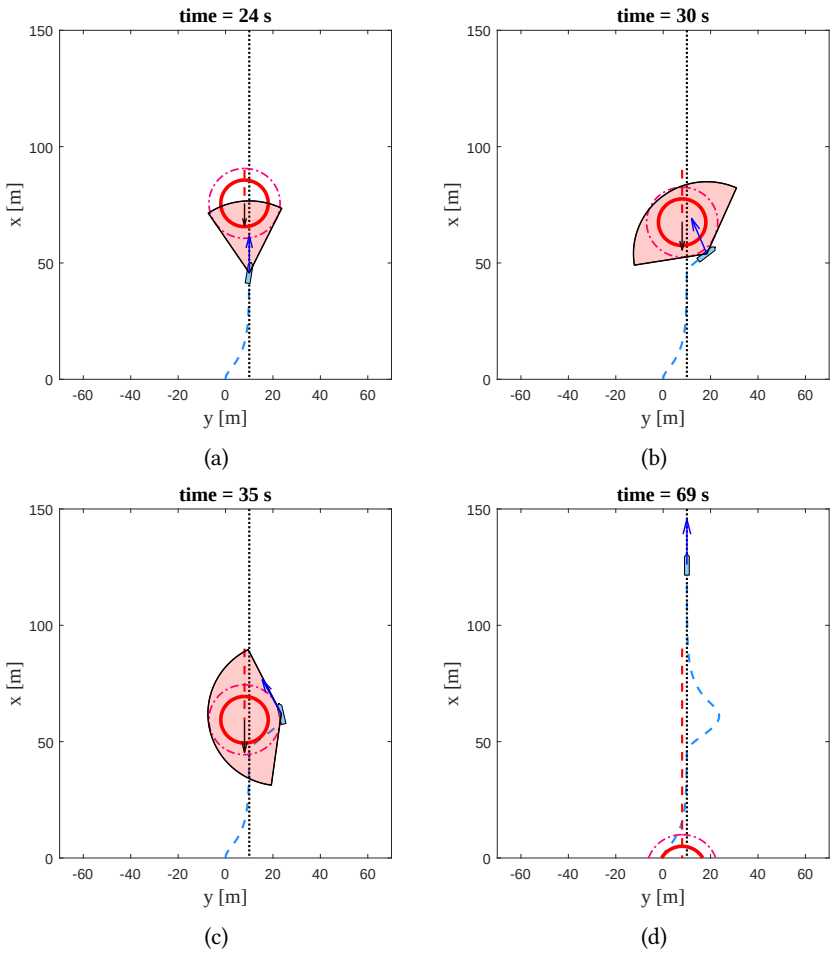

Figure 6.5: Second simulation scenario of a nonholonomic vehicle reactively avoiding collision, guided by the LOS guidance law. The path $\mathcal{P}$ is represented by the dotted line.

Chapter 7

The Velocity Obstacle Algorithm for Vehicles with Underactuated Dynamics

In this chapter, we extend the unicycle model to include the underactuated sway dynamics of the marine vehicle modeled in Chapter 3. Even though the vehicle cannot produce control forces in the sway direction, swaying motions will naturally be induced by the vehicle's turning motion. Recall from Chapter 4 that the vehicle's heading will deviate from its course for nonzero sway speeds. Since the course cannot be controlled directly, the control system needs to continuously compensate for the crab angle induced by the sway speed in order to track the desired course.

In order to derive a minimum threshold distance, deciding when to start the avoidance maneuver, the size of the sway speed needs to be bounded. Since the vehicle is required to turn during both guidance and collision avoidance, measures must be taken to ensure that this is achieved. This means, among other things, that we need to limit the vehicle's turning motion during collision avoidance, and also during the vehicle's nominal behaviour. Such limitations will be dealt with in this chapter, in

order to guarantee safety of the vehicle in the underactuated case.

7.1 System description

In this section, we will present the model used to describe a vehicle with underactuated dynamics, the vehicle's control objective, and the model used to describe a moving obstacle.

7.1.1 Vehicle model

The vehicle is modeled as an underactuated, marine vehicle moving in 3 DOF, modeled in Chapter 3. In this part of the thesis, we will assume that the surge speed and yaw rate can be perfectly controlled, thus acting as virtual control inputs:

Assumption 7.1. The surge speed, u_b, and yaw rate, r_b, can be perfectly controlled. Moreover, the surge speed $u_b > 0$ is constant.

The model becomes:

$$\dot{x}_b^n = u_b \cos(\psi_b^n) - v_b \sin(\psi_b^n), \tag{7.1a}$$
$$\dot{y}_b^n = u_b \sin(\psi_b^n) + v_b \cos(\psi_b^n), \tag{7.1b}$$
$$\dot{\psi}_b^n = r_b, \tag{7.1c}$$
$$\dot{v}_b = f_v(u_b, v_b, r_b), \tag{7.1d}$$

where the expression of $f_v(\cdot)$ is given in Appendix 7.A. The surge and yaw dynamics will be included later on, in Chapter 8. The term $f_v(u_b, v_b, r_b)$ can be expressed as

$$f_v(u_b, v_b, r_b) \triangleq X(u_b) r_b + Y(u_b) v_b, \tag{7.2}$$

where $X(u_b)$ and $Y(u_b)$ are given in Appendix 7.A. It can be noticed that the terms are constant by Assumption 7.1.

Assumption 7.2. The term $Y(u_b)$ satisfies

$$Y(u_b) < 0. \tag{7.3}$$

Assumption 7.2 ensures that the vehicle is nominally stable in sway, which is the case for most commercial vessels by design.

7.1.2 Control objective

In this chapter we only consider target reaching, as the results can easily be extended to yield safe path-following, as is done in the subsequent chapter. Hence, the control objective of the vehicle is to come within an acceptable distance $d_{\mathrm{a}} > 0$ of a target position $\boldsymbol{p}_{\mathrm{t}}^n \triangleq [x_{\mathrm{t}}^n, y_{\mathrm{t}}^n]^\top$, at an unspecified point in time $t_{\mathrm{f}} \in [t_0, \infty)$, while keeping at least a minimum safety distance, d_ϵ, from the obstacle at all times:

$$d_{b,o}(t) - R_o \geq d_\epsilon > 0, \quad \forall t \in [t_0, t_{\mathrm{f}}]\,. \tag{7.4}$$

Furthermore, in order to prevent the vehicle from colliding side-ways into the obstacle, the vehicle is required to maintain a limited sway speed, satisfying

$$|v_b(t)| \leq v_{b,\max}, \ \ \forall t \in [t_0, t_{\mathrm{f}}]\,, \tag{7.5}$$

where $v_{b,\max} > 0$ is a constant design parameter. To ensure this, the following assumption must hold:

Assumption 7.3. The vehicle's initial sway speed, $v_b(t_0)$, satisfies

$$|v_b(t_0)| \leq v_{b,\max}. \tag{7.6}$$

7.1.3 Obstacle model

As in Chapter 6, the obstacle is modeled as a moving, circular domain $\mathcal{D}_o$, with radius R_o, described by the kinematic equations:

$$\dot{x}_o^n = u_o \cos(\psi_o^n), \tag{7.7a}$$
$$\dot{y}_o^n = u_o \sin(\psi_o^n), \tag{7.7b}$$
$$\dot{\psi}_o^n = r_o, \tag{7.7c}$$
$$\dot{u}_o = a_o. \tag{7.7d}$$

The obstacle is subject to the kinematic constraints:

Assumption 7.4. The obstacle's heading rate, r_o, and forward acceleration, a_o, are bounded by

$$\begin{aligned} r_o &\in [-r_{o,\max},\, r_{o,\max}], \\ a_o &\in [-a_{o,\max},\, a_{o,\max}], \end{aligned} \tag{7.8}$$

where $r_{o,\max} \geq 0$ and $a_{o,\max} \geq 0$ are constant parameters.

In order to ensure the vehicle is able to avoid a collision with the obstacle, the following assumption must be met:

Assumption 7.5. The obstacle's forward speed $0 \leq u_o \leq u_{o,\max}$ satisfies

$$u_{o,\max} < \begin{cases} u_b, & \text{if } X(u_b) > -\frac{1}{2}u_b, \\ -\frac{u_b^2}{X(u_b)} - u_b, & \text{if } -\frac{1}{2}u_b \geq X(u_b) > -u_b. \end{cases} \tag{7.9}$$

Remark 7.1. Assumption 7.5 ensures that the vehicle's required turning rate during collision avoidance is well-defined, derived in the analysis given in Section 7.4.

7.2 Guidance and control

In guidance mode, the pure pursuit guidance law will be employed for guiding the vehicle towards a static position in the world frame. In order to follow the course references generated by the guidance system and the collision avoidance algorithm, the vehicle employs a proportional heading controller, while compensating for the crab angle induced by the sway speed.

7.2.1 Guidance law

In nominal guidance mode, the vehicle's course references will be given by the pure pursuit guidance law, generating a velocity vector along the line of sight vector between the vehicle and the target:

$$\boldsymbol{v}_{\text{pp}}^n \triangleq -U_b \frac{\tilde{\boldsymbol{p}}^n}{\|\tilde{\boldsymbol{p}}^n\|}, \tag{7.10}$$

where $\tilde{\boldsymbol{p}}^n \triangleq \boldsymbol{p}_{nb}^n - \boldsymbol{p}_{\text{t}}^n$, and $U_b \triangleq \sqrt{u_b^2 + v_b^2} > 0$ is the speed of vehicle. The desired course is given by

$$\chi_{\text{pp}}^n \triangleq \angle \boldsymbol{v}_{\text{pp}}^n. \tag{7.11}$$

7.2.2 Heading controller

The heading controller is stated as in [25]:

$$r_b = \dot{\psi}_{\text{db}}^n - \lambda_\psi \tilde{\psi}, \tag{7.12}$$

where $\lambda_\psi > 0$ is the heading control gain, and the heading error $\tilde{\psi} \triangleq \psi_b^n - \psi_{\text{db}}^n$ is mapped to the interval $(-\pi, \pi]$ to ensure that the vehicle always takes the shortest turn. It is straight-forward to verify that the heading controller ensures exponential stabilization of the heading error dynamics by (7.1c), for a positive gain $\lambda_\psi > 0$. We will derive the expressions of the desired heading, ψ_{db}^n, and its derivative, $\dot{\psi}_{\text{db}}^n$, below.

The vehicle's course is defined as the angle from the positive x^n axis to the velocity vector of the vehicle:

$$\chi_b^n \triangleq \angle \boldsymbol{v}_{nb}^n. \tag{7.13}$$

As presented in Chapter 4, the course may be written

$$\chi_b^n = \psi_b^n + \beta_c. \tag{7.14}$$

To obtain the desired heading angle, the crab angle must thus be subtracted from the desired course, defined as

$$\beta_c \triangleq \tan^{-1}\left(\frac{v_b}{u_b}\right). \tag{7.15}$$

Hence,

$$\psi_{\mathrm{d}b}^n \triangleq \chi_{\mathrm{d}b}^n - \beta_c, \tag{7.16}$$

where $\chi_{\mathrm{d}b}^n$ is desired course.

The time-derivative of the course is computed from (7.14) and (7.15), as

$$\dot{\chi}_b^n = \dot{\psi}_b^n \frac{U_b^2 + X(u_b)u_b}{U_b^2} + \frac{Y(u_b)v_b u_b}{U_b^2}. \tag{7.17}$$

Solving (7.17) for $\dot{\psi}_b^n$ yields

$$\dot{\psi}_b^n = \frac{U_b^2 \dot{\chi}_b^n - Y(u_b)v_b u_b}{U_b^2 + X(u_b)u_b}. \tag{7.18}$$

The control law (7.12) is well-defined if the denominator of (7.18) is nonzero. This is ensured by the assumption:

Assumption 7.6. The term $X(u_b)$ satisfies

$$u_b + X(u_b) > 0. \tag{7.19}$$

Remark 7.2. Assumption 7.6 ensures that a change in the vehicle's heading results in a change in the vehicle's course. This is the case for most commercial vessels by design.

It can be verified that Assumption 7.6 yields the following lower bound:

$$U_b^2 + X(u_b)u_b \geq au_b, \ a > 0, \tag{7.20}$$

thus ensuring that $\dot{\psi}_{\mathrm{db}}^n$ is well-defined. Furthermore, substituting the control law $\dot{\psi}_b^n = \dot{\psi}_{\mathrm{db}}^n - \lambda_\psi \tilde{\psi}$ into (7.17) where

$$\dot{\psi}_{\mathrm{db}}^n \triangleq \frac{U_b^2 \dot{\chi}_{\mathrm{db}}^n - Y(u_b)v_b u_b}{U_b^2 + X(u_b)u_b}, \tag{7.21}$$

and $\tilde{\psi} \triangleq \tilde{\chi}$, yields the course error dynamics given by

$$\dot{\tilde{\chi}} = -\lambda_\chi \tilde{\chi}, \tag{7.22}$$

where

$$\lambda_\chi \triangleq \lambda_\psi \frac{U_b^2 + X(u_b)u_b}{U_b^2}. \tag{7.23}$$

Remark 7.3. Assumption 7.6 ensures that $\lambda_\chi > 0$.

Thus, the heading controller (7.12) ensures exponential stabilization of the course error dynamics, when Assumption 7.6 holds.

7.3 Collision avoidance

The collision avoidance algorithm described in Chapter 5 will be used to generate course references for the vehicle in collision avoidance mode. The algorithm is summarized in this section. Note that the implementation of the algorithm is slightly different from what was presented in previous chapters, and that we operate with course rather than heading, as the sway speed can be nonzero.

The geometry of the velocity obstacle algorithm is shown in Figure 7.1. The edges of the collision cone can be described geometrically as

$$\psi_{\mathrm{t}}^{\pm} \triangleq \alpha \pm \beta, \tag{7.24}$$

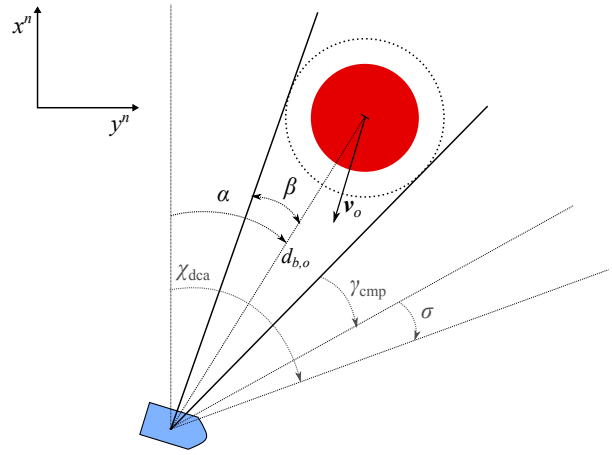

Figure 7.1: Geometric representation of the VO algorithm.

where

$$\beta \triangleq \sin^{-1}\left(\frac{R_{o|\epsilon}}{d_{b,o}}\right) \in \left(0, \frac{\pi}{2}\right]. \tag{7.25}$$

The vehicle is said to be in a conflict with the obstacle if $\chi^n_{bo} \triangleq \angle \boldsymbol{v}^n_{nbo}$ lies within the angular boundaries of collision cone:

$$|\chi^n_{bo} - \alpha| < \beta. \tag{7.26}$$

The edges of the absolute collision cone are defined geometrically as

$$\psi^{\pm}_{\text{abs}} \triangleq \gamma^{\pm}_{\text{cmp}} + \psi^{\pm}_{\text{t}}, \tag{7.27}$$

where the angle $\gamma^{\pm}_{\text{cmp}}$ compensates for the obstacle velocity, and is given by

$$\gamma^{\pm}_{\text{cmp}} = \sin^{-1}\left(\frac{u_o \sin(\gamma^{\pm}_o)}{U_b}\right). \tag{7.28}$$

The angle $\gamma_o^{\pm}$ is found geometrically as

$$\gamma_o^{\pm} = \pi + \psi_{\mathrm{t}}^{\pm} - \psi_o^n. \tag{7.29}$$

Recall in Chapter 6 that we made the vehicle maintain a constant, angular safety distance away from a conflict in collision avoidance mode. We now extend the collision cone (and equivalently the velocity obstacle), by a constant angle $\sigma > 0$ on each side. We denote the extended cones as $\mathcal{CC}_\sigma$ and $\mathcal{VO}_\sigma$, respectively.

Remark 7.4. The angle σ is an additional safety measure, ensuring that the vehicle cannot come too close to the obstacle. The choice of this angle will become apparent in the analysis given in Section 7.4.

The control system is switched to collision avoidance mode if the obstacle is too close the vehicle, simultaneously as the guidance velocity is unsafe:

$$d_{b,o}(t_1) \leq d_{\text{threshold}}, \;\; \boldsymbol{v}_{ndg}^n(t_1) \in \mathcal{VO}_\sigma(t_1), \tag{7.30}$$

where $\mathcal{VO}_\sigma$ is the extended velocity obstacle. Nominal guidance towards the target will resume when the guidance velocity is safe:

$$\boldsymbol{v}_{ndg}^n(t_2) \notin \mathcal{VO}_\sigma(t_2). \tag{7.31}$$

If the distance equals $d_{b,o} = d_{\text{threshold}}$ when CA mode is entered, the turning direction makes the vehicle seek to pass behind the obstacle:

$$d_{b,o} = d_{\text{threshold}}, \;\; j = \underset{j\in\{\pm\}}{\arg\max} \left| \psi_o^n - \psi_{\text{abs}}^{(j)} \right|, \tag{7.32}$$

where j is the turning parameter. If the distance is less than $d_{\text{threshold}}$, the vehicle will instead turn away from the nearest conflict to ensure safety:

$$d_{b,o} < d_{\text{threshold}}, \;\; j = \underset{j\in\{\pm\}}{\arg\min} \left| \chi_b^n - \psi_{\text{abs}}^{(j)} \right|. \tag{7.33}$$

The course references in collision avoidance mode will make the vehicle avoid a collision with a nearby obstacle, given by

$$\chi^n_{\text{dca}j} \triangleq \psi^{(j)}_{\text{abs}} \pm \sigma, \ j \in \{\pm\}, \tag{7.34}$$

where the turning direction j is chosen by the rules presented above. It can noticed that the course candidates (7.34) correspond to the edges of the extended, absolute collision cone, as illustrated in Figure 7.1.

7.4 Analysis

In this section, we present a mathematical analysis of the velocity obstacle algorithm described in Section 7.3, applied to a vehicle with underactuated dynamics, modeled by (7.1), for collision avoidance of a single, circular obstacle, described by the kinematic model (7.7).

In the first lemma, we will prove that the safety angle, σ, introduced in Section 7.3 makes the vehicle maintain a constant distance from the obstacle, providing an upper bound of the angle β.

Lemma 7.1. *Consider an obstacle moving with a time-varying velocity $\boldsymbol{v}^n_{no}(t)$, and let the vehicle and the obstacle initially be separated by a distance $d_{b,o}(t_0) > \frac{R_{o|\epsilon}}{\cos(\sigma)}$, for a constant angle $\sigma \in (0, \pi/2]$. If the vehicle maintains a course angle satisfying*

$$|\chi^n_{bo}(t) - \alpha(t)| = \beta(t) + \sigma, \ \forall t \geq t_0, \tag{7.35}$$

where β is defined in (7.25), then the vehicle will converge to a circle with radius

$$\frac{R_{o|\epsilon}}{\cos(\sigma)}, \tag{7.36}$$

and center in the obstacle center, $\boldsymbol{p}^n_{no}$. Moreover, if the vehicle maintains a course angle satisfying

$$|\chi^n_{bo}(t) - \alpha(t)| \geq \beta(t) + \sigma, \ \forall t \geq t_0, \tag{7.37}$$

then

$$d_{b,o}(t) \geq \frac{R_{o|\epsilon}}{\cos(\sigma)}, \ \forall t \geq t_0, \tag{7.38}$$

and

$$\beta(t) \in [0, \frac{\pi}{2} - \sigma], \ \forall t \geq t_0. \tag{7.39}$$

Proof. Consider the line segment going from the vehicle center, $\boldsymbol{p}^n_{nb}$, to the obstacle center, $\boldsymbol{p}^n_{no}$, with length $d_{b,o}$ and orientation α. The time-derivative of $d_{b,o}$ is found geometrically as

$$\dot{d}_{b,o} = -U_{bo} \cos(\chi^n_{bo} - \alpha), \tag{7.40}$$

where $U_{bo} \triangleq \|\boldsymbol{v}^n_{nb} - \boldsymbol{v}^n_{no}\|$. Let (7.35) hold, we can then write (7.40) as

$$\dot{d}_{b,o} = -U_{bo} \cos(\beta + \sigma). \tag{7.41}$$

Notice that $(\beta + \sigma) \in (0, \pi]$. Hence, from (7.41), if $\beta < \pi/2 - \sigma$ then $\dot{d}_{b,o} < 0$. If $\beta > \pi/2 - \sigma$ then $\dot{d}_{b,o} > 0$, and if and only if $\beta = \pi/2 - \sigma$ then $\dot{d}_{b,o} = 0$. Thus, $\dot{d}_{b,o} \to 0$ and $\beta \to \pi/2 - \sigma$ as $t \to \infty$. Since β is defined as (7.25), we can solve for the distance $d_{b,o}$:

$$\sin^{-1}\left(\frac{R_{o|\epsilon}}{d_{b,o}}\right) = \frac{\pi}{2} - \sigma \implies d_{b,o} = \frac{R_{o|\epsilon}}{\cos(\sigma)}. \tag{7.42}$$

Now, let (7.37) hold. By (7.40) the angle β then satisfies

$$\beta \leq \left|\cos^{-1}\left(-\frac{\dot{d}_{b,o}}{U_{bo}}\right)\right| - \sigma. \tag{7.43}$$

Since the initial distance satisfies $d_{b,o}(t_0) > \frac{R_{o|\epsilon}}{\cos(\sigma)}$, then $\beta(t_0) < \pi/2 - \sigma$. Thus, we only need to consider when $\dot{d}_{b,o} \leq 0$, since β is decreasing for $\dot{d}_{b,o} > 0$ by (7.25). The maximum of (7.43) is then found at $\dot{d}_{b,o} = 0$. Hence,

$$\frac{\pi}{2} - \sigma \geq \beta \geq 0, \tag{7.44}$$

and

$$d_{b,o} \geq \frac{R_{o|\epsilon}}{\cos(\sigma)}, \tag{7.45}$$

which concludes the proof.

□

When the vehicle turns, a swaying motion will be induced, seen by (7.1d). Since the sway dynamics are underactuated, we cannot control this speed directly. Thus, in order to satisfy the control objective (7.5), the control input r_b cannot be chosen arbitrarily large. The next lemma provides the necessary conditions ensuring that the magnitude of the sway speed is upper bounded, adopted from Wiig et al. [25].

Lemma 7.2. *Consider a vehicle described by* (7.1)*, and let Assumption* 7.2 *hold. Suppose the heading rate,* r_b*, is dependent on the sway speed,* v_b*, in a way that the following holds:*

$$|r_b(v_{b,\max})| < \frac{|Y(u_b)|}{|X(u_b)|} v_{b,\max}. \tag{7.46}$$

Then, if $|v_b(t_0)| \leq v_{b,\max}$*,*

$$|v_b(t)| \leq v_{b,\max}, \ \forall t \geq t_0. \tag{7.47}$$

Proof. Consider the Lyapunov function candidate given by

$$V = \frac{1}{2} v_b^2. \tag{7.48}$$

The time derivative of V along the trajectories of (7.1d) is

$$\dot{V} = X(u_b) r_b v_b + Y(u_b) v_b^2. \tag{7.49}$$

By Assumption 7.2, Equation (7.49) is bounded by

$$\dot{V} \leq |X(u_b)| \, |r_b| \, |v_b| - |Y(u_b)| \, v_b^2. \tag{7.50}$$

It follows from (7.50) values of r_b satisfying

$$|r_b| < \frac{|Y(u_b)|}{|X(u_b)|}|v_b| \tag{7.51}$$

ensures

$$\dot{V} < 0 \ \forall v_b \in \mathbb{R}/\{0\}. \tag{7.52}$$

Define the level set

$$\Omega_c = \{ v_b \in \mathbb{R} \mid V \leq \frac{1}{2} v_{b,\max}^2 \}. \tag{7.53}$$

The condition (7.52) ensures that any trajectory starting inside the set Ω_c can never come out again. Hence, if (7.46) holds, then any initial value of v_b satisfying $|v_b(t_0)| \leq v_{b,\max}$ ensures $|v_b(t)| \leq v_{b,\max}, \ \forall t \geq t_0$. □

We have established that the angle σ can be used to bound β and the distance $d_{b,o}$, and the choice of r_b can be used to bound the sway speed. To ensure that the control objective is satisfied, we must design the control law (7.12) with the conditions of Lemma 7.1 and 7.2 in mind. The maximum sway velocity, $v_{b,\max}$, and the safety angle, σ, act as design parameters in this regard. Before stating the next lemma, we define the following term for conciseness:

$$\begin{aligned} f_\psi(u_b, \sigma) \triangleq v_{b,\max} |Y(u_b)| \left(\frac{1}{|X(u_b)|} - \frac{2}{U_{b,\max}^2} \left(\frac{u_{o,\max} v_{b,\max}}{\sqrt{U_{b,\max}^2 - u_{o,\max}^2}} + u_b \right) \right) \\ - r_{o,\max} \frac{u_{o,\max}}{u_b} - \frac{a_{o,\max}}{\sqrt{u_b^2 - u_{o,\max}^2}} - \left(1 + \frac{u_{o,\max}}{U_{b,\max}} \right) \frac{U_{bo,\max}}{(R_o + d_\epsilon)\tan(\sigma)}, \end{aligned} \tag{7.54}$$

where we define $U_{b,\max} \triangleq \sqrt{v_{b,\max}^2 + u_b^2}$, and

$$U_{bo,\max} \triangleq \sqrt{u_b^2 + v_{b,\max}^2 + u_{o,\max}^2 + 2u_{o,\max}(v_{b,\max} + u_b)}.$$

Lemma 7.3. *Consider an obstacle described by (7.7), and a vehicle described by (7.1).*

Let the vehicle's course references be given by the collision avoidance algorithm, defined in (7.34). Suppose the vehicle maintains a distance to the obstacle satisfying

$$d_{b,o}(t) \geq \frac{R_{o|\epsilon}}{\cos(\sigma)}, \ \forall t \geq t_0, \tag{7.55}$$

where $\sigma \in (0, \pi/2]$ is a constant angle. If Assumption 7.1-7.5 hold, and the vehicle is controlled by the heading controller (7.12) where $\lambda_\psi > 0$ satisfies

$$\lambda_\psi \leq \frac{f_\psi(u_b, \sigma)}{\pi}. \tag{7.56}$$

Then, if $|v_b(t_0)| \leq v_{b,\max}$,

$$|v_b(t)| \leq v_{b,\max}, \ \forall t \geq t_0. \tag{7.57}$$

Proof. The desired heading is computed from the desired course by subtracting the crab angle, as

$$\psi_{db}^n = \chi_{\text{dca}j}^n - \beta_c, \tag{7.58}$$

where $j \in \{\pm\}$ is the turning parameter. The time-derivative of ψ_{db}^n is computed by substituting (7.24) and (7.27) into (7.34) as

$$\dot{\psi}_{db}^n = \dot{\alpha} \pm \dot{\beta} + \dot{\gamma}_{\text{abs}}^{(j)} - \dot{\beta}_c. \tag{7.59}$$

The terms can be computed in the same manner as in Chapter 6. The time-derivatives of α and β are found geometrically and by (7.25), as

$$\dot{\alpha} = -\frac{U_{bo}}{d_{b,o}} \sin(\chi_{bo}^n - \alpha), \tag{7.60}$$

$$\dot{\beta} = \frac{U_{bo}}{d_{b,o}} \cos(\chi_{bo}^n - \alpha) \tan(\beta). \tag{7.61}$$

The time-derivative of $\gamma_{\text{cmp}}^{(j)}$ can be computed from (7.28) as

$$\dot{\gamma}_{\text{cmp}}^{(j)} = (-r_o + \dot{\alpha} \pm \dot{\beta})P(\gamma_o^{(j)}) + a_o Q(\gamma_o^{(j)}) + \dot{v}_b \frac{\partial \gamma_{\text{cmp}}^{(j)}}{\partial v_b}, \tag{7.62}$$

where the expressions of $P(\gamma_o)$ and $Q(\gamma_o)$ are given in Appendix 7.A. The last term can be computed from (7.28) as

$$\frac{\partial \gamma_{\text{cmp}}^{(j)}}{\partial v_b} = \frac{\partial}{\partial v_b}\left(\sin^{-1}\left(\frac{u_o}{U_b}\sin(\gamma_o^{(j)})\right)\right) \tag{7.63}$$

$$= -v_b \frac{u_o \sin(\gamma_o^{(j)})}{U_b^3\sqrt{1-(u_o/U_b)^2\sin^2(\gamma_o^{(j)})}}. \tag{7.64}$$

For convenience, we define

$$\begin{aligned} R(\gamma_o) &\triangleq \frac{u_o \sin(\gamma_o)}{U_b^3\sqrt{1-(u_o/U_b)^2\sin^2(\gamma_o)}} \\ &\in \left[-\frac{u_o}{U_b^2\sqrt{U_b^2-u_o^2}}, \frac{u_o}{U_b^2\sqrt{U_b^2-u_o^2}}\right]. \end{aligned} \tag{7.65}$$

The time-derivative of the crab angle β_c is computed from (7.15) as

$$\dot{\beta}_c = \frac{d}{dt}\left(\tan^{-1}\left(\frac{v_b}{u_b}\right)\right) = \dot{v}_b \frac{u_b}{U_b^2}. \tag{7.66}$$

Finally, we find $\dot{\psi}_{\text{db}}^n$ as

$$\dot{\psi}_{\text{db}}^n = \left(1 + P(\gamma_o^{(j)})\right)\dot{\psi}_{\alpha\beta}^{(j)} - r_o P(\gamma_o^{(j)}) + a_o Q(\gamma_o^{(j)}) - \dot{v}_b\left(v_b R(\gamma_o^{(j)}) + \frac{u_b}{U_b^2}\right), \tag{7.67}$$

where $\dot{\psi}_{\alpha\beta}^{(j)} \triangleq \dot{\alpha} \pm \dot{\beta}$. Inserting the control law (7.12) and the dynamics of v_b given by

(7.1d) yields

$$r_b = \left(1 + P(\gamma_o^{(j)})\right) \dot{\psi}_{\alpha\beta}^{(j)} - r_o P(\gamma_o^{(j)}) + a_o Q(\gamma_o^{(j)}) - \lambda_\psi \tilde{\psi} \dots \\ - \left(X(u_b) r_b + Y(u_b) v_b\right) \left(v_b R(\gamma_o^{(j)}) + \frac{u_b}{U_b^2}\right). \tag{7.68}$$

Solving (7.68) for r_b gives the expression:

$$r_b = \frac{G_{\text{num}}}{G_{\text{den}}}, \tag{7.69}$$

where

$$G_{\text{den}} = 1 + X(u_b) \left(v_b R(\gamma_o^{(j)}) + \frac{u_b}{U_b^2}\right), \tag{7.70}$$

$$G_{\text{num}} = \left(1 + P(\gamma_o^{(j)})\right) \dot{\psi}_{\alpha\beta}^{(j)} - r_o P(\gamma_o^{(j)}) + a_o Q(\gamma_o^{(j)}) - \lambda_\psi \tilde{\psi} \dots \\ - Y(u_b) v_b \left(v_b R(\gamma_o^{(j)}) + \frac{u_b}{U_b^2}\right). \tag{7.71}$$

To ensure that (7.69) is well-defined, G_{den} must be nonzero. If $X(u_b) \geq 0$, we can write (7.70) as

$$G_{\text{den}} > 1 + \frac{X(u_b)}{U_b^2} \left(\frac{v_b u_{o,\max}}{\sqrt{U_b^2 + u_{o,\max}^2}} + u_b\right), \tag{7.72}$$

by (7.65) which bounds $R(\gamma_o)$, and Assumption 7.5 which bounds the obstacle speed. Since $u_b > u_{o,\max}$, it is then ensured that $G_{\text{den}} > 0, \ \forall X(u_b) \geq 0$. If $X(u_b) < 0$, a lower bound of (7.70) can similarly be found by (7.65) and Assumption 7.5, as

$$G_{\text{den}} > 1 - \frac{|X(u_b)|}{U_b^2} \left(\frac{|v_b| u_{o,\max}}{\sqrt{U_b^2 - u_{o,\max}^2}} + u_b\right) := G_{\text{d,min}}. \tag{7.73}$$

If $u_{o,\max} = 0$, then (7.73) satisfies

$$G_{\text{den}} > 1 - \frac{|X(u_b)|}{U_b^2} u_b. \tag{7.74}$$

The minimum is found at $v_b = 0$, thus we require $X(u_b) > -u_b$ which is satisfied by Assumption 7.6. For $u_{o,\max} \neq 0$, we find a lower bound by minimizing (7.73) with respect to v_b, as

$$G_{\text{den}} > 1 - \frac{|X(u_b)|}{u_b^2} \left(u_{o,\max} + u_b\right). \tag{7.75}$$

Hence, we require the obstacle speed to satisfy

$$u_{o,\max} < \begin{cases} u_b, & \text{if } X(u_b) > -\frac{1}{2}u_b, \\ -\frac{u_b^2}{X(u_b)} - u_b, & \text{if } -\frac{1}{2}u_b \geq X(u_b) > -u_b. \end{cases} \tag{7.76}$$

Remark 7.5. Assumption 7.5 ensures that (7.76) always holds.

An upper bound of G_{num} can be found by maximizing $P(\gamma_o)$, $Q(\gamma_o)$ and $R(\gamma_o)$, Assumption 7.4 bounding the obstacle's turning rate and forward acceleration, Assumption 7.5 bounding the obstacle's speed, and Assumption 7.2 stating that $Y(u_b) < 0$, as

$$\begin{aligned} G_{\text{num}} < (1 + \frac{u_{o,\max}}{U_b})\dot{\psi}_{\alpha\beta,\max} + r_{o,\max}\frac{u_{o,\max}}{u_b} + \frac{a_{o,\max}}{\sqrt{u_b^2 - u_{o,\max}^2}} \dots \\ + \lambda_\psi \pi + \frac{|Y(u_b)||v_b|}{U_b^2}\left(\frac{|v_b| u_{o,\max}}{\sqrt{U_b^2 - u_{o,\max}^2}} + u_b\right) \coloneqq G_{\text{n,max}}. \end{aligned} \tag{7.77}$$

To bound $\dot{\psi}_{\alpha\beta}^{(j)}$ we make use the trigonometric identity given by

$$\tan(x) \pm \tan(y) = \frac{\sin(x) \pm \sin(y)}{\cos(x)\cos(y)}, \tag{7.78}$$

which, by (7.60) and (7.61), yields

$$\dot{\alpha} \pm \dot{\beta} = \frac{U_{bo}}{d_{b,o}} \left(-\sin(\chi_{bo}^n - \alpha) \pm \cos(\chi_{bo}^n - \alpha) \tan(\beta) \right) \tag{7.79}$$

$$= -\frac{U_{bo}}{d_{b,o}} \cos(\chi_{bo}^n - \alpha) \left(\tan(\chi_{bo}^n - \alpha) \mp \tan(\beta) \right) \tag{7.80}$$

$$= -\frac{U_{bo}}{d_{b,o}} \frac{\sin(\chi_{bo}^n - \alpha \mp \beta)}{\cos(\beta)}. \tag{7.81}$$

The distance $d_{b,o}$ is lower bounded by (7.55), which ensures that $\beta \in [0,\ \pi/2 - \sigma)$ by (7.25). Hence,

$$\dot{\psi}_{\alpha\beta}^{(j)} < \frac{U_{bo,\max}}{(R_o + d_\epsilon)\tan(\sigma)} := \dot{\psi}_{\alpha\beta,\max}. \tag{7.82}$$

The angle σ can be used as a design parameter to bound this term, as a larger angle yields a lower value of $\dot{\psi}_{\alpha\beta,\max}$. However, this requires the vehicle to maintain a larger distance from the obstacle.

By evaluating $G_{\text{d,min}}$ and $G_{\text{n,max}}$ at $v_{b,\max}$ we obtain:

$$|r_b(v_{b,\max})| < \frac{G_{\text{n,max}}}{G_{\text{d,min}}}. \tag{7.83}$$

It is then straight-forward to verify that

$$\lambda_\psi \leq \frac{f_\psi(u_b, \sigma)}{\pi} \tag{7.84}$$

ensures that if $|v_b(t_0)| \leq v_{b,\max}$, then

$$|v_b(t)| \leq v_{b,\max},\ \ \forall t \geq t_0, \tag{7.85}$$

by Lemma 7.2. □

We need to ensure that the vehicle is able to turn out of a conflict before a collision occurs. By the same reasoning as presented in Chapter 6, we must then choose the threshold distance of the switching condition (7.30) above a lower bound. The lower

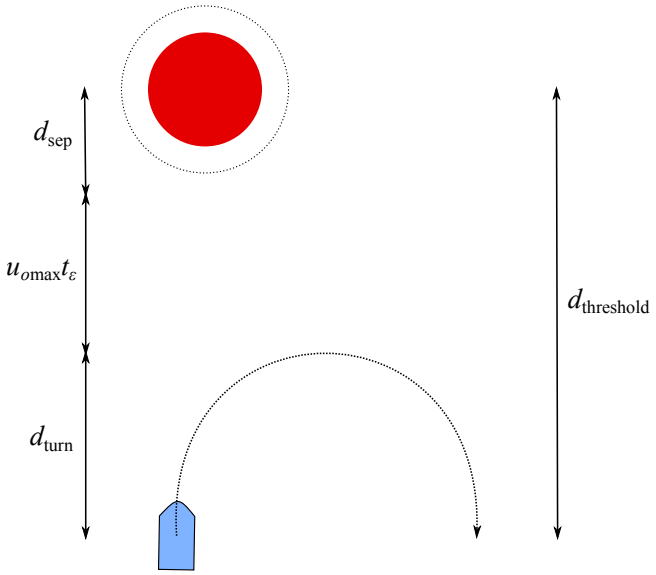

Figure 7.2: Illustration of the collision avoidance scenario of Lemma 7.4.

bound should be based on the amount of time it takes for the vehicle to turn to the desired course, and the maximum distance the vehicle and the obstacle hypothetically can travel towards each other during the maneuver. For this we need to define the Sine integral function, given by

$$\text{Si}(\tau) = \int_0^\tau \frac{\sin(t)}{t} dt. \tag{7.86a}$$

The following lemma provides an explicit lower bound of the threshold distance, based on the analysis presented in Wiig et al. [25].

Lemma 7.4. *Consider an obstacle described by* (7.7)*, and a vehicle described by* (7.1)*. Let the vehicle enter collision avoidance mode according to the switching rule* (7.30)*, as the distance satisfies* $d_{b,o} = d_{\text{threshold}}$*. Let the vehicle, controlled by the heading controller* (7.12)*, follow the course references defined in* (7.34)*, with the turning direction chosen by the turning rules* (7.32)-(7.33)*. Let Assumption 7.1-7.6 hold, and suppose the vehicle speed*

satisfies $U_b \leq U_{b,\max},\ \forall t \geq t_0$. *If the threshold distance satisfies*

$$d_{\text{threshold}} \geq u_{o,\max} t_\varepsilon + d_{\text{sep}} + d_{\text{turn}}, \tag{7.87}$$

where

$$t_\varepsilon := -\frac{\ln(\varepsilon/\pi)}{\lambda_\chi} \tag{7.88}$$

is an upper bound of the time it takes for the vehicle to converge to within ε *rad of the desired course, and*

$$d_{\text{turn}} := \frac{U_{b,\max}}{\lambda_\chi} \text{Si}\left(\frac{\pi}{2}\right), \tag{7.89}$$

is an upper bound of the distance traveled by the vehicle towards the obstacle when making a π *rad turn, where* λ_χ *is defined in* (7.23). *Then, the vehicle will converge to within* ε *rad of the desired course before the obstacle is within the distance* d_{sep} *of the vehicle.*

Proof. The proof of this lemma follows along the lines of the proof presented in [25], where a minimum switching distance is derived by evaluating the worst case collision avoidance scenario between the vehicle and the obstacle. The scenario is illustrated in Figure 7.2, describing a situation where the vehicle must turn π rad while the obstacle moves directly towards the turning circle of the vehicle.

Let the vehicle and the obstacle move with maximum speeds, i.e. $U_b = U_{b,\max}$ and $u_o = u_{o,\max}$, and let $R_{o|\epsilon} \to \infty$ such that $\beta \to \pi/2$. The course error is then upper bounded by $|\tilde{\chi}| = \pi$. To find a lower bound of the required threshold distance, we will analyse the course error dynamics given by (7.22), with the solution:

$$\tilde{\chi} = \tilde{\chi}(t_0) e^{-\lambda_\chi (t - t_0)}. \tag{7.90}$$

The course error $\tilde{\chi}$ is bounded by definition, thus $|\tilde{\chi}(t_0)| \leq \pi$. Since $\lambda_\chi > 0$, then (7.90) is bounded. It follows that the convergence time of the course error to $|\tilde{\chi}| \leq \varepsilon$ is given by

$$t - t_0 \leq -\frac{\ln(\varepsilon/\pi)}{\lambda_\chi} := t_\varepsilon,\ \varepsilon \in (0, \pi]\,. \tag{7.91}$$

The distance covered by the obstacle is upper bounded by $u_{o,\max} t_\varepsilon$. The distance covered by the vehicle is less straight-forward to compute, since the course rate is time-varying. From Figure 7.2 it can be seen that the distance the vehicle travels over the time t_ε is upper bounded by the distance the vehicle travels when making a $\pi/2$ turn. Without loss of generality, let the initial vehicle course be $\chi_b^n(t_0) = 0$, the obstacle heading be $\psi_o^n = \pi$, and let $x_b^n < x_o^n$. From Chapter 4 we can recall that the time-derivative of x_b^n can be found from the course, as

$$\dot{x}_b^n = U_{b,\max} \cos(\chi_b^n). \tag{7.92}$$

The maximum distance the vehicle travels towards the obstacle is found by solving (7.92) for $\tilde{\chi} = -\frac{\pi}{2} e^{-\lambda_\chi (t - t_0)}$, as

$$\int_0^\infty U_{b,\max} \cos\left(\tilde{\chi} + \chi_{db}^n\right) dt \tag{7.93}$$

$$= \int_0^\infty U_{b,\max} \cos\left(\frac{\pi}{2} - \frac{\pi}{2} e^{-\lambda_\chi (t - t_0)}\right) dt = \frac{U_{b,\max}}{\lambda_\chi} \mathrm{Si}\left(\frac{\pi}{2}\right). \tag{7.94}$$

It follows that if the threshold distance satisfies (7.87), then the vehicle will converge to within ε rad of the desired course, before the distance between the vehicle and the obstacle, $d_{b,o}$, is less than the distance d_{sep}.

□

The main theorem of the chapter is now ready to be stated. First, we state the general assumption:

Assumption 7.7. The vehicle and the obstacle are initially separated by a distance satisfying

$$d_{b,o}(t_0) \geq d_{\text{threshold}}. \tag{7.95}$$

The final theorem will provide the conditions under which a vehicle modeled by (7.1) will navigate safely in the presence of a moving obstacle described by (7.7), combined with guidance towards a target by the pure pursuit guidance law (7.10), while also maintaining a limited sway speed satisfying the required bound defined in (7.5).

Theorem 7.1. *Consider an obstacle described by (7.7) and a vehicle described by (7.1). Let Assumption 7.1-7.7 hold, the threshold distance satisfy*

$$d_{\text{threshold}} \geq u_{o,\max} t_\varepsilon + \frac{R_{o|\epsilon}}{\cos(\sigma)} + d_{\text{turn}}, \tag{7.96}$$

where t_ε and d_{turn} are defined in Lemma 7.4, and the safety angle $\sigma \in (0, \pi/2]$ satisfy

$$\sigma = \bar{\sigma} + \varepsilon, \quad \bar{\sigma} > 0, \, \varepsilon > 0. \tag{7.97}$$

Furthermore, let the heading control gain λ_ψ satisfy

$$\lambda_\psi \leq \frac{f_\psi(u_b, \bar{\sigma})}{\pi}, \tag{7.98}$$

and the acceptance distance satisfy

$$d_a > \frac{|X(u_b)| U_{b,\max}}{|Y(u_b)| v_{b,\max} - |X(u_b)| \lambda_\chi \pi}, \tag{7.99}$$

where λ_χ is defined in (7.23). Then, the vehicle controlled by the heading controller (7.12), following the guidance law (7.10), the switching rules (7.30)-(7.31), the turning rules (7.32)-(7.33), and the collision avoidance law (7.34), will converge to within d_a of the target position $\boldsymbol{p}_{\text{t}}^n$ at an unspecified point in time $t_{\text{f}} < \infty$, and furthermore satisfy

$$d_{b,o}(t) - R_o \geq d_\epsilon, \ \forall t \in [t_0, \, t_{\text{f}}] \,, \tag{7.100}$$

while ensuring that

$$|v_b(t)| \leq v_{b,\max}, \ \forall t \in [t_0, \, t_{\text{f}}] \,. \tag{7.101}$$

Proof. The required course rate when the vehicle follows the pure pursuit guidance law is computed from (7.11) as

$$\dot{\chi}_{\text{pp}}^n = \frac{(x_b^n - x_t^n)\dot{y}_b^n - (y_b^n - y_t^n)\dot{x}_b^n}{(x_b^n - x_t^n)^2 + (y_b^n - y_t^n)^2}, \tag{7.102}$$

which yields the upper bound:

$$|\dot{\chi}^n_{\text{pp}}| \leq \frac{U_b}{\sqrt{(x^n_b - x^n_t)^2 + (y^n_b - y^n_t)^2}}. \tag{7.103}$$

An upper bound of the required course rate during pure pursuit guidance is then found as

$$|\dot{\chi}^n_{\text{db}}| \leq \frac{U_{b,\max}}{d_a}. \tag{7.104}$$

The required heading rate is found from the course rate by the relation (7.18), yielding

$$|\dot{\psi}^n_{\text{db}}| \leq \left(\frac{U_{b,\max}}{d_a} - \frac{|Y(u_b)| v_{b,\max} u_b}{U^2_{b,\max}} \right) \frac{U^2_{b,\max}}{U^2_{b,\max} - |X(u_b)| u_b} \tag{7.105}$$

Inserting the control law (7.12) yields

$$|r_b| \leq \left(\frac{U_{b,\max}}{d_a} - \frac{|Y(u_b)| v_{b,\max} u_b}{U^2_{b,\max}} \right) \frac{U^2_{b,\max}}{U^2_{b,\max} - |X(u_b)| u_b} + \lambda_\psi \pi \tag{7.106}$$

Hence, by Lemma 7.2 the acceptance distance d_a must satisfy

$$d_a > \frac{|X(u_b)| U_{b,\max}}{|Y(u_b)| v_{b,\max} - |X(u_b)| \lambda_\chi \pi}, \tag{7.107}$$

where λ_χ is defined in (7.23), in order to ensure that the sway speed satisfies $|v_b(t)| \leq v_{b,\max}, \ \forall t \geq t_0$ in the presence of zero obstacles.

Let the vehicle enter collision avoidance mode at the time $t_1 \geq t_0$, as the distance satisfies $d_{b,o}(t_1) = d_{\text{threshold}}$. Lemma 7.4 and condition (7.96) ensures that there exists a time $t_2 > t_1$, in which the vehicle satisfies

$$d_{b,o}(t_2) \geq \frac{R_{o|\epsilon}}{\cos(\sigma)}, \tag{7.108}$$

and $|\tilde{\chi}(t_2)| = \left|\chi^n_b(t_2) - \chi^n_{\text{dca}j}(t_2)\right| \leq \varepsilon$. Since $\tilde{\chi} = 0$ is an exponentially stable

equilibrium, it is then ensured that

$$\left|\chi_b^n(t) - \chi_{\text{dca}j}^n(t)\right| \leq \varepsilon, \ \ \forall t \in [t_2,\, t_3\,], \tag{7.109}$$

where $t_3 \geq t_2$ is the time in which the vehicle exits collision avoidance mode. Condition (7.109) furthermore ensures that

$$|\chi_{bo}^n(t) - \alpha(t)| \geq \beta(t) + \bar{\sigma}, \ \ \forall t \in [t_2,\, t_3\,]. \tag{7.110}$$

Hence,

$$d_{b,o}(t) \geq \frac{R_{o|\epsilon}}{\cos(\bar{\sigma})}, \ \ \forall t \in [t_1,\, t_3\,], \tag{7.111}$$

by Lemma 7.1. Finally, Lemma 7.3 along with condition (7.98) then ensures that

$$|v_b(t)| \leq v_{b,\max}, \ \ \forall t \in [t_1,\, t_3\,]. \tag{7.112}$$

The obstacle may turn, causing the vehicle to enter collision avoidance mode as the distance satisfies $d_{b,o} < d_{\text{threshold}}$. Since $\chi_{\text{dca}j}^n$ is first-time differentiable, and the desired course is chosen as the nearest of the two course candidates, the vehicle will then immediately be able to follow the desired course, ensuring that the vehicle satisfies (7.110) at all times, which furthermore ensures that condition (7.100) is satisfied, by Lemma 7.1.

Finally, since $u_b > u_{o,\max}$, the vehicle will escape the obstacle at some point in time, and proceed to the target $\boldsymbol{p}_{\text{t}}^n$. By Lemma 6.2 and Assumption 7.1 the vehicle will converge to within d_a of the target position at some point in time $t_{\text{f}} < \infty$. By the above analysis, we can conclude that the conditions (7.100) and (7.101) are satisfied. □

7.5 Simulations

This section presents two numerical simulations of a vehicle with underactuated dynamics, modeled as (7.1), controlled by the heading controller (7.12) and following the VO algorithm presented in Section 7.3, for collision avoidance of a moving obstacle

modeled by (7.7). The vehicle drives towards a static target chosen as $\boldsymbol{p}_{\mathrm{t}}^{n} = [140,\ 0]$ m, by following the pure pursuit guidance law (7.10). In both scenarios, the vehicle maintains a constant forward speed $u_b = 2$ m/s, with initial heading equal to $\psi_b^n(t_0) = 0$ rad, and position $\boldsymbol{p}_{nb}^{n}(t_0) = [0,\ 0]^\top$ m. To model the underactuated sway dynamics, we use the model parameters of an LAUV (light AUV) [4]. We can verify that Assumption 7.2 and 7.6 holds with $Y(u_b) = -2.8161$ and $X(u_b) = -1.0242$. The maximum allowed sway speed was set to $v_{b,\max} = 3$ m/s. The radius of the obstacle was chosen equal to $R_o = 10$ m, and the safety distance equal to $d_\epsilon = 5$ m. The convergence parameter was chosen as $\varepsilon = 0.09$ rad.

In the first scenario, the obstacle maintains a constant forward speed equal to $u_o = u_{o,\max} = 1.5$ m/s, satisfying Assumption 7.5. The angular safety distance was chosen as $\sigma = 0.7$ rad. With these parameters ($a_{o,\max} = 0$, $r_{o,\max} = 0$), the heading control gain was computed as $\lambda_\psi = 0.489\ \mathrm{s}^{-1}$, and the threshold distance chosen as $d_{\text{threshold}} = 45$ m, satisfying the conditions of Theorem 7.1. The acceptance distance was set to $d_a = 1$ m, also complying with the conditions of Theorem 7.1.

The obstacle approaches the vehicle from the port side as seen in Figure 7.4, where the obstacle and vehicle trajectories have been plotted at four moments in time. The extended collision cone, $\mathcal{CC}_\sigma$, is shown as the red, transparent cone, and has length equal to $d_{\text{threshold}}$. The vehicle enters CA mode as the distance is reduced to $d_{b,o} = d_{\text{threshold}}$, and turns left in order to pass on the rear side of the obstacle, seen in Figure 7.4a and 7.4b. The vehicle exits collision avoidance mode at $t = 29$ s according to the switching rule (7.31), and reaches the target without collision at $t = 80$ s, seen in Figure 7.4c and 7.4d.

The distance between the vehicle and obstacle centers, $d_{b,o}(t)$, is plotted in Figure 7.6a along with the threshold distance, $d_{\text{threshold}}$, and the minimum required separation distance, $R_{o|\epsilon}$. We have also included the distance $\frac{R_{o|\epsilon}}{\cos(\bar{\sigma})}$, where $\bar{\sigma} \triangleq \sigma - \varepsilon$, in order to demonstrate that the conditions of Lemma 7.3 are satisfied, which is a requirement for Theorem 7.1 to hold. It can be seen that the distance remains above the minimum safety distance $R_{o|\epsilon}$, and also above $\frac{R_{o|\epsilon}}{\cos(\bar{\sigma})}$, thus verifying the theoretical result of Theorem 7.1.

In the second scenario, the obstacle both turns and increases its forward speed,

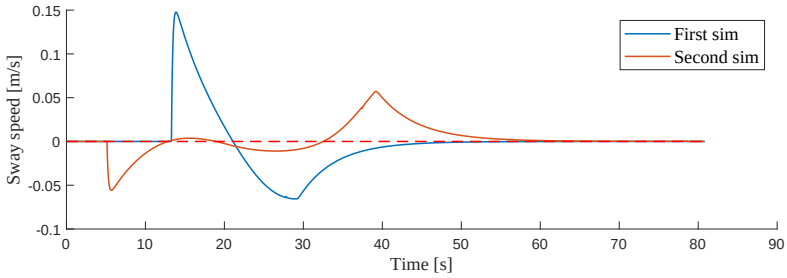

Figure 7.3: Vehicle sway speed, v_b, during both simulations.

with constant turning rate $r_o = r_{o,\max} = 0.1$ rad/s, and forward acceleration $a_o = a_{o,\max} = 0.05$ m/s^2. The initial speed of the obstacles was set to $u_o(t_0) = 0$ m/s, and the maximum speed to $u_{o,\max} = 1$ m/s, satisfying Assumption 7.5. The angular safety distance was chosen as $\sigma = 0.53$ rad. With these parameters, the heading control gain was chosen as $\lambda_\psi = 0.46$ s^{-1}, the threshold distance as $d_{\text{threshold}} = 40$ m, and the acceptance distance as $d_a = 1$ m, satisfying the conditions of Theorem 7.1.

The trajectories of the vehicle and the obstacle can be seen in Figure 7.5. The obstacle turns in a clockwise circle as it increases its forward speed. The vehicle enters collision avoidance mode as the distance is reduced to $d_{b,o} = d_{\text{threshold}}$, and turns right according to the turning rule (7.32), seen in Figure 7.5a and 7.5b. The vehicle follows the desired course along the edges of the extended, absolute collision cone until it exits CA mode at $t = 39$ s, seen in Figure 7.5c. The target is reached safely at $t = 78$ s, in Figure 7.5d. The distance between the vehicle and the obstacle during the collision avoidance scenario is plotted in Figure 7.6b. From the figure it is verified that the conditions of Lemma 7.3 are satisfied, and the result of Theorem 7.1 holds.

Finally, the sway speed of the vehicle during both simulation scenarios are given in Figure 7.3. The sway speed becomes nonzero during the vehicle's turning motion, and converges to zero once the turning ends. It can be noticed that magnitude of the sway speed remains far below the maximum $v_{b,\max} = 3$ m/s, which indicates that the theoretical upper bound of the heading control gain is conservative. However, it does verify the result of Theorem 7.1.

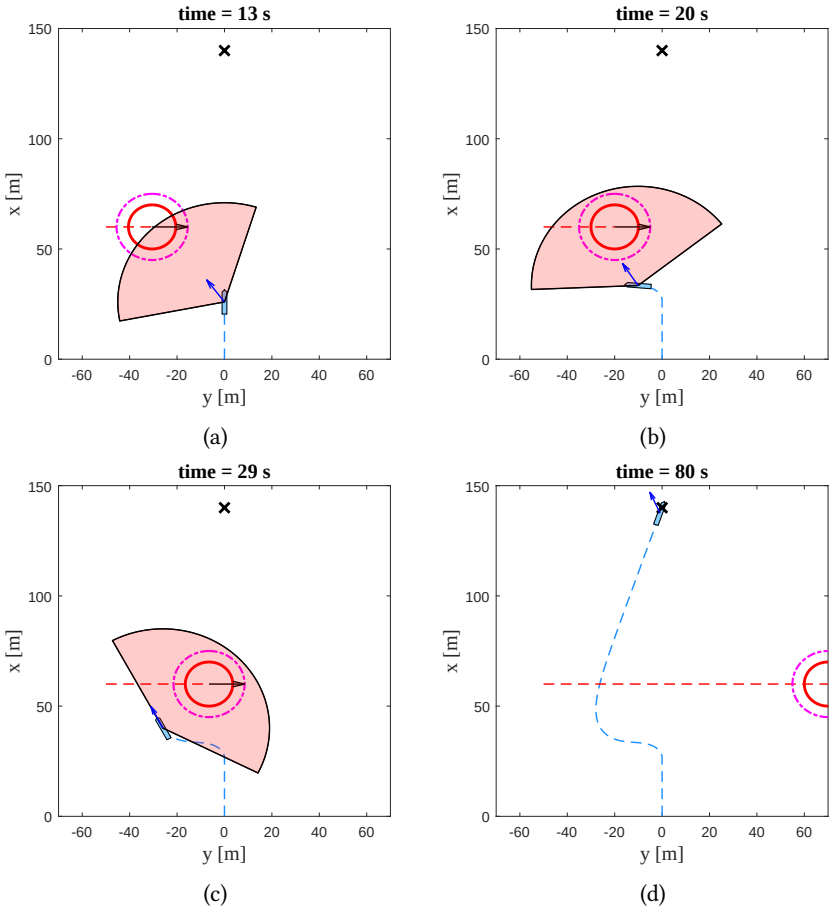

Figure 7.4: First simulation scenario of a vehicle with underactuated dynamics, reactively avoiding collision with a moving obstacle. The obstacle is the red circle, the vehicle is the blue polygon, and the safety distance is the magenta line encircling the obstacle. The trajectories of the vehicle and the obstacle are the blue and red, dashed lines, respectively. The extended collision cone, $\mathcal{CC}_\sigma$, is the red cone, and the relative guidance velocity, $\boldsymbol{v}^n_{ndgo}$, is the blue arrow. The target position is marked as an 'X'.

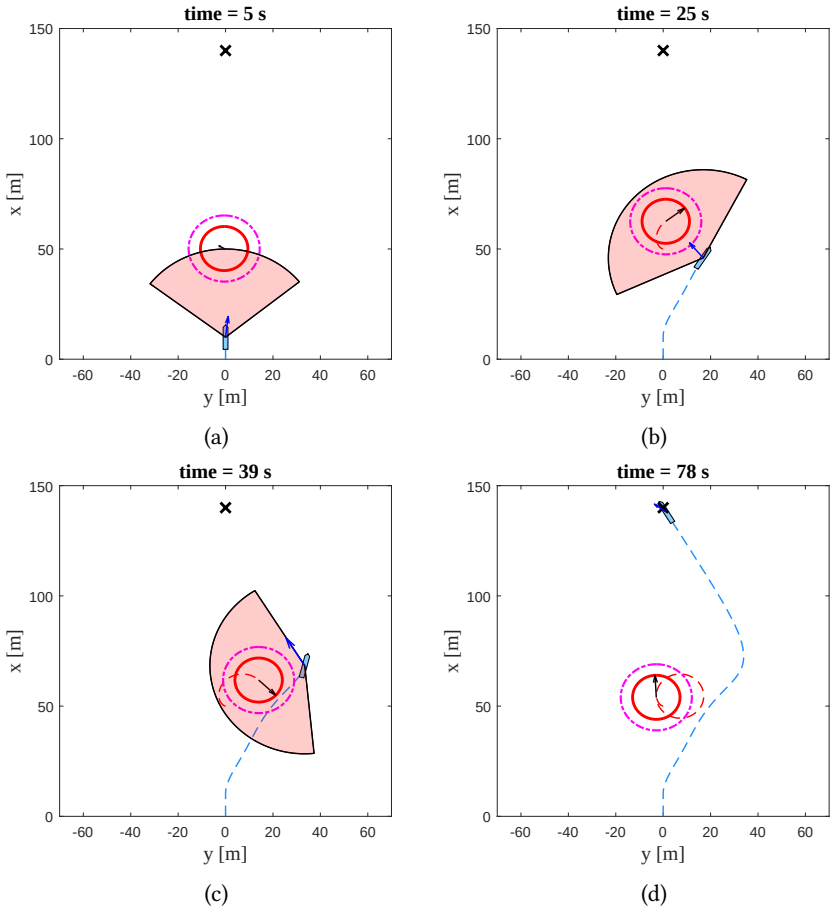

Figure 7.5: Second simulation scenario of a vehicle with underactuated dynamics, reactively avoiding collision with an obstacle that both turns and increases its forward speed.

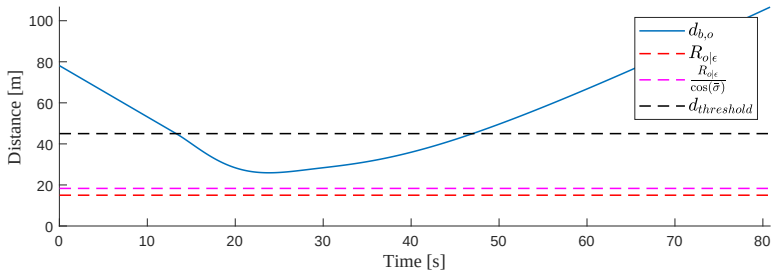

(a) Distance, $d_{b,o}$, during the first simulation.

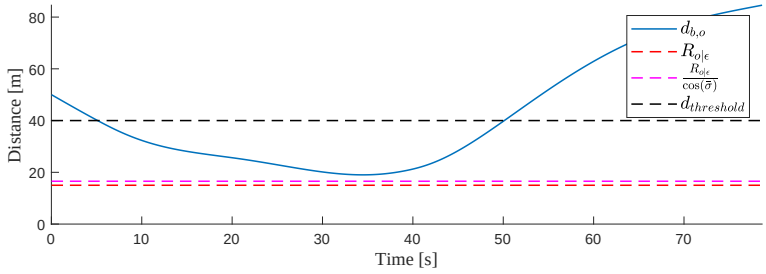

(b) Distance, $d_{b,o}$, during the second simulation.

Figure 7.6: Distance between the vehicle and the obstacle during both simulations.

7.A Functional expressions

The expression derived in Chapter 3 is restated here for convenience:

$$f_v(u_b, v_b, r_b) \triangleq Y(u_b)v_b + X(u_b)r_b, \tag{7.113}$$

where

$$X(u_b) \triangleq \frac{d_{32}m_{23} - d_{33}m_{22} + u_b m_{23}\,(m_{11} - m_{22})}{m_{22}m_{33} - m_{23}^2}, \tag{7.114}$$

$$Y(u_b) \triangleq \frac{d_{22}m_{23} - d_{32}m_{22} - u_b m_{22}\left(m_{22} + m_{11}\right)}{m_{22}m_{33} - m_{23}^2}. \tag{7.115}$$

In Chapter 6 we defined the following expressions:

$$P(\gamma_o) \triangleq \frac{(u_o/U_b)\cos(\gamma_o)}{\sqrt{1 - (u_o/U_b)^2 \sin^2(\gamma_o)}} \in \left[-\frac{u_o}{U_b}, \frac{u_o}{U_b}\right], \tag{7.116}$$

$$Q(\gamma_o) \triangleq \frac{\sin(\gamma_o)}{U_b\sqrt{1 - (u_o/U_b)^2 \sin^2(\gamma_o)}} \in \left[-\frac{1}{\sqrt{U_b^2 - u_o^2}}, \frac{1}{\sqrt{U_b^2 - u_o^2}}\right]. \tag{7.117}$$

Chapter 8

The Velocity Obstacle Algorithm for Underactuated Surface Vehicles

This chapter presents the velocity obstacle algorithm applied to the full model of an underactuated marine vehicle. In contrast to the previous chapter, we will now include the yaw and surge dynamics of the surface vehicle, and consider path following in addition to target reaching, as sub-goals for the vehicle.

As in the previous chapter, we need to take precautions regarding the underactuated sway dynamics. Since we formulated the conditions ensuring that the vehicle's sway speed is bounded in the previous chapter, we can apply these results with only minor alterations.

To ensure that the vehicle follows the desired surge speed and yaw rate, considering they are no longer perfectly controlled, we apply two feedback stabilizing controllers, ensuring exponential stabilization of the surge and yaw error dynamics. To ensure that the yaw rate input signal is given as a continuous function, we introduce a smoothing function which makes the yaw rate signal continuous in the case of a jump. However,

this leads an additional smoothing time to reach the desired yaw rate, which must be accounted for when deriving a minimum threshold distance for initiating the avoidance maneuver.

8.1 System description

In this section, we will present the model of an underactuated marine vehicle, moving in the horizontal plane, its associated control objective, and the model used to describe a moving obstacle.

8.1.1 Vehicle model

The vehicle is modeled as an underactuated, marine vehicle moving in 3 DOF, modeled in Chapter 3. The full model is stated as

$$\dot{x}_b^n = u_b \cos(\psi_b^n) - v_b \sin(\psi_b^n), \tag{8.1a}$$
$$\dot{y}_b^n = u_b \sin(\psi_b^n) + v_b \cos(\psi_b^n), \tag{8.1b}$$
$$\dot{\psi}_b^n = r_b, \tag{8.1c}$$
$$\dot{u}_b = f_u(v_b, r_b) + g_u, \tag{8.1d}$$
$$\dot{v}_b = f_v(u_b, v_b, r_b), \tag{8.1e}$$
$$\dot{r}_b = f_r(u_b, v_b, r_b) + g_r, \tag{8.1f}$$

where the expressions of $f_u(\cdot)$, $f_v(\cdot)$, and $f_r(\cdot)$ are given in Appendix 8.A, and g_u and g_r are the control forces in surge and yaw, respectively. The term $f_v(u_b, v_b, r_b)$ can be expressed as

$$f_v(u_b, v_b, r_b) \triangleq X(u_b) r_b + Y(u_b) v_b, \tag{8.2}$$

where the terms $X(u_b)$ and $Y(u_b)$ are given in Appendix 8.A.

Assumption 8.1. The vehicle's surge speed u_b satisfies

$$u_b \geq u_{b,\min}, \ \forall t \geq t_0, \tag{8.3}$$

where $u_{b,\min} > 0$ is a constant parameter.

Assumption 8.2. The term $Y(u_b)$ satisfies

$$Y(u_b) < 0 \ \forall u_b \geq u_{b,\min}. \tag{8.4}$$

Assumption 8.2 ensures that the vehicle is nominally stable in sway for surge speeds above a certain minimum speed, $u_{b,\min}$. This is the case for most commercial vessels by design.

8.1.2 Control objective

The vehicle's control objective varies, depending on the nominal guidance mode of the vehicle. We distinguish between two guidance modes; target reaching and path following.

In target reaching mode, the control objective of the vehicle is to come within an acceptable distance $d_a > 0$ of a target position $\boldsymbol{p}_{\mathrm{t}}^n \triangleq [x_{\mathrm{t}}^n, y_{\mathrm{t}}^n]^\top$, at an unspecified point in time $t_{\mathrm{f}} \in [t_0, \infty)$. In path following mode, the control objective of the vehicle is to converge to, and follow a straight line path parallel to the positive x^n axis, defined as

$$\mathcal{P} \triangleq \{(x, y) \in \mathbb{R}^2 \mid y = y_{\mathrm{t}}^n\}, \tag{8.5}$$

where y_{t}^n is the desired vehicle position along the y^n axis. Both goals should be achieved while keeping at least a minimum safety distance to the obstacle:

$$d_{b,o}(t) - R_o \geq d_\epsilon > 0, \ \forall t \geq t_0. \tag{8.6}$$

Finally, to prevent the vehicle from colliding side-ways into the obstacle, the vehicle's sway velocity should satisfy

$$|v_b(t)| \leq v_{b,\max} \ \forall t \geq t_0, \tag{8.7}$$

where $v_{b,\max} > 0$ is a constant design parameter.

Assumption 8.3. The initial sway speed, $v_b(t_0)$, satisfies

$$|v_b(t_0)| \leq v_{b,\max}. \tag{8.8}$$

8.1.3 Obstacle model

As in Chapter 6 and 7, the obstacle is modeled as a moving, circular domain $\mathcal{D}_o$, with radius R_o, described by the kinematic equations:

$$\dot{x}_o^n = u_o \cos(\psi_o^n), \tag{8.9a}$$
$$\dot{y}_o^n = u_o \sin(\psi_o^n), \tag{8.9b}$$
$$\dot{\psi}_o^n = r_o, \tag{8.9c}$$
$$\dot{u}_o = a_o. \tag{8.9d}$$

The obstacle is subject to the kinematic constraints:

Assumption 8.4. The obstacle's heading rate, r_o, and forward acceleration, a_o, are bounded by

$$\begin{aligned} r_o &\in [-r_{o,\max},\, r_{o,\max}], \\ a_o &\in [-a_{o,\max},\, a_{o,\max}], \end{aligned} \tag{8.10}$$

where $r_{o,\max} \geq 0$ and $a_{o,\max} \geq 0$ are constant parameters.

As introduced in Chapter 7, the following assumption needs to be met in order to ensure that the vehicle's desired yaw rate during collision avoidance is well-defined:

Assumption 8.5. The obstacle's forward speed $0 \leq u_o \leq u_{o,\max}$ satisfies

$$u_{o,\max} < \begin{cases} u_{\mathrm{d}b}, & \text{if } X(u_{\mathrm{d}b}) > -\frac{1}{2}u_{\mathrm{d}b}, \\ -\frac{u_{\mathrm{d}b}^2}{X(u_{\mathrm{d}b})} - u_{\mathrm{d}b}, & \text{if } -\frac{1}{2}u_{\mathrm{d}b} \geq X(u_{\mathrm{d}b}) > -u_{\mathrm{d}b}. \end{cases} \tag{8.11}$$

8.2 Guidance

In nominal guidance mode, the vehicle's course references will be generated by the pure pursuit guidance law during target reaching, and the line of sight guidance law during path following. Both of the guidance schemes are summarized below.

8.2.1 Pure pursuit guidance

When the control system is in target reaching mode, the vehicle's nominal course references will be generated by the pure pursuit guidance law. The guidance law generates a velocity vector along the line of sight vector between the vehicle and the target, given by

$$\boldsymbol{v}_{\text{pp}}^n \triangleq -U_b \frac{\tilde{\boldsymbol{p}}^n}{\|\tilde{\boldsymbol{p}}^n\|}, \tag{8.12}$$

where $\tilde{\boldsymbol{p}}^n \triangleq \boldsymbol{p}_{nb}^n - \boldsymbol{p}_{\text{t}}^n$, and $U_b > 0$ is the speed of the vehicle. The course reference is given by

$$\chi_{\text{pp}}^n = \angle \boldsymbol{v}_{\text{pp}}^n. \tag{8.13}$$

The pure pursuit guidance law ensures that the vehicle reaches a static target. However, it results in a tail chase of faster moving targets.

8.2.2 Line of sight guidance

In path following mode, the vehicle's course references will be generated by the line of sight guidance law. The straight line path is constructed from two points, $\boldsymbol{p}_{k-1}^n = \left[x_{k-1}^n, y_{k-1}^n\right]^\top$ and $\boldsymbol{p}_k^n = [x_k^n, y_k^n]^\top$, chosen to comply with the desired path, defined in (8.5).

The line of sight vector points towards a point along the path, located a constant lookahead distance $\Delta > 0$ from the direct projection of the vehicle position onto the path. The desired course is given by

$$\chi_{\text{los}}^n(y_{\text{e}}) \triangleq \chi_p + \arctan\left(\frac{-y_{\text{e}}}{\Delta}\right), \tag{8.14}$$

where the path-tangential angle χ_p, and the cross-track error y_{e}, are defined as

$$\chi_p = \mathrm{atan2}\left(y_k^n - y_{k-1}^n, x_k^n - x_{k-1}^n\right), \tag{8.15}$$

$$y_{\mathrm{e}} = -\left(x_b^n - x_k^n\right)\sin(\chi_p) + \left(y_b^n - y_k^n\right)\cos(\chi_p). \tag{8.16}$$

The guidance velocity during LOS guidance is computed as

$$\boldsymbol{v}_{\mathrm{los}}^n \triangleq U_b \left[\cos(\chi_{\mathrm{los}}^n),\ \sin(\chi_{\mathrm{los}}^n)\right]^\top. \tag{8.17}$$

8.3 Control

For the vehicle to follow the course references generated by the guidance system and the collision avoidance algorithm, the vehicle employs a saturated heading controller while directly compensating for the crab angle induced by the sway speed. Furthermore, in order to track the desired surge speed and yaw rate, the vehicle employs two feedback linearizing controllers, which ensures exponential stabilization of the surge and yaw error dynamics.

8.3.1 Heading controller

The heading controller is given by, [26]:

$$r_d = \dot{\psi}_{\mathrm{db}}^n - \mathrm{sat}\big(\lambda_\psi \tilde{\psi},\ k_\psi\big), \tag{8.18}$$

where $\lambda_\psi > 0$ is the heading control gain, and r_d is the desired yaw rate. The heading error $\tilde{\psi} \triangleq \psi_b^n - \psi_{\mathrm{db}}^n$ is mapped to the interval $(-\pi, \pi]$ to ensure that the vehicle always takes the shortest turn. Furthermore, the saturation function $\mathrm{sat}(a, b)$ is defined as

$$\mathrm{sat}(a,b) \triangleq \begin{cases} b & \text{if } a \geq b, \\ a & \text{if } a \in (-b,\ b), \\ -b & \text{if } a \leq -b, \end{cases} \tag{8.19}$$

and $k_\psi \in (0,\, \lambda_\psi \pi)$ is the heading saturation gain, representing a constant design parameter. The saturation term will allow us to relax the constraint we imposed on the heading control gain in the previous chapter, motivated by Wiig et al. [26].

The desired heading is found from the desired course as

$$\psi_{db}^n \triangleq \chi_{db}^n - \beta_c, \tag{8.20}$$

where

$$\beta_c \triangleq \tan^{-1}\left(\frac{v_b}{u_b}\right) \tag{8.21}$$

is the crab angle.

The relationship between the course rate and the heading rate is found by computing the time-derivative of the course, given by

$$\dot{\chi}_b^n = \dot{\psi}_b^n \frac{U_b^2 + X(u_b)u_b}{U_b^2} + \frac{Y(u_b)v_b u_b + \dot{u}_b v_b}{U_b^2}. \tag{8.22}$$

To ensure that the control law (8.18) is well-defined, the following assumption must be met:

Assumption 8.6. The term $X(u_b)$ satisfies

$$u_b + X(u_b) > 0 \;\forall u_b \geq u_{b,\min}. \tag{8.23}$$

Remark 8.1. Assumption 8.6 ensures that a change in the vehicle's heading results in a change in the vehicle's course in the nominal case when $\dot{u}_b = 0$. This is the case for most commercial vessels by design.

Furthermore, the relation (8.22) together with the heading controller (8.18) yields the course error dynamics:

$$r_\chi = \dot{\chi}_{db}^n - \text{sat}\big(\lambda_\chi \tilde{\chi},\, k_\chi\big), \tag{8.24}$$

where r_χ is the course rate, $\tilde{\chi} \triangleq \chi_b^n - \chi_{db}^n$ is the course error, and

$$\lambda_\chi \triangleq \lambda_\psi \frac{U_b^2 + X(u_b)u_b}{U_b^2}, \tag{8.25}$$

$$k_\chi \triangleq k_\psi \frac{U_b^2 + X(u_b)u_b}{U_b^2}. \tag{8.26}$$

Remark 8.2. Assumption 8.6 ensures that $\lambda_\chi > 0$.

Hence, the heading controller (8.18) ensures local, exponential stabilization of the course error dynamics.

8.3.2 Yaw rate smoother

For the vehicle to be able to track the desired yaw rate, the input signal must be given as a continuous function, which is usually satisfied. However, when the vehicle switches from guidance mode to collision avoidance mode, the vehicle may experience a jump in the desired yaw rate if the course reference signal is discontinuous during the switch.

To prevent discontinuities in the yaw rate, we introduce the yaw rate smoothing function, defined as

$$r_{\text{jump}}(r_{k-1}, r_k) \triangleq \begin{cases} \tilde{r}_{\max}, & \text{if } r_k - r_{k-1} > \tilde{r}_{\max} \quad | \ \text{sgn}(r_k) \geq \text{sgn}(r_{k-1}), \\ -\tilde{r}_{\max}, & \text{if } r_k - r_{k-1} < -\tilde{r}_{\max} \ | \ \text{sgn}(r_k) \leq \text{sgn}(r_{k-1}), \\ r_k - r_{k-1}, & \text{otherwise}, \end{cases} \tag{8.27}$$

where the $\text{sgn}(x)$ function is defined as

$$\text{sgn}(x) \triangleq \begin{cases} 1 & \text{if } x > 0, \\ 0 & \text{if } x = 0, \\ -1 & \text{if } x < 0, \end{cases} \tag{8.28}$$

and $\tilde{r}_{\max} > 0$ is the maximum allowed change in the yaw rate over the time interval

from t_{k-1} to t_k, chosen to comply with the vehicle's actuation constraints. Furthermore, the desired yaw rate is chosen as

$$r_{\mathrm{db}} = r_b(t_{k-1}) + r_{\mathrm{jump}}(r_b(t_{k-1}), r_d(t_k)). \tag{8.29}$$

The desired yaw rate remains equal to the input signal generated by the heading controller, i.e. r_d defined in (8.18), if the change is within the feasible area. Otherwise, the change in the yaw rate is taken as $\tilde{r}_{\max}$.

8.3.3 Surge controller

The surge dynamics are controlled using a feedback linearizing controller. The control force in surge is given by

$$g_u = \dot{u}_{\mathrm{db}} - f_u(v_b, r_b) - \lambda_u \tilde{u}, \tag{8.30}$$

where $\tilde{u} \triangleq u_b - u_{\mathrm{db}}$, and u_{db} is the desired surge speed. The surge control gain satisfies $\lambda_u > 0$.

The control law (8.30) yields the surge error dynamics by (8.1d):

$$\dot{\tilde{u}} = -\lambda_u \tilde{u}. \tag{8.31}$$

The surge error dynamics (8.31) are linear and globally exponentially stable at the origin. Thus, as long as the following assumption holds, the vehicle will be able to follow the desired speed:

Assumption 8.7. At the time t_0, the system has operated long enough for the surge speed to converge, i.e. $\tilde{u}(t_0) = 0$.

8.3.4 Yaw rate controller

The yaw dynamics are controlled using a feedback linearizing controller. The control force in yaw is given by

$$g_r = \dot{r}_{db} - f_r(u_b, v_b, r_b) - \lambda_r \tilde{r}, \tag{8.32}$$

where $\tilde{r} \triangleq r_b - r_{db}$, and r_{db} is the desired yaw rate defined in (8.29). The yaw control gain satisfies $\lambda_r > 0$.

The control law (8.32) yields the yaw rate error dynamics by (8.1f):

$$\dot{\tilde{r}} = -\lambda_r \tilde{r}. \tag{8.33}$$

The error dynamics (8.33) are linear, and globally exponentially stable at the origin. Thus, the vehicle will track the desired yaw rate when r_{db} is given as a continuous control input, which is ensured by the yaw rate smoother, and the following assumption holds:

Assumption 8.8. At the time t_0, the system has operated long enough for the yaw rate to converge, i.e. $\tilde{r}(t_0) = 0$.

Remark 8.3. Assumption 8.7 and 8.8 requires that the vehicle is properly initialized before any operations requiring collision avoidance is initiated, which is a reasonable assumption.

8.4 Collision avoidance

The velocity obstacles algorithm described in Chapter 5 will be used to generate course references for the vehicle in collision avoidance mode. The algorithm is briefly summarized in this section.

The geometry of the algorithm is shown in Figure 8.1. The edges of the collision

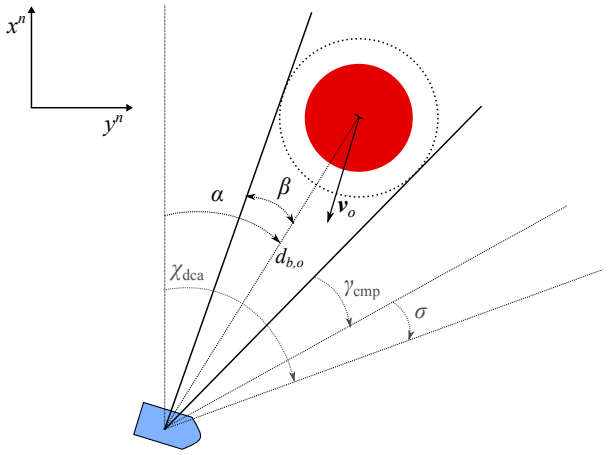

Figure 8.1: Geometric representation of the VO algorithm.

cone can be described geometrically as

$$\psi_{\text{t}}^{\pm} \triangleq \alpha \pm \beta, \tag{8.34}$$

where

$$\beta \triangleq \sin^{-1}\left(\frac{R_{o|\epsilon}}{d_{b,o}}\right) \in \left(0, \frac{\pi}{2}\right]. \tag{8.35}$$

The vehicle is said to be in a conflict with the obstacle if χ_{bo}^n lies within the angular boundaries of the collision cone:

$$|\chi_{bo}^n - \alpha| < \beta. \tag{8.36}$$

The edges of the absolute collision cone are defined geometrically as

$$\psi_{\text{abs}}^{\pm} \triangleq \gamma_{\text{cmp}}^{\pm} + \psi_{\text{t}}^{\pm}, \tag{8.37}$$

where the angle $\gamma_{\text{cmp}}^{\pm}$ compensates for the obstacle velocity.

The control system is switched to collision avoidance mode if the obstacle is too

close the vehicle, simultaneously as the guidance velocity is unsafe:

$$d_{b,o}(t_1) \leq d_{\text{threshold}}, \;\; \boldsymbol{v}^n_{ndg}(t_1) \in \mathcal{VO}_\sigma(t_1). \tag{8.38}$$

Nominal guidance will resume when the guidance velocity is safe:

$$\boldsymbol{v}^n_{ndg}(t_2) \notin \mathcal{VO}_\sigma(t_2). \tag{8.39}$$

If the distance equals $d_{b,o} = d_{\text{threshold}}$ when CA mode is entered, the turning direction makes the vehicle seek to pass behind the obstacle:

$$d_{b,o} = d_{\text{threshold}}, \;\; j = \arg\max_{j \in \{\pm\}} \left| \psi^n_o - \psi^{(j)}_{\text{abs}} \right|, \tag{8.40}$$

where j is the turning parameter. If the distance is less than $d_{\text{threshold}}$, the vehicle will instead turn away from the nearest conflict to ensure safety:

$$d_{b,o} < d_{\text{threshold}}, \;\; j = \arg\min_{j \in \{\pm\}} \left| \chi^n_b - \psi^{(j)}_{\text{abs}} \right|. \tag{8.41}$$

The course references in collision avoidance mode will make the vehicle avoid a collision with a nearby obstacle, given by

$$\chi^n_{\text{dca}j} \triangleq \psi^{(j)}_{\text{abs}} \pm \sigma, \;\; j \in \{\pm\}, \tag{8.42}$$

where $\sigma > 0$ is a constant design angle, and j is chosen by the turning rules presented before.

8.5 Analysis

In this section, we present the final analysis of the velocity obstacle algorithm described in Chapter 5, applied to an underactuated surface vehicle modeled by (8.1), for avoiding a moving obstacle described by (8.9), capable of both turning and accelerating towards the vehicle. We will prove that the vehicle can safely switch between nominal

guidance, in which the vehicle moves towards a target or follows along a path, and collision avoidance, in which the vehicle reactively avoids a moving obstacle in its presence. Furthermore, we will prove that the course references in collision avoidance mode makes the vehicle avoid a collision with the obstacle, provided that all stated assumptions hold. This will be achieved while simultaneously ensuring that the vehicle's sway speed is limited.

8.5.1 Bound on the sway speed

When the vehicle turns, a swaying motion will be induced, seen by the sway dynamics in (8.1e). The vehicle is underactuated in sway, meaning that the vehicle cannot produce control forces in the side-ways direction to stabilize the swaying motion. The purpose of the first lemma is to formulate the conditions ensuring that the vehicle's sway speed is bounded. By choosing the yaw rate based on this condition, we ensure that the magnitude of the sway speed cannot exceed the upper bound $v_{b,\max}$.

Lemma 8.1. *Consider a vehicle described by* (8.1)*, and let Assumption 8.2 and 8.7 hold. Suppose the yaw rate, r_b, is dependent on the sway speed, v_b, in a way that the following holds:*

$$|r_b(v_{b,\max})| < \frac{|Y(u_{\mathrm{db}})|}{|X(u_{\mathrm{db}})|} v_{b,\max}. \tag{8.43}$$

Then, if $|v_b(t_0)| \leq v_{b,\max}$,

$$|v_b(t)| \leq v_{b,\max}, \ \forall t \geq t_0. \tag{8.44}$$

Proof. Assumption 8.7 ensures that $u_b = u_{\mathrm{db}}, \ \forall t \geq t_0$. Hence, the proof of Lemma 7.2 applies. □

8.5.2 Upper bound on the heading saturation gain

In order to bound the sway speed, we must design the heading control law (8.18) to comply with the result of Lemma 8.1, which is achieved as long as the heading saturation gain satisfies an upper bound. Before presenting the next lemma, we define

the following expression for conciseness:

$$f_\psi(u_{\mathrm{db}}, \sigma) \triangleq v_{b,\max} |Y(u_{\mathrm{db}})| \left(\frac{1}{|X(u_{\mathrm{db}})|} - \frac{2}{U_{b,\max}^2} \left(\frac{u_{o,\max} v_{b,\max}}{\sqrt{U_{b,\max}^2 - u_{o,\max}^2}} + u_{\mathrm{db}} \right) \right)$$
$$- r_{o,\max} \frac{u_{o,\max}}{u_{\mathrm{db}}} - \frac{a_{o,\max}}{\sqrt{u_{\mathrm{db}}^2 - u_{o,\max}^2}} - \left(1 + \frac{u_{o,\max}}{U_{b,\max}} \right) \frac{U_{bo,\max}}{(R_o + d_\epsilon) \tan(\sigma)}, \tag{8.45}$$

where we define $U_{b,\max} \triangleq \sqrt{v_{b,\max}^2 + u_{\mathrm{db}}^2}$, and

$$U_{bo,\max} \triangleq \sqrt{u_{\mathrm{db}}^2 + v_{b,\max}^2 + u_{o,\max}^2 + 2u_{o,\max}(v_{b,\max} + u_{\mathrm{db}})}.$$

Lemma 8.2. *Consider an obstacle described by (8.9), and a vehicle described by (8.1). Let the vehicle's course references be given by the collision avoidance algorithm, defined in (8.42). Furthermore, let the vehicle be controlled by the the heading controller (8.18), the surge controller (8.30), and the yaw rate controller (8.32). Suppose that the vehicle maintains a distance to the obstacle satisfying*

$$d_{b,o}(t) \geq \frac{R_{o|\epsilon}}{\cos(\sigma)}, \ \forall t \geq t_0, \tag{8.46}$$

where $\sigma \in (0, \pi/2]$ is a constant angle. If Assumption 8.1-8.8 hold, and the heading saturation gain $k_\psi > 0$ satisfies

$$k_\psi \leq f_\psi(u_{\mathrm{db}}, \sigma). \tag{8.47}$$

Then, if $|v_b(t_0)| \leq v_{b,\max}$,

$$|v_b(t)| \leq v_{b,\max}, \ \forall t \geq t_0. \tag{8.48}$$

Proof. When Assumption 8.7 and 8.8 hold, we can apply the proof of Lemma 7.3 to

show that

$$|r_b| < \frac{|Y(u_{\text{db}})|}{|X(u_{\text{db}})|} v_{b,\max}, \ \forall\, k_\psi \leq f_\psi(u_{\text{db}}, \sigma), \tag{8.49}$$

provided condition (8.46) holds. Thus, condition (8.47) ensures that if $|v_b(t_0)| \leq v_{b,\max}$, then

$$|v_b(t)| \leq v_{b,\max}, \ \forall t \geq t_0, \tag{8.50}$$

by Lemma 8.1. □

The main difference from Lemma 7.3 is that we relax the upper bound on the heading control gain λ_ψ, by imposing the constraint on the heading saturation gain instead. Clearly, since $\lambda_\psi|\tilde{\psi}| \leq k_\psi, \ \forall \tilde{\psi}$ by the saturation term, we still satisfy the conditions of Lemma 8.1, while gaining more flexibility in the choice of λ_ψ.

8.5.3 Lower bound on the threshold distance

In order to ensure that the vehicle is able to turn out of a conflict before a collision occurs, we must derive a lower bound on the threshold distance for the switching condition (8.38), which is the purpose of the next lemma.

Lemma 8.3. *Consider an obstacle described by (8.9), and a vehicle described by (8.1). Let the vehicle enter collision avoidance mode according to the switching rule (8.38), as the distance satisfies $d_{b,o} = d_{\text{threshold}}$. Let the vehicle, controlled by the heading controller (8.18), the surge controller (8.30), and the yaw rate controller (8.32), follow the course references defined in (8.42), with the turning direction chosen by the turning rules (8.40)-(8.41). Let Assumption 8.1-8.8 hold, and suppose the vehicle speed satisfies $U_b \leq U_{b,\max}$, $\forall t \geq t_0$, and the yaw rate satisfies $r_b \leq r_{b,\max}$. If the threshold distance satisfies*

$$d_{\text{threshold}} \geq u_{o,\max} t_{\text{turn}} + d_{\text{sep}} + d_{\text{turn}}, \tag{8.51}$$

where

$$t_{\text{turn}} \coloneqq t_{\text{smooth}} + \left(\frac{\pi}{k_\chi} - \frac{1}{\lambda_\chi}\right) - \frac{\ln\left(\frac{\lambda_\psi}{k_\psi}\varepsilon\right)}{\lambda_\chi} \tag{8.52}$$

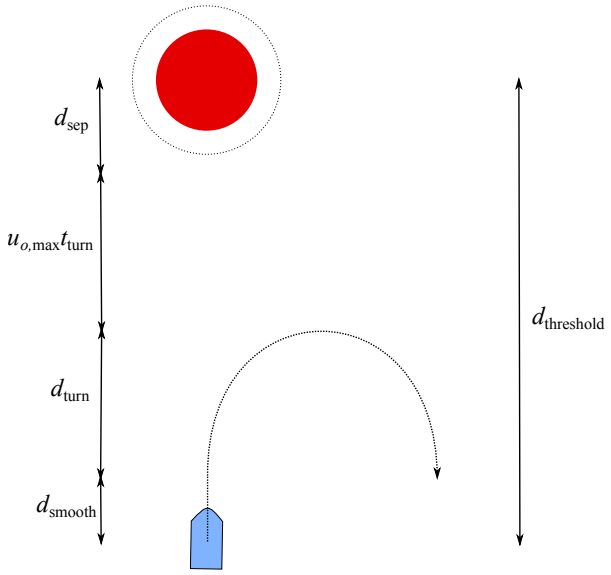

Figure 8.2: Illustration of the worst case collision avoidance scenario, including the smoothing distance.

is an upper bound of the time it takes for the vehicle to converge to within ε rad of the desired course, and

$$d_{\text{turn}} := U_{b\max} \left(t_{\text{smooth}} + \frac{1}{\min\left(k_\chi,\, \lambda_\chi \frac{\pi}{2}\right)} \right) \tag{8.53}$$

is an upper bound of the distance traveled by the vehicle towards the obstacle when making a π rad turn. Then, the vehicle is able to converge to within ε rad of the desired course before the obstacle is within the distance d_{sep} of the vehicle.

Proof. The proof of this lemma follows along the lines of the proof presented in Wiig et al. [26], which derives a minimum threshold distance by evaluating the worst case collision avoidance scenario between the vehicle and the obstacle. Let the radius of the obstacle be infinitely large, such that $\beta \to \pi/2$. The initial course error is then upper bounded by $|\tilde{\chi}| = \pi$. Moreover, the vehicle and obstacle speeds are upper bounded by

$U_{b,\max}$ and $u_{o,\max}$, respectively.

When the vehicle enters collision avoidance mode it will start turning towards the desired course by changing its heading. Suppose that the vehicle's initial yaw rate is zero. A jump in the yaw rate input signal will then be present, which is made continuous by the yaw rate smoothing function defined in (8.27). Recall that the largest feasible jump is defined as $\tilde{r}_{\max}$, over a time interval from t_{k-1} to t_k. For convenience, we assume the interval is 1 s. The largest jump is then found when $r_b(t_{k-1}) = 0$ and $r_d(t_k) = r_{b,\max}$. The time it takes for the vehicle to arrive at the desired turning rate is thus upper bounded by

$$t_{\text{smooth}} \coloneqq \frac{r_{b,\max}}{\tilde{r}_{\max}}. \tag{8.54}$$

Remark 8.4. An upper bound of r_b can always be found by Lemma 8.1 when the conditions of Lemma 8.2 holds.

Furthermore, the distance the vehicle travels towards the obstacle during the smoothing time is upper bounded by

$$d_{\text{smooth}} \coloneqq U_{b,\max} t_{\text{smooth}}. \tag{8.55}$$

After the smoothing time, the magnitude of the course error remains upper bounded by π. Since $\tilde{\chi} \triangleq \tilde{\psi}$, the heading controller (8.18) will saturate when $|\tilde{\chi}| > \frac{k_\psi}{\lambda_\psi}$. The time from $|\tilde{\chi}| = \pi$ to $|\tilde{\chi}| = \frac{k_\psi}{\lambda_\psi}$ can be found by considering the course error dynamics given by (8.24). Without loss of generality, let $\tilde{\chi} > \frac{k_\psi}{\lambda_\psi}$. The solution of (8.24) is then

$$\tilde{\chi}(t) - \tilde{\chi}(t_0) = -k_\chi (t - t_0), \tag{8.56}$$

where k_χ is defined in (8.26). Solving (8.56) for $\tilde{\chi}(t) = \frac{k_\psi}{\lambda_\psi}$ and $\tilde{\chi}(t_0) = \pi$, yields

$$t - t_0 = \frac{\pi}{k_\chi} - \frac{1}{\lambda_\chi} \coloneqq t_{\text{sat}}, \tag{8.57}$$

where λ_χ is defined in (8.25). Note that since $k_\chi < \lambda_\chi \pi$, it is ensured that $t_{\text{sat}} > 0$. From this point on, the course will converge exponentially. The solution of (8.24) is

then

$$\tilde{\chi}(t) = \tilde{\chi}(t_0)e^{-\lambda_\chi(t-t_0)}. \tag{8.58}$$

The time it takes for the vehicle to converge to within ε rad of the desired course is thus given by

$$t_\varepsilon := -\frac{\ln\left(\varepsilon\frac{\lambda_\psi}{k_\psi}\right)}{\lambda_\chi}, \ \forall \varepsilon \in \left(0, \ \frac{k_\psi}{\lambda_\psi}\right]. \tag{8.59}$$

The complete maneuver will be finished at $t_{\text{turn}} := t_{\text{smooth}} + t_{\text{sat}} + t_\varepsilon$. The distance the obstacle travels during the maneuver is upper bounded by $u_{o,\max}t_{\text{turn}}$.

The distance the vehicle travels towards the obstacle after the smoothing time is upper bounded by the distance the vehicle travels when making a $\pi/2$ rad turn, as illustrated in Figure 8.2. A lower bound of the course rate when the controller saturates is found from (8.24) as $|r_\chi| = k_\chi$. This can be seen as the vehicle moves towards the obstacle during the $\pi/2$ turn. This causes the angle β to increase by (8.35), which causes $\chi^n_{\text{db}} = \chi^n_{\text{dca}j}$ to increase as well. Hence, $\dot{\chi}^n_{\text{db}} \geq 0$, and the minimum course rate is found when $\dot{\chi}^n_{\text{db}} = 0$. If the course converges exponentially, the course error will be at least $\pi/2$ during the turn by the same argument, i.e. the desired course is either constant or increasing as the vehicle moves closer to the obstacle. The minimum course rate is thus $|r_\chi| = \lambda_\chi\frac{\pi}{2}$ by (8.24). An upper bound of the distance the vehicle travels when making a $\pi/2$ rad turn is then found as

$$d_{\pi/2} := \frac{U_{b,\max}}{\min\left(k_\chi, \ \lambda_\chi\frac{\pi}{2}\right)}. \tag{8.60}$$

The distance the vehicle travels towards the obstacle when making a π rad turn is upper bounded by the distance the vehicle travels during the smoothing interval, and the distance the vehicle travels when making a $\pi/2$ rad turn:

$$d_{\text{turn}} := d_{\text{smooth}} + d_{\pi/2}. \tag{8.61}$$

Finally, it follows that if the threshold distance satisfies (8.51), then the vehicle will converge to within ε rad of the desired course, before the distance between the vehicle

and the obstacle, $d_{b,o}$, is less than the distance d_{sep}. □

We are now ready to present the main theorems of the chapter. The following assumption must hold:

Assumption 8.9. The vehicle and the obstacle are initially separated by a distance satisfying

$$d_{b,o}(t_0) \geq d_{\text{threshold}}. \tag{8.62}$$

Finally, to ensure that the smoothing time presented in Lemma 8.3, i.e. the time it takes for the vehicle to reach the desired yaw rate, is not large enough to cause a collision, the following assumption needs to be met:

Assumption 8.10. The smoothing time t_{smooth} is small enough to be neglected:

$$(u_{o,\max} + U_{b,\max})t_{\text{smooth}} \ll R_{o|\epsilon}. \tag{8.63}$$

Remark 8.5. If Assumption 8.10 does not hold, which for instance is the case for exceptionally heavy vessels, then the obstacle's motion must be restricted at a close range, otherwise a collision will likely occur. In such cases, it is necessary to assume that the obstacle's decisions are not ill-advised, e.g. by assuming the obstacle obeys the International Regulations for Preventing Ship Collision at Sea (COLREGS). In this thesis, we consider the case where Assumption 8.10 holds.

8.5.4 Safe target reaching

In this section, we will provide the conditions ensuring that an underactuated surface vehicle modeled by (8.1), can travel safely towards a static position in the world frame, in the presence of a moving obstacle modeled by (8.9), while also maintaining a limited sway speed in accordance with (8.43).

Theorem 8.1. *Consider an obstacle described by (8.9) and a vehicle described by (8.1). Let Assumption 8.1-8.10 hold, the threshold distance satisfy*

$$d_{\text{threshold}} \geq u_{o,\max} t_{\text{turn}} + \frac{R_o + d_\epsilon}{\cos(\sigma)} + d_{\text{turn}}, \tag{8.64}$$

where t_{turn} and d_{turn} are defined in Lemma 8.3, and the safety angle $\sigma \in (0, \pi/2]$ satisfy

$$\sigma = \bar{\sigma} + \varepsilon, \quad \bar{\sigma} > 0, \, \varepsilon > 0. \tag{8.65}$$

Furthermore, let the heading saturation gain k_ψ satisfy

$$k_\psi \leq f_\psi(u_{\text{db}}, \bar{\sigma}), \tag{8.66}$$

where $f_\psi(\cdot)$ is defined in (8.45), and the acceptance distance satisfy

$$d_a > \frac{|X(u_{\text{db}})| U_{b,\max}}{|Y(u_{\text{db}})| v_{b,\max} - |X(u_{\text{db}})| k_\chi}, \tag{8.67}$$

where k_χ is defined in (8.26). Then, the vehicle controlled by the heading controller (8.18), the surge controller (8.30), and the yaw rate controller (8.32), following the pure pursuit guidance law (8.12), the switching rules (8.38)-(8.39), the turning rules (8.40)-(8.41), and the collision avoidance law (8.42), will converge to within d_a of the target position $\boldsymbol{p}_{\text{t}}^n$ at an unspecified point in time $t_{\text{f}} < \infty$, and furthermore satisfy

$$d_{b,o}(t) - R_o \geq d_\epsilon, \ \forall t \in [t_0, \, t_{\text{f}}], \tag{8.68}$$

while ensuring that

$$|v_b(t)| \leq v_{b,\max}, \ \forall t \in [t_0, \, t_{\text{f}}]. \tag{8.69}$$

Proof. An upper bound of the required course rate when the vehicle follows the pure pursuit guidance law is given by

$$|\dot{\chi}_{\text{pp}}^n| \leq \frac{U_{b,\max}}{d_a}. \tag{8.70}$$

Inserting (8.70) and the upper bound of the control law (8.18) into the relation (8.22), with $\dot{u}_b = 0$ ensured by Assumption 8.7, yields the following upper bound:

$$|r_b| \leq \left(\frac{U_{b,\max}}{d_a} - \frac{|Y(u_{\mathrm{db}})| v_{b,\max} u_{\mathrm{db}}}{U_{b,\max}^2} \right) \frac{U_{b,\max}^2}{U_{b,\max}^2 - |X(u_{\mathrm{db}})| u_{\mathrm{db}}} + k_\psi \tag{8.71}$$

Hence, by Lemma 8.1 the acceptance distance d_a must satisfy

$$d_a > \frac{|X(u_{\mathrm{db}})| U_{b,\max}}{|Y(u_{\mathrm{db}})| v_{b,\max} - |X(u_{\mathrm{db}})| k_\chi}, \tag{8.72}$$

where k_χ is defined in (8.26), in order to ensure that the sway speed satisfies $|v_b(t)| \leq v_{b,\max},\ \forall t \geq t_0$ in the presence of zero obstacles.

Let the vehicle enter collision avoidance mode at $t_1 \geq t_0$, as the distance satisfies $d_{b,o}(t_1) = d_{\text{threshold}}$. Lemma 8.3 and condition (8.64) ensures that there exists a time $t_2 > t_1$, in which the vehicle satisfies

$$d_{b,o}(t_2) \geq \frac{R_o + d_\epsilon}{\cos(\sigma)}, \tag{8.73}$$

and $\left|\chi_b^n(t_2) - \chi_{\mathrm{dca}j}^n(t_2)\right| \leq \varepsilon$. Since the desired yaw rate is given as a continuous input signal, and $\tilde{\chi} = 0$ is a locally stable equilibrium when the heading controller (8.18) is employed, it is ensured that

$$\left|\chi_b^n(t) - \chi_{\mathrm{dca}j}^n(t)\right| \leq \varepsilon,\ \forall t \in [t_2,\, t_3]\,, \tag{8.74}$$

where $t_3 \geq t_2$ is the time the vehicle exits CA mode. Condition (8.74) furthermore ensures that $|\chi_{bo}^n(t) - \alpha(t)| \geq \beta(t) + \bar{\sigma},\ \forall t \in [t_2,\, t_3]$. Hence,

$$d_{b,o}(t) \geq \frac{R_o + d_\epsilon}{\cos(\bar{\sigma})},\ \ \forall t \in [t_1,\, t_3\,]\,, \tag{8.75}$$

by Lemma 7.1. Finally, Lemma 8.2 along with condition (8.66) then ensures that

$$|v_b(t)| \leq v_{b,\max},\ \forall t \in [t_1,\, t_3\,]\,. \tag{8.76}$$

If collision avoidance mode is entered as $d_{b,o} < d_{\text{threshold}}$, Assumption 8.10 ensures that the smoothing time is small enough to be neglected. Since $\chi^n_{\text{dca}j}$ is first-time differentiable, the vehicle will immediately be able to follow desired course, and satisfy (8.74) until it exits collision avoidance mode.

Finally, since $u_{\text{db}} > u_{o,\max}$, the vehicle will escape the obstacle at some point in time, and proceed to the target $\boldsymbol{p}^n_{\text{t}}$. By Lemma 6.2 and Assumption 8.8 the vehicle will converge to within d_a of the target at some point in time $t_{\text{f}} < \infty$. By the above analysis, we can conclude that the conditions (8.68) and (8.69) are satisfied. □

8.5.5 Safe path following

In this section, we will formulate the conditions ensuring that an underactuated surface vehicle modeled by (8.1), will converge to and stay on the path defined in (8.5), by following the LOS guidance law (8.14), while also avoiding a collision with an obstacle modeled by (8.9), and maintaining a limited sway speed complying with (8.43). Before presenting the main theorem, we must restate Lemma 6.3 to comply with the system (8.1).

Lemma 8.4. *Let the path-tangential angle χ_p be defined as (8.15), the cross-track error y_{e} be defined as (8.16), and the lookahead distance satisfy $\Delta > 0$. Then, the LOS guidance law*

$$\chi^n_{\text{los}}(y_{\text{e}}) = \chi_p + \arctan\left(\frac{-y_{\text{e}}}{\Delta}\right) \tag{8.77}$$

ensures that the cross-track error y_e of the system (8.1) converges globally uniformly asymptotically to the origin.

Proof. The proof is equivalent to the proof of Lemma 6.3 if we write the time-derivatives of x^n_b and y^n_b in terms of the vehicle's course, as

$$\dot{x}^n_b = U_b \cos(\chi^n_b), \tag{8.78}$$

$$\dot{y}^n_b = U_b \sin(\chi^n_b). \tag{8.79}$$

Following the method presented in Lemma 6.3, we use the Lyapunov function candidate

given by

$$V = \frac{1}{2} y_e^2, \tag{8.80}$$

and the guidance law stated in (8.77), to show that the time-derivative of (8.80) satisfies

$$\dot{V} = -U_b \frac{y_e^2}{\Delta \sqrt{\left(\frac{y_e}{\Delta}\right)^2 + 1}} < 0, \ \forall y_e \neq 0. \tag{8.81}$$

Hence, the origin of $\dot{y}_e$ is UGAS. □

Theorem 8.2. *Consider an obstacle described by (8.9) and a vehicle described by (8.1). Let Assumption 8.1-8.10 hold, the threshold distance satisfy*

$$d_{\text{threshold}} \geq u_{o,\max} t_{\text{turn}} + \frac{R_o + d_\epsilon}{\cos(\sigma)} + d_{\text{turn}}, \tag{8.82}$$

where t_{turn} and d_{turn} are defined in Lemma 8.3, and the safety angle $\sigma \in (0, \pi/2]$ satisfy

$$\sigma = \bar{\sigma} + \varepsilon, \quad \bar{\sigma} > 0, \varepsilon > 0. \tag{8.83}$$

Furthermore, let the heading saturation gain k_ψ satisfy

$$k_\psi \leq f_\psi(u_{\text{db}}, \bar{\sigma}), \tag{8.84}$$

where $f_\psi(\cdot)$ is defined in (8.45), and the lookahead distance satisfy

$$\Delta > \frac{|X(u_{\text{db}})| U_{b,\max}}{|Y(u_{\text{db}})| v_{b,\max} - |X(u_{\text{db}})| k_\chi}, \tag{8.85}$$

where k_χ is defined in (8.26). Then, the vehicle controlled by the heading controller (8.18), the surge controller (8.30), and the yaw rate controller (8.32), following the LOS guidance law (8.14), the switching rules (8.38)-(8.39), the turning rules (8.40)-(8.41), and the collision avoidance law (8.42), will converge to, and follow along the path $\mathcal{P}$, and furthermore satisfy

$$d_{b,o}(t) - R_o \geq d_\epsilon, \ \forall t \geq t_0, \tag{8.86}$$

while ensuring that

$$|v_b(t)| \leq v_{b,\max}, \ \forall t \geq t_0. \tag{8.87}$$

Proof. The required course rate when the vehicle follows the LOS guidance law is computed from (8.14) as

$$\dot{\chi}^n_{\text{los}} = -\frac{\Delta \dot{y}_e}{\Delta^2 + y_e^2}, \tag{8.88}$$

where y_e is the cross-track error defined in (8.16), and $\Delta > 0$ is the lookahead distance. The time-derivative of the cross-track error is bounded by $|\dot{y}_e| \leq U_b$, and

$$\frac{\Delta}{\Delta^2 + y_e^2} \leq \frac{\Delta}{\Delta^2} = \frac{1}{\Delta}. \tag{8.89}$$

Hence, the required course rate during LOS guidance is upper bounded by

$$|\dot{\chi}^n_{\text{db}}| \leq \frac{U_{b,\max}}{\Delta}. \tag{8.90}$$

Inserting (8.90) and the upper bound of the control law (8.18) into the relation (8.22), with $\dot{u}_b = 0$ ensured by Assumption 8.7, yields the following upper bound:

$$|r_b| \leq \left(\frac{U_{b,\max}}{\Delta} - \frac{|Y(u_{\text{db}})| v_{b,\max} u_{\text{db}}}{U^2_{b,\max}} \right) \frac{U^2_{b,\max}}{U^2_{b,\max} - |X(u_{\text{db}})| u_{\text{db}}} + k_\psi \tag{8.91}$$

Hence, by Lemma 8.1 the lookahead distance Δ must satisfy

$$\Delta > \frac{|X(u_{\text{db}})| U_{b,\max}}{|Y(u_{\text{db}})| v_{b,\max} - |X(u_{\text{db}})| k_\chi}, \tag{8.92}$$

where k_χ is defined in (8.26), in order to ensure that the sway speed satisfies $|v_b(t)| \leq v_{b,\max}, \ \forall t \geq t_0$ in the presence of zero obstacles.

The rest of the proof is equivalent to the proof of Theorem 8.1. Moreover, the vehicle will escape from the obstacle at some point in time, since $u_{\text{db}} > u_{o,\max}$. By Lemma 8.4 and Assumption 8.8 the vehicle will converge to the path in finite time, and for the remainder of the time, follow along it. □

8.6 Simulations

This section presents two numerical simulations of an underactuated surface vehicle, whose model is stated in (8.1), following the velocity obstacle algorithm for reactive collision avoidance of a moving obstacle modeled as (8.9). Specific parts of the implantation of the algorithm can be found in Section 8.4. The vehicle's model parameters belong to an LAUV (light AUV) [4], operating in 3 DOF, i.e. the horizontal plane.

In all simulations, the vehicle's initial and desired surge speed was chosen as $u_b(t_0) = u_{db} = 2$ m/s. We can verify that Assumption 8.2 holds with $Y(u_{db}) = -2.8161$, and Assumption 8.6 is satisfied with $X(u_{db}) = -1.0242$. The sway speed should not exceed the surge speed, i.e. $v_{b,\max} = 2$ m/s. The initial heading of the vehicle was chosen as $\psi_b^n(t_0) = 0$ rad, and the initial NED position as $\boldsymbol{p}_{nb}^n(t_0) = [0,\ 0]^\top$ m. The obstacle radius was chosen as $R_o = 10$ m and the safety distance as $d_\epsilon = 5$ m. Finally, the convergence parameter was set to $\varepsilon = 0.09$ rad and the angular safety distance was chosen equal to $\sigma = 0.7$ rad.

8.6.1 Target reaching

This section presents a simulation of the vehicle following the pure pursuit guidance law (8.12) in combination with collision avoidance of an obstacle. The target position was chosen as $\boldsymbol{p}_{\text{t}}^n = [140,\ 0]^\top$ m. The obstacle turns in a clockwise circle, with constant turning rate $r_o = r_{o,\max} = 0.1$ rad/s, and constant forward speed $u_o = u_{o,\max} = 1.3$ m/s, satisfying Assumption 8.5. The heading saturation gain was chosen according to Theorem 8.1 as $k_\psi = 0.538$ rad/s, satisfying the required bound which was verified by direct computation. The heading control gain was chosen as $\lambda_\psi = 0.8\ \text{s}^{-1}$. Finally, the threshold distance was set to $d_{\text{threshold}} = 51$ m and the acceptance distance to $d_a = 1$ m, satisfying the conditions of Theorem 8.1.

Trajectories of the vehicle and the obstacle are shown in Figure 8.5. In Figure 8.5a the obstacle can be seen to turn in a uniform circle as the vehicle enters CA mode according to the switching rule (8.38), with $d_{b,o} = d_{\text{threshold}}$. The vehicle turns right according to the turning rule (8.40), and converges to within ε rad of the desired course before the obstacle is within the safety distance of it. The vehicle safely exits CA mode

at $t = 51$ s, seen in Figure 8.5c, and reaches the target at $t = 74$ s, in Figure 8.5d.

Figure 8.3a shows the distance between the vehicle and the obstacle, $d_{b,o}(t)$, plotted against the threshold distance, $d_{\text{threshold}}$, and the minimum required separation distance, $R_{o|\epsilon}$. Additionally, the distance $\frac{R_{o|\epsilon}}{\cos(\bar{\sigma})}$, where $\bar{\sigma} \triangleq \sigma - \varepsilon$, is included to verify that the conditions of Lemma 8.2 hold. The distance between the vehicle and the obstacle remains above $\frac{R_{o|\epsilon}}{\cos(\bar{\sigma})}$ at all times, thus verifying the theoretical result of Theorem 8.1.

8.6.2 Path following

This section presents a simulation of the vehicle following the LOS guidance law (8.14) in combination with collision avoidance of an obstacle. The path was chosen parallel to the x^n axis, with $y^n_{\text{t}} = -20$ m. The obstacle approaches the vehicle head on with constant acceleration $a_o = a_{o,\max} = 0.05$ m/s^2, initial speed $u_o(t_0) = 0$ m/s and maximum speed $u_{o,\max} = 1.4$ m/s, satisfying Assumption 8.5. The heading saturation gain was then computed as $k_\psi = 0.38$ rad/s, satisfying the condition of Theorem 8.2. The heading control gain was set to $\lambda_\psi = 0.6$ s^{-1}. The threshold distance was chosen as $d_{\text{threshold}} = 60$ m, and the lookahead distance as $\Delta = 10$ m, satisfying the conditions of Theorem 8.2.

The trajectories of the vehicle and the obstacle are shown in Figure 8.6. The vehicle enters CA mode close to path, as seen in Figure 8.6a, but is forced to move aside in order to avoid the incoming obstacle. By turning to the left, the vehicle is able to maintain a safe course as obstacle passes, seen in Figure 8.6b. The vehicle leaves collision avoidance mode at $t = 41$ s as the guidance velocity becomes safe, in Figure 8.6c. From this point on, the vehicle converges to the path and follows along it, as seen in Figure 8.6d. The distance between the vehicle and the obstacle is shown in Figure 8.3b. We can then verify that the distance remains above the requirement, and thus supports the theoretical result of Theorem 8.2.

The sway speed of the vehicle during both simulations is shown in Figure 8.4. As we saw in Chapter 7, the size of sway speed is small during both collision avoidance scenarios, and remains far below the maximum $v_{b,\max}$. Hence, the simulation results support the theoretical results of Theorem 8.1 and 8.2, although it also indicates that

the theoretical upper bound on the heading saturation gain is conservative.

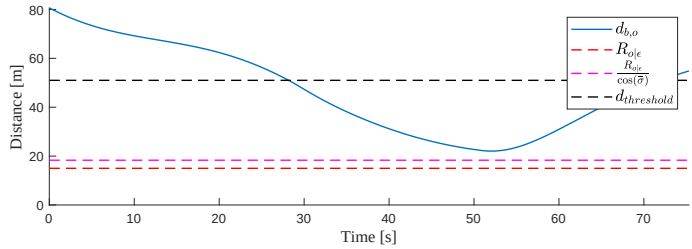

(a) Distance, $d_{b,o}$, during the first simulation.

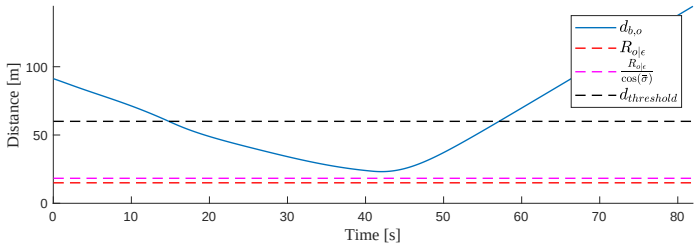

(b) Distance, $d_{b,o}$, during the second simulation.

Figure 8.3: Distance between the vehicle and the obstacle during both simulations.

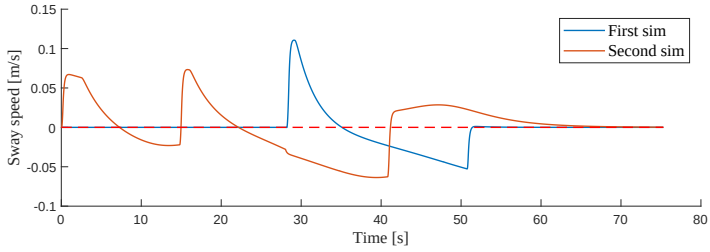

Figure 8.4: Vehicle sway speed, v_b, during both simulations.

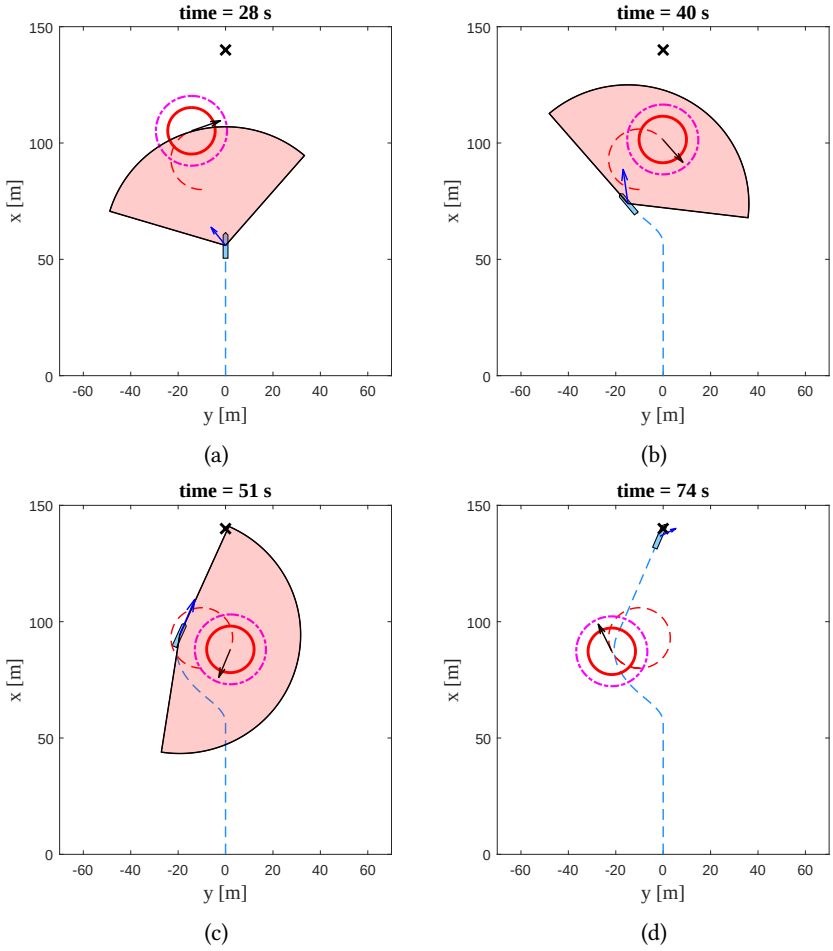

Figure 8.5: First simulation of an underactuated surface vehicle following the velocity obstacle algorithm in combination with pure pursuit guidance, in the presence of a turning obstacle. The obstacle is the red circle, the vehicle is the blue polygon, and the safety distance is the magenta line encircling the obstacle. The trajectories of the vehicle and the obstacle are the blue and red, dashed lines, respectively. The extended collision cone, $\mathcal{CC}_\sigma$, is the red cone, and the relative guidance velocity, $\boldsymbol{v}^n_{ndgo}$, is the blue arrow. The target position is marked as an 'X'.

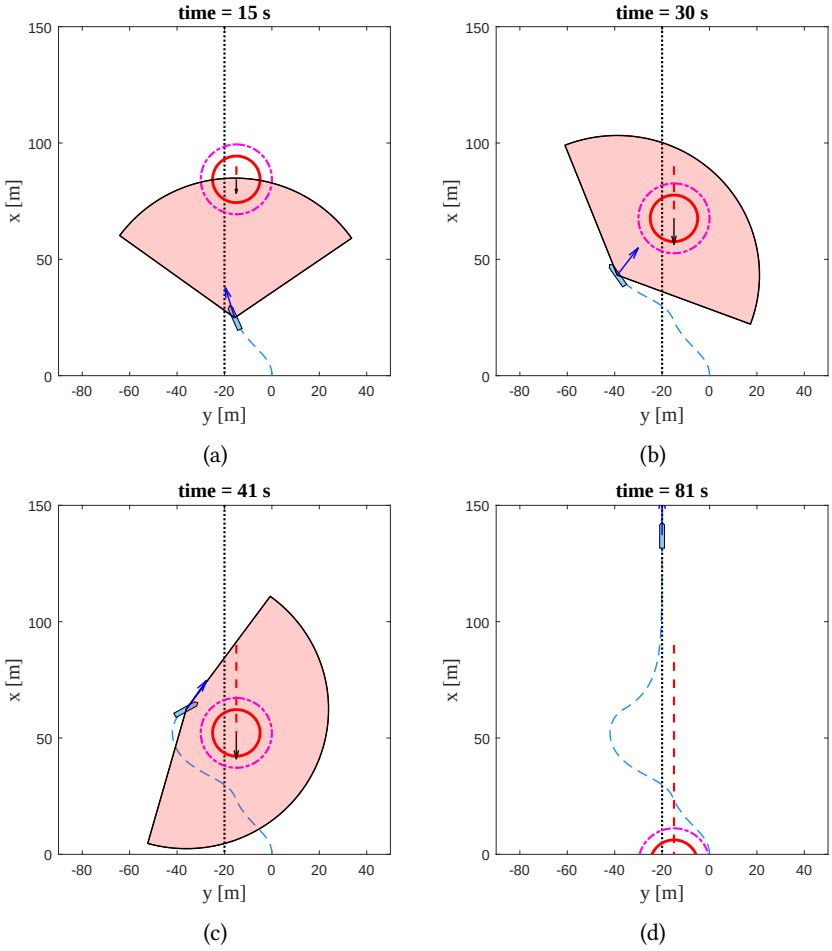

Figure 8.6: Second simulation of an underactuated surface vehicle following the velocity obstacle algorithm in combination with LOS guidance, in the presence of an accelerating obstacle. The path $\mathcal{P}$ is represented by the dotted line.

8.A Functional expressions

The expressions derived in Chapter 3 are restated here for convenience:

$$f_u(v_b, r_b) \triangleq r_b \frac{r_b m_{23} + v_b m_{22}}{m_{11}} - v_b \frac{d_{11}}{m_{11}}, \tag{8.93}$$

$$f_v(u_b, v_b, r_b) \triangleq Y(u_b) v_b + X(u_b) r_b, \tag{8.94}$$

$$\begin{aligned} f_r(u_b, v_b, r_b) \triangleq\ & v_b \frac{d_{32} m_{23} - d_{22} m_{33} + u_b m_{23} (m_{11} + m_{22})}{m_{22} m_{33} - m_{23}^2} \\ & + r_b \frac{d_{33} m_{23} - d_{23} m_{33} + u_b \left(m_{23}^2 - m_{11} m_{33}\right)}{m_{22} m_{33} - m_{23}^2}, \end{aligned} \tag{8.95}$$

where

$$X(u_b) \triangleq \frac{d_{32} m_{23} - d_{33} m_{22} + u_b m_{23} (m_{11} - m_{22})}{m_{22} m_{33} - m_{23}^2}, \tag{8.96}$$

$$Y(u_b) \triangleq \frac{d_{22} m_{23} - d_{32} m_{22} - u_b m_{22} (m_{22} + m_{11})}{m_{22} m_{33} - m_{23}^2}. \tag{8.97}$$

Chapter 9

Conclusions and future work

In this thesis, we have implemented, applied, and analyzed the velocity obstacle algorithm for collision avoidance of a single, moving obstacle. The algorithm makes the vehicle avoid a collision with a nearby obstacle by generating safe velocity references for it to follow. Any velocities outside of the set of unsafe velocities, called the velocity obstacle, are considered safe. The vehicle followed these references when an obstacle came within a chosen threshold distance of it, until the vehicle's nominal behaviour was considered safe again.

In Chapter 5 we introduced the algorithm and the obstacle model, and presented a preliminary analysis of the fundamental concept of this method, proving that collision avoidance of a circular obstacle, moving with time-varying velocity, was achieved. In Chapter 6 we investigated the collision avoidance algorithm applied to a kinematic model, the unicycle, subject to nonholonomic constraints. In Chapter 7 we extended this model to include the underactuated sway dynamics of a surface vehicle, while in Chapter 8 we analyzed the full dynamical model of this vehicle. In all chapters, we investigated collision avoidance in combination with other vehicle goals, specifically in the form of target reaching and/or path following. We provided numerical simulations of the kinematic and the dynamical models, following the collision avoidance algorithm in combination with guidance laws for path following and target reaching, to support

the theoretical results.

Chapter 6 - The VO algorithm for unicycles

In this chapter, we investigated the safety of a kinematic vehicle that was subject to kinematic constraints, when following the VO algorithm in the presence of a moving obstacle. The vehicle was restricted to maintain a constant forward speed, and had limited turning rate, showing that the algorithm suitable for vehicles with heavy linear acceleration constraints and/or limited turning capabilities.

With these constraints, we derived a minimum threshold distance which ensured that the vehicle was able to turn out of an entered conflict before a collision could occur with the obstacle. To avoid collision, we made the vehicle turn with maximum turning power towards a safe heading as it entered collision avoidance mode. The vehicle maintained this behaviour until nominal guidance could safely resume.

Through a mathematical analysis of the algorithm we derived a lower bound on the required turning rate of the vehicle. The lower bound ensured that collision avoidance was achieved in any scenario with a non-cooperative obstacle, dependent on the obstacle's speed and turning capabilities. Hence, the bound has intuitive meaning in that the vehicle's required turning rate increases/decreases with the obstacle's maximum turning rate, speed and forward acceleration. Furthermore, we combined the proofs with target reaching and path following, ensuring that the vehicle not only avoided collision, but also reached its other goals.

The theoretical bounds were supported by numerical simulations, which showed that the vehicle, satisfying the necessary conditions and following the collision avoidance algorithm, was able to circumvent an obstacle and maintaining a minimum distance from it at all times, even in scenarios where the obstacle accelerated and turned directly towards the vehicle for some time. We also verified that the vehicle achieved its separate goals in the presence of an obstacle.

Chapter 7 - The VO algorithm for vehicles with underactuated dynamics

In this chapter, we extended the kinematic model to include underactuated dynamics. In particular, we included the underactuated sway dynamics of the marine vehicle modeled in Chapter 3.

Although the vehicle cannot produce forces in the side-ways (sway) direction, swaying motions are induced by the vehicle's turning motion. At times, this can cause the vehicle to glide side-ways rather than moving forward, which in effect may bring the vehicle closer to the obstacle than intended. We addressed this issue by compensating for the crab angle induced by the nonzero sway speed when controlling the vehicle's heading, and by letting the guidance- and collision avoidance algorithm generate course references instead of heading references.

As in the previous chapter, we restricted the vehicle to maintain a constant forward speed, while directly controlling the heading rate, showing that the algorithm is applicable to vehicle's with heavy acceleration constraints and limited speed envelopes. To deal with the added velocity component, we derived conditions under which the sway speed was bounded, by the assumption that the vehicle was nominally stable in sway. This allowed us to derive a minimum threshold distance deciding when to start the vehicle's maneuver to safety. The conditions were derived by allowing the sway speed to be within a chosen interval. Furthermore, we introduced a constant safety angle ensuring that the vehicle remained a constant safety distance from the obstacle. These design parameters were used to derive an upper bound of the heading control gain. Increasing the safety angle and the maximum sway speed allowed us to increase this gain. In return, the vehicle needed to maintain a larger distance from the obstacle, and we allowed for a larger sway speed.

We showed that as long as the control gain was chosen positive, the vehicle's course dynamics were exponentially stable. Thus, the vehicle was ensured to track the desired course once the course had converged. Since the desired course in collision avoidance mode was chosen to lie outside the edges of the absolute collision cone, and the threshold distance was chosen large enough to ensure that the vehicle had

converged to the desired course before a collision, this proved that a collision with the obstacle was avoided. Finally, target reaching of a static target was considered along side collision avoidance. It was then necessary to derive a lower bound of the acceptance distance which ensured that the vehicle's sway speed remained bounded during nominal guidance as well.

We presented simulation results in order to verity the theoretical results. These showed that collision avoidance was achieved in combination with target reaching of a static target, under the presented assumptions and conditions. Furthermore, the vehicle's sway speed remained far below the maximum allowed value, which indicates that the theoretical upper bound on the yaw rate is somewhat conservative. Due to the complexity of the problem, and the shear number of parameters that had to be considered, it is difficult to derive a tighter bound without loss of generality. However, the importance was that the size of the sway speed remained below an upper limit, which was clearly achieved.

Chapter 8 - The VO algorithm for underactuated surface vehicles

We analyzed the full 3 DOF model of an underactuated surface vehicle in this chapter, by including the actuated surge and yaw dynamics of the vehicle we modeled in Chapter 3.

We applied two feedback linearizing controllers to stabilize the yaw and surge dynamics, thus ensuring that the vehicle tracked the desired surge speed and yaw rate, on the condition that the references were given as continuous signals. As in the two previous chapters, the vehicle was restricted to maintain a constant forward speed, ensuring that this condition was satisfied for the surge controller.

A saturated heading controller was employed in order to generate yaw rate references. By compensating for the crab angle, we showed that the controller ensured local, exponential stabilization of the course error dynamics. The input to the heading controller was furthermore generated by the collision avoidance algorithm in collision avoidance mode, and the guidance law in guidance mode. During the transition between these two modes, the course reference may be discontinuous, which in turn

causes a jump in the yaw rate input signal. To deal with issue, we introduced a yaw rate smoothing function, which made the yaw rate signal continuous in the case of a jump. However, this introduced an additional smoothing time that had to be accounted for.

We derived a minimum threshold distance which accounted for the smoothing time, and extended the results of the previous chapter to apply for the full dynamical model. This required only minor alterations. The results were furthermore combined with both target reaching and path following in this chapter, where we derived sufficient lower bounds on the acceptance distance and the lookahead distance, ensuring that the sway speed remained bounded during nominal guidance as well as during collision avoidance. Simulations were provided in order to support the presented theoretical results.

Future work

In this thesis, we have examined scenarios with a circular obstacle. This is not a requirement of the algorithm; if the obstacle shape is non-circular, the collision cone may be computed to fit the exact shape of the obstacle by substituting the circular domain $\mathcal{D}_o$ with any shaped domain $\mathcal{D}$. However, the performance of the algorithm in such cases remains to be analysed and is a topic of future research. Other topics concern the issue of avoiding multiple moving obstacles, and avoidance of other agents in multi-agent scenarios. In such cases, the vehicle must avoid the velocities inside the combined set of velocity obstacles. Analysis of such scenarios is inherently more complex and remains a subject for future work. Finally, extending the analysis to guarantee collision avoidance for underwater vehicles, capable of movement in more than 3 degrees of freedom, is an interesting topic to consider, left to future research.

References

[1] Alonso-Mora, J., Naegeli, T., Siegwart, R., and Beardsley, P. (2015). Collision avoidance for aerial vehicles in multi-agent scenarios. *Autonomous Robots*, 39(1):101–121.

[2] Bareiss, D. and van den Berg, J. (2015). Generalized reciprocal collision avoidance. *The International Journal of Robotics Research*, 34(12):1501–1514.

[3] Cho, Y., Han, J., Kim, J., Lee, P., and Park, S.-B. (2019). Experimental validation of a velocity obstacle based collision avoidance algorithm for unmanned surface vehicles. In *Proc. Conference on Control Applications in Marine Systems, Robotics, and Vehicles*, pages 329 – 334.

[4] Estrela da Silva, J., Terra, B., Martins, R., and Sousa, J. (2007). Modeling and simulation of the LAUV autonomous underwater vehicle. In *Proc. IEEE IFAC International Conference on Methods and Models in Automation and Robotics*.

[5] Fiorini, P. and Shiller, Z. (1998). Motion planning in dynamic environments using velocity obstacles. *The International Journal of Robotics Research*, 17(7):760–772.

[6] Fossen, T. I. (2011). *Handbook of Marine Craft Hydrodynamics and Motion Control*. John Wiley & Sons.

[7] Hoy, M., Matveev, A. S., and Savkin, A. V. (2015). Algorithms for collision-free navigation of mobile robots in complex cluttered environments: a survey. *Robotica*, 33:463–497.

[8] Huang, Y., Chen, L., Chen, P., Negenborn, R. R., and [van Gelder], P. (2020). Ship collision avoidance methods: State-of-the-art. *Safety Science*, 121:451 – 473.

[9] Huang, Y., Chen, L., and Gelder, P. (2019). Generalized velocity obstacle algorithm for preventing ship collisions at sea. *Ocean Engineering*, 173:142–156.

[10] Jenie, Y. I., Kampen, E.-J. V., de Visser, C. C., Ellerbroek, J., and Hoekstra, J. M. (2015). Three-dimensional velocity obstacle method for UAV deconflicting maneuvers. In *Proc. AIAA Guidance, Navigation, and Control Conference*.

[11] Jenie, Y. I., Kampen, E.-J. V., de Visser, C. C., Ellerbroek, J., and Hoekstra, J. M. (2016). Three-dimensional velocity obstacle method for uncoordinated avoidance maneuvers of unmanned aerial vehicles. *Journal of Guidance, Control, and Dynamics*, 39(10):2312 – 2323.

[12] Johansen, T. A. and Fossen, T. I. (2013). Control allocation—a survey. *Automatica*, 49(5):1087 – 1103.

[13] Khalil, H. K. (2002). *Nonlinear Systems*. Prentice Hall, Upper Saddle River.

[14] Koren, Y. and Borenstein, J. (1991). Potential field methods and their inherent limitations for mobile robot navigation. In *Proc. IEEE International Conference on Robotics and Automation*, pages 1398–1404.

[15] Kuwata, Y., Wolf, M., Zarzhitsky, D., and Huntsberger, T. (2014). Safe maritime autonomous navigation with COLREGS, using velocity obstacles. *IEEE Journal of Oceanic Engineering*, 39:110–119.

[16] Lalish, E. and Morgansen, K. A. (2012). Distributed reactive collision avoidance. *Autonomous Robots*, 32:207 – 226.

[17] Lalish, E., Morgansen, K. A., and Tsukamaki, T. (2008). Decentralized reactive collision avoidance for multiple unicycle-type vehicles. In *Proc. 47th IEEE Conference on Decision and Control*, pages 5055 – 5061.

[18] Large, F., Sckhavat, S., Shiller, Z., and Laugier, C. (2002). Using non-linear velocity obstacles to plan motions in a dynamic environment. In *Proc. 7th International Conference on Control, Automation, Robotics and Vision*, pages 734–739.

[19] Mercado Velasco, G. A., C. Borst, J. E., van Paassen, M. M., and Mulder, M. (2015). The use of intent information in conflict detection and resolution models based on dynamic velocity obstacles. *IEEE Transactions on Intelligent Transportation Systems*, 16(4):2297–2302.

[20] Owen, E. and Montano, L. (2005). Motion planning in dynamic environments using the velocity space. In *Proc. IEEE/RSJ International Conference on Intelligent Robots and Systems*, pages 2833–2838.

[21] Shiller, Z., Large, F., and Sekhavat, S. (2001). Motion planning in dynamic environments: obstacles moving along arbitrary trajectories. In *Proc. IEEE International Conference on Robotics and Automation*, pages 3716–3721.

[22] Snape, J., van den Berg, J., Guy, S., and Manocha, D. (2011). The hybrid reciprocal velocity obstacle. *IEEE Transactions on Robotics*, 27(4):696–706.

[23] van den Berg, J., Lin, M. C., and Manocha, D. (2008). Reciprocal velocity obstacles for real-time multi-agent navigation. In *Proc. IEEE International Conference on Robotics and Automation*, pages 1928–1935.

[24] van den Berg, J., Snape, J., Guy, S. J., and Manocha, D. (2011). Reciprocal collision avoidance with acceleration-velocity obstacles. In *Proc. IEEE International Conference on Robotics and Automation*, pages 3475–3482.

[25] Wiig, M. S., Pettersen, K. Y., and Krogstad, T. R. (2017a). A reactive collision avoidance algorithm for vehicles with underactuated dynamics. In *Proc. IEEE 56th Annual Conference on Decision and Control*, pages 1452–1459.

[26] Wiig, M. S., Pettersen, K. Y., and Krogstad, T. R. (2020). Collision avoidance for underactuated marine vehicles using the constant avoidance angle algorithm. *IEEE Transactions on Control Systems Technology*, 28(3):951–966.

[27] Wiig, M. S., Pettersen, K. Y., and Savkin, A. V. (2017b). A reactive collision avoidance algorithm for nonholonomic vehicles. In *Proc. IEEE Conference on Control Technology and Applications*, pages 1776–1783.

[28] Wilkie, D., van den Berg, J., and Manocha, D. (2009). Generalized velocity obstacles. In *Proc. IEEE/RSJ International Conference on Intelligent Robots and Systems*, pages 5573–5578.

[29] Zhang, W., Wei, S., Teng, Y., Zhang, J., Wang, X., and Yan, Z. (2017). Dynamic obstacle avoidance for unmanned underwater vehicles based on an improved velocity obstacle method. *Sensors*, 17(12):2742.

[30] Zhuang, J., Zhang, L., and Zhao, S. (2016). Radar-based collision avoidance for unmanned surface vehicles. *China Ocean Engineering*, 30:867–883.